INDIVIDUAL TRANSITIONS IN (n,α) REACTIONS AT 14 MeV.

by

CHARLES SPIRA

Submitted in partial fulfillment
of the requirements for the degree of
Doctor of Philosophy

Department of Physics,
Faculty of Pure and Applied Science,
The University of Ottawa,
Ottawa, Canada.

1968

A B S T R A C T

This work deals with the study of (n, α) reactions at 14.6 Mev incident neutron energy. Cross sections are reported for transitions which lead to individual states (or to a group of states) in the residual nucleus.

Alpha particle spectra are presented for 12 isotopes. These were obtained using a counter telescope consisting of two transmission proportional counters placed in front of a lithium drifted silicon detector. Coincidences were taken and particle identification was carried out to reduce the background.

The experimental data are first compared with the predictions of the statistical theory. Fits are obtained for the approximate model known as the (2I+ 1) - rule and results of detailed Hauser Feshbach calculations are reported.

The variation of the experimental ground state transition cross section with target nucleus is compared with the theoretical variation deduced from a direct interaction model, in which two protons and a neutron are successively picked up from the target.

The data for ^{58}Ni are also examined in the light of two models which treat the reaction as a ^{3}He pick-up. One of them takes exchange effects into account.

STATEMENT OF ORIGINALITY

Much work has been previously published on (n,α) reactions initiated by 14 MeV neutrons, but this project constitutes the first systematic search for transitions to individual levels in the residual nucleus.

As far as the author is aware, he is the first to have observed (n,α) spectra from the following target isotopes: ^{60}Ni, ^{61}Ni, ^{47}Ti, ^{56}Fe and ^{138}Ba.

It is customary to compare the total reaction cross section with the predictions of the statistical theory. In this work, however, the experimental cross sections for individual transitions are compared with the yields to single levels in the residual nucleus, as predicted by two versions of the statistical theory. This procedure does not seem to have been considered previously in the literature dealing with (n,α) reactions. These calculations also show quantitatively that the predictions of the $(2I + 1)$-rule and the Hauser Feshbach theory are identical for (n,α) reactions at 14 MeV. Although it is known that the agreement between the two models should improve when higher angular

momentum states participate in the incoming channel, no detailed calculations have come to our attention.

It is also shown for the first time that the successive nucleon pick-up model, used by Bayman et al. to analyse (p,α) data, can be successfully modified to predict ratios of ground state transition cross sections in (n,α) reactions.

ACKNOWLEDGEMENTS

I would like to express my most sincere gratitude to Professor J. M. Robson for his constant guidance and encouragement during this long project.

I am greatly indebted to Dr. R. L. Clarke of Carleton University for several interesting discussions and the sacrifice of much time in making it possible for me to use the Chalk River computer program for Hauser Feshbach calculations.

Thanks are extended to Dr. B. Hird for his interest in the theoretical calculations and to Dr. H. L. Pai for valuable advice on statistical theory calculations.

I would also like to acknowledge discussions of various aspects of the problem with Drs. R. C. Smith, Y. P. Varshni, I. L. Fairweather and B. A. Logan.

I am grateful to former graduate student D. A. Gedke from whose enthusiastic explanations I acquired much electronic know-how in the early stages of the project.

Others to whom thanks are due are:
Dr. K. G. McNeill of the University of Toronto who

lent an enriched titanium target; Mr. W. Perry of the Chalk River Nuclear Laboratories who constructed a thin iron foil, and Dr. W. R. Dixon, of the Applied Physics Division of NRC, who arranged for the preparation of a cobalt target.

Further assistance was also received from: Mr. G. L. Cornish who kept the neutron generator in working order and helped solve several electronic problems; Mr. R. Hart who built the target chamber; Messrs. N. Goodchild and D. Kingswell who machined various objects; Mr. F. Prat who inked the drawings and assisted with some of the computer work; Mr. L. Bunning who took the photographs and Miss S. Daoust who skilfully typed a large part of the manuscript on very short notice.

I finally want to express my gratitude to the Province of Ontario for financial assistance through scholarships.

TABLE OF CONTENTS.

LIST OF ILLUSTRATIONS

I INTRODUCTION

1.1 Motivation for this project.

In 1953 Paul and Clarke used the activation method to measure the cross sections for (n, 2n), (n,p) and (n, α) reactions induced by 14.5 Mev neutrons (Paul 1953). When they compared their experimental results with the evaporation theory, they found a good agreement for (n, 2n) reactions, but the theoretical (n, α) cross sections were nearly always too small (up to four orders of magnitude for targets with mass numbers greater than 100). The (n, p) data followed a pattern similar to (n,α), but less pronounced.

These results were interpreted as follows: in the evaporation theory the excitation energy introduced into the system by the incoming neutron is rapidly shared by all nucleons of the compound system. Particles boiling off the compound nucleus, therefore, carry on the average low energies. If they are charged many emissions will be suppressed by the coulomb barrier. The presence of the coulomb barrier will consequently, favour those processes in which considerable energy is transferred to the outgoing charged particle.

Large energy transfers are typical for direct reaction processes. The difference between the experimental cross sections and the statistical theory predictions was, therefore, attributed to direct reactions.

Many experimental (n, α) cross section data have been published since 1953 and a compilation of the results up to 1964 has been given by Chatterjee (1964 A). These measurements are difficult because of the inherent low cross sections of the (n, α) process and the large background caused by the interaction of the neutrons with all surrounding materials. The necessity of using thin targets ($\sim$ 2mg/cm^2) makes the difficulties more acute. One is, therefore, not surprised that the cross sections quoted by various authors often differ considerably.

The introduction of pairing energy corrections (Newton 1956) in the level density expressions which are used in the statistical theory, resulted in better agreement between compound nucleus theory and experiment. Facchini et al. found good agreement between experimental (n, α) data and statistical theory for nuclei with A < 80 (Facchini 1964). For heavy nuclei the theoretical cross sections were, however, still much too small. It would be imprudent to conclude

from Facchini's work that direct effects are absent in nuclei having A < 80. It is more appropriate to say that in general the total direct contribution is rather small in comparison with the total compound nucleus cross section.

The spectra of the alpha particles emitted in the reactions have also been recorded by various workers. (Numerous references are given in section 1.2). Until the advent of solid state radiation detectors these spectra showed only the gross structure of the energy distributions because of the limited resolution of the then available detection methods. The use of semiconductor detectors led to the observation of resolved alpha particle groups, populating individual levels in the residual nucleus of the reaction (McDicken 1966, Knellwolf 1966).

Measurements of cross sections for resolved individual transitions enable one to make a more useful interpretation of the role of direct interactions in this type of reaction since they would be expected to show the greatest influence of such processes.

The calculation of the theoretical cross sections is complicated, however, especially for the direct interaction process where three nucleon transfers are involved. Single

nucleon transfers as encountered in the (n, d) reaction require already a complex treatment (Valkovic 1965). Glendenning has treated two nucleon transfer reactions in detail (Glendenning 1962, 1965). Three nucleon transfer processes have also been treated by various authors: Massot et al. have considered the (n, α) process as a mixture of pick-up and knock-out events (Massot 1964). Lamot et al. have analysed the same reaction with the DWBA method (Lamot 1967). These treatments, however, do not as yet predict absolute cross sections: several parameters must be adjusted to fit the theoretical angular distributions to experiment.

Recently, Hird and Li have published an analysis of the $^{19}F(p, \alpha)\ ^{16}O$ reaction by means of the DWBA method and come very close to predicting the absolute cross section for this three nucleon transfer process (Hird 1968). A large number of parameters appear in the DWBA process, but these authors allow only two sets to vary freely: the optical potential parameters for the triton (the picked up cluster) and for the alpha particle. In the case of the alpha particle optical parameters "free variation" is an overstatement, because the choice is restricted to four sets of parameters which equally well describe α-particle elastic scattering from ^{16}O.

The aim of the present work was to measure the cross sections for transitions to isolated states in the residual nucleus for as many isotopes as possible and to compare the values with the predictions of compound nucleus theories and with direct interaction theories.

The measurement of the angular distribution of the various alpha groups would have enabled further comparisons to be made, but was not included in this project.

The angular aperture of the detecting system was 78°, enabling a complete set of data for one isotope (including background spectrum) to be accumulated in about 14 hours with a total neutron production rate of 5×10^{8} n/sec.

If the angular resolution of the system had been improved to 20° to enable angular distributions to be attempted, a neutron production of 2.5×10^{11} n/sec would have been needed to accumulate data at the same rate as before. Such high neutron fluxes were not available at the time of the experiment.

1.2 Review of previous work on (n, α) reactions.

The experimental methods which have been used in the study of (n, α) reactions are subdivided in this section into seven categories. The accompanying references serve as a

guide to the literature.

i) Cloud chamber measurements

If the target material is introduced in the cloud chamber as a vapour, not only the emerging alpha particles are recorded, but also the recoiling residual nuclei. Unfortunately, the range energy relation for low-energy recoil nuclei is uncertain because their charge changes during the slowing down process. This, and the need of many photographs, each requiring a painstaking analysis renders the method less attractive (Lillie 1952, Hsu 1967).

ii) Gas filled detection devices

Sometimes the isotope of interest has been introduced into a proportional counter (Ribe 1956). Gridded ionization chambers have also been used (Davis 1964), as well as high pressure gas scintillation counters (Shamu 1962). These methods do not yield angular distribution data. Often the gas filling is also the target and the method could then be mentioned under iv).

iii) The emulsion technique

In some cases the emulsion has been loaded with the target material (Kaul 1962), in others external targets have been used (Kumabe 1957). The alpha particle tracks have been

distinguished from fast proton tracks by special developing techniques, but unfortunately the emulsion nuclei always give rise to a large background.

iv) The detector constitutes also the target

The only instance in which thick targets can be used in the study of (n, α) reactions, is when the detector material constitutes at the same time the target. Experimenters have exploited this opportunity by bombarding silicon detectors (Colli 1963), lithium drifted germanium counters (Aitken 1965) as well as detectors using NaI(Tl) (Bizzeti 1962), CsI(Tl) (Marcazzan 1961), CsBr(Tl) and RbI(Tl) (König 1965), as scintillators. Unless special techniques are employed (Forti 1966, Morgenstern 1966) angular distributions cannot be obtained by this method.

v) Use of a single counter without coincidence requirements

In some experiments useful spectra have been obtained by simply placing a detector in front of the sample target (Cindro 1961, Marcazzan 1963, Cuzzocrea 1964 and Rubbino 1966). The wall material of the vacuum chamber must be properly chosen and the neutron flux must be low in order that small background pulses cannot pile up and contaminate the high energy end of the spectrum.

vi) Counter telescopes

Various counter telescopes consisting of one or two dE/dx counters and a totally absorbing detector are described in the literature (Irfan 1963, Slinn 1963, Kulisic 1964, McDicken 1966 and Maxson 1968). The totally absorbing detector has usually been a semiconductor device or a CsI(Tl) scintillator, and the dE/dx counters have been gas filled or totally depleted silicon detectors. The use of a telescope allows considerable background reduction through coincidence techniques and particle identification.

vii) The activation method

A large number of total (n, α) cross sections have been determined by activation analysis (Paul 1953, Jeronymo 1963, Yu 1967). The method, of course, requires that the residual nucleus be unstable and the measurement is then made by estimating the induced activity.

II - GENERAL DESCRIPTION OF THE APPARATUS

This section gives an over-all picture of the experimental method that has been employed in the present work. The experimental assembly consists of a vacuum chamber mounted in the vicinity of the neutron producing target of a 100 kV Cockraft-Walton accelerator. Fig. 2.1 gives a schematic picture of the system. The vacuum chamber which is filled with 200 mm Hg of A and 20 mm Hg of CO_2 houses the sample target, a counter telescope consisting of two proportional counters and a lithium drifted solid state detector. Each detector has its own amplification and discriminator system. Alpha particles emitted by the sample target can only reach the semiconductor detector by traversing first the two proportional counters, whose cathodes are tungsten wire grids, easily penetrated by the alpha particles. The latter lose only a small fraction of their energy in the proportional counters (dE/dx counters). All the remaining energy is deposited in the semiconductor detector (E-counter).

The discriminator output from each amplifier is connected to one input of a triple coincidence circuit. The output from the latter triggers a particle identification system which singles out the events corresponding to alpha particles. The necessary information for particle identifi-

THE EXPERIMENTAL ASSEMBLY — SIMPLIFIED DIAGRAM

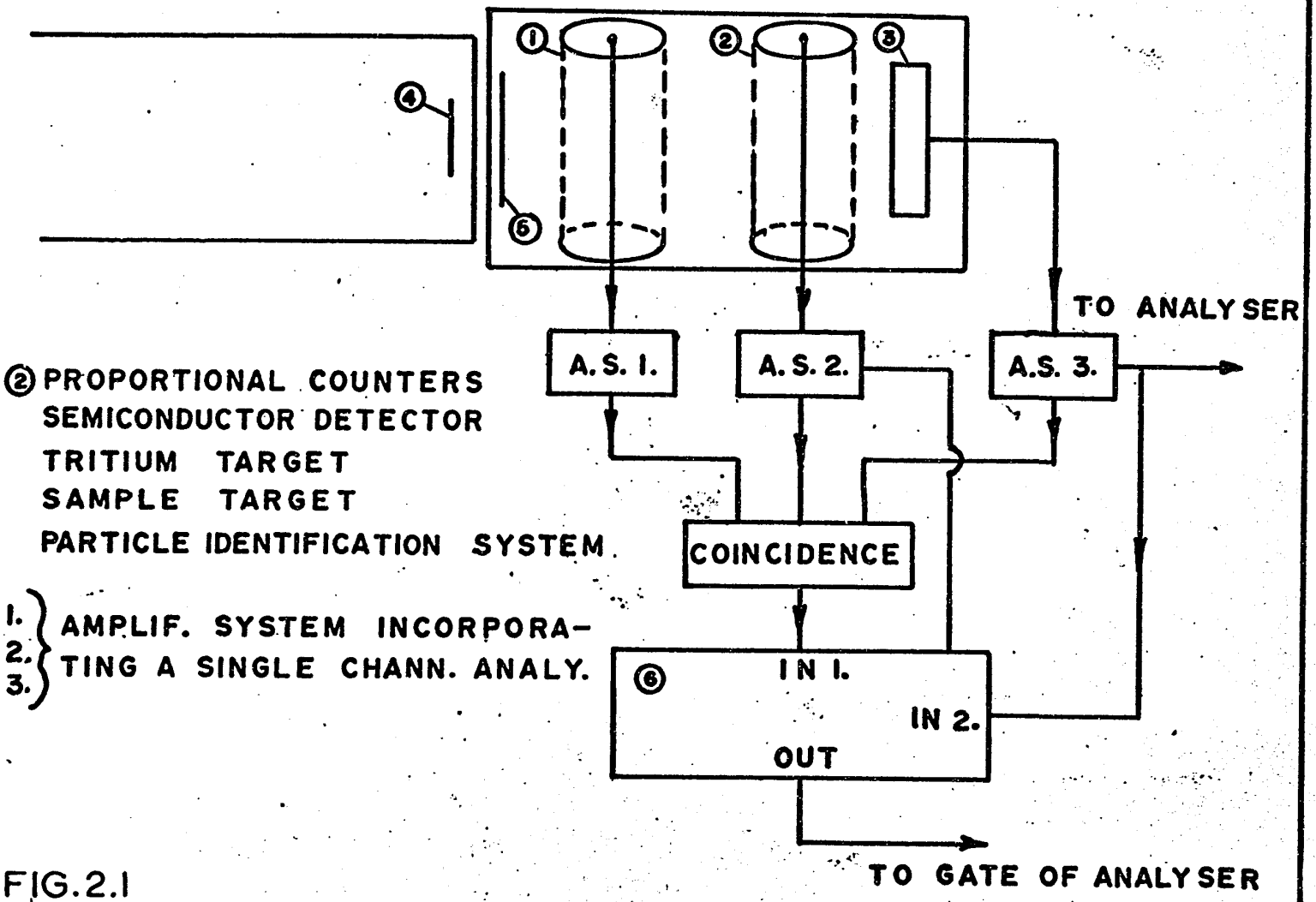

① ② PROPORTIONAL COUNTERS
③ SEMICONDUCTOR DETECTOR
④ TRITIUM TARGET
⑤ SAMPLE TARGET
⑥ PARTICLE IDENTIFICATION SYSTEM.

A.S. 1.
A.S. 2.
A.S. 3.
} AMPLIF. SYSTEM INCORPORATING A SINGLE CHANN. ANALY.

FIG. 2.1

cation is provided by the semiconductor detector and the adjacent proportional counter. The signals from the semiconductor detector due to alpha particles are further processed and recorded.

III - VACUUM CHAMBER AND COUNTER ASSEMBLY

The vacuum chamber and counter assembly have been designed after it was decided that:

a) no angular distribution measurements would be attempted.

b) only the high energy part of the alpha spectrum would be recorded.

3.1 General design criteria.

Two important conditions have to be met by the design:

i) the alpha particles emitted by the sample should be counted as efficiently as possible.

ii) the sensitivity to background radiation produced by materials other than the sample target should be as small as possible.

Fig. 3.1 shows the design of the vacuum chamber and the counter geometry that was finally adopted.
This choice will now be justified.

3.1.1 Achieving optimum efficiency.

Maximum counting efficiency will be achieved if the detector area is large and if the detector is placed as close as possible to the sample target. But the counting geometry affects the energy resolution. From the reaction kinematics it follows that the energy of an alpha particle

THE TARGET CHAMBER

1. SEMICONDUCTOR DETECTOR
2. PROPORTIONAL COUNTER
3. TARGET
4. TARGETWHEEL
5. ROTATING VACUUM SEAL
6. TRITIUM TARGET
7. PUMPING LINE AND GAS INLET

BRASS

GRAPHITE

SCALE 1:1

FIG. 3.1

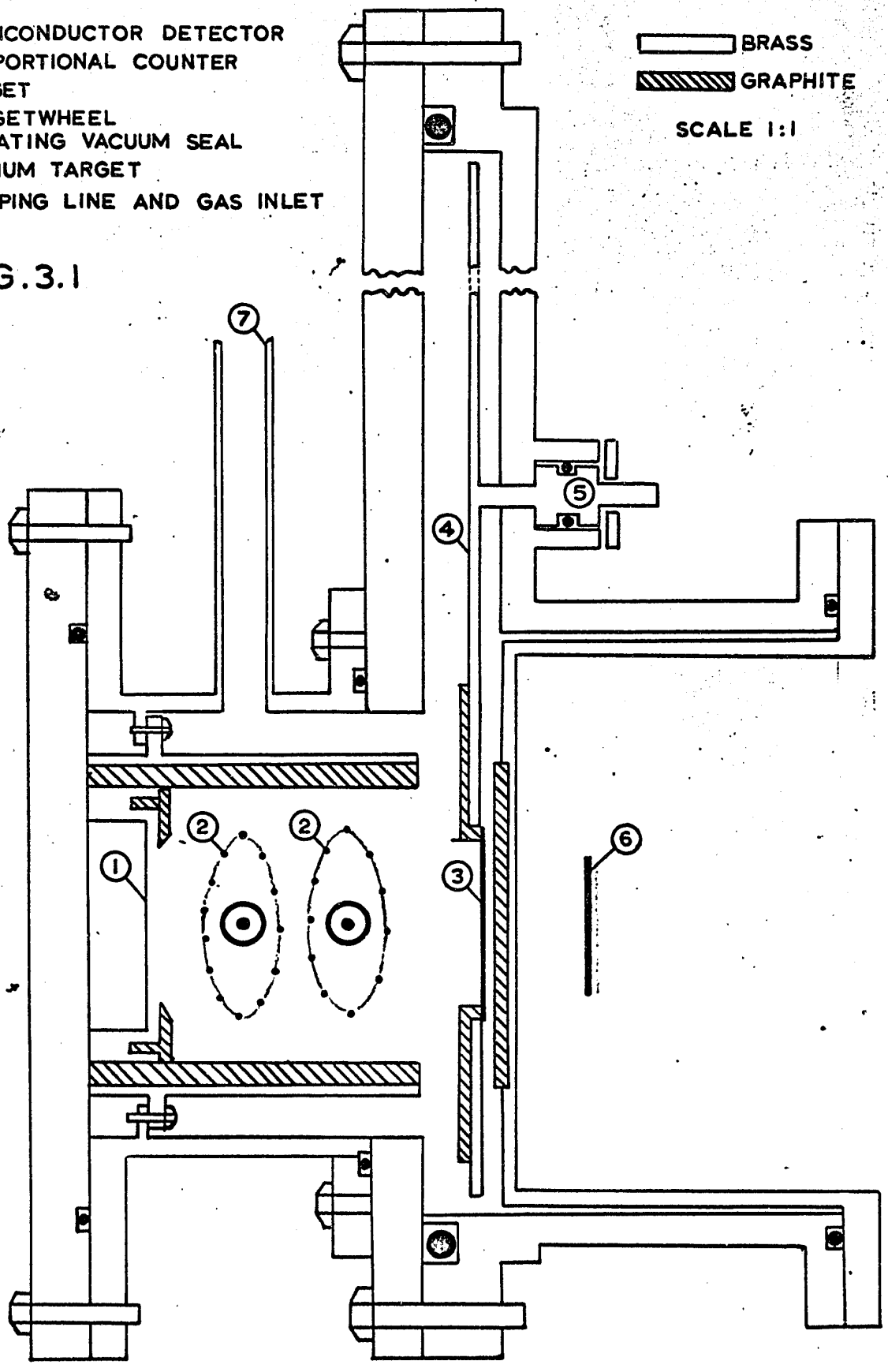

emitted in a (n, α) reaction and leaving the residual nucleus in a definite state, will depend on the angle between its path and that of the neutron that initiated the reaction. If one wants to observe sharp peaks in the energy spectrum for alpha particles leaving the residual nucleus in a definite state, the acceptance angle of the E-counter must be limited. This limitation is more drastic for lighter target nuclei. The minimum sample-detector distance is dictated by the detector area and the maximum tolerable energy spread. One should also keep in mind that the tritium target-sample target distance plays a part in fixing the maximum possible angle between an ingoing neutron and an outgoing alpha particle, in order that the latter still be counted.

3.1.2 Minimizing the background.

The background radiation in the vacuum chamber includes all radiation emitted by materials other than the sample and particles other than alphas produced in the latter. The sources of this background radiation are:

a) the silicon of the semiconductor detector.

b) the walls of the vacuum chamber.

c) the proportional counter gas.

d) the tungsten wires which constitute the anodes and cathodes of the proportional counters.

The background originating in the E-detector can be reduced in two ways which complement each other:

i) One can choose a type of detector whose main constituant element has a very small cross section for (n, α) reactions.

ii) By installing at least one proportional counter between sample target and E-counter, and demanding a time coincidence between the signals from both detectors, the alpha particles generated in the E-counter can be eliminated from the spectrum. Only those alpha particles which are generated near the front window of the solid state detector and travel backwards can give rise to a coincidence. Fortunately, these deposit only little energy in the E-counter and will not contaminate the high energy end of the spectrum.

In the present work a silicon lithium drifted detector was used, which is not a good choice in view of i): both ^{28}Si and ^{29}Si have a large cross section for (n, α) reactions at 14 Mev (with Q-values of respectively - 2.6 and -0.035 Mev). This type of detector was selected for other reasons given below.

Most materials emit alpha particles when subjected to a bombardment with 14 Mev neutrons. The maximum energy of the

emitted alphas depends on the Q-values of the respective (n, α) reactions. Two policies can be adopted to minimize the background:

i) One can arrange that the E-detector only sees high Z-materials which generate few alphas on account of their high Coulomb barriers. The emitted particles necessarily have energies not much lower than the barrier height and up to a maximum value governed by the Q-value of the reaction. The resulting background covers nevertheless the whole spectrum, down to zero energy, because many alpha particles originate from well below the surface of the material and may lose considerable energy before emerging. Although the background covers the whole spectrum, it remains small, which might be an important asset.

ii) The E-counter only sees materials which have a strongly negative Q-value for (n, α) reactions. The background alpha particles will be numerous but all will have low energy. If the neutron flux is such that no pile-up occurs in the E-counter amplification channel, the background spectrum will feature a high counting rate in the low energy region, but will be clean at high energies.

Graphite is highly suitable as a wall material to meet objective (ii). The percentage abundances and Q-values are respectively 98.9% and 1.1%,- 5.70 Mev and - 3.83 Mev for ^{12}C and ^{13}C. These isotopes also have negative Q-values in excess of 12 Mev for the (n, p) reaction, which reduces the high energy proton background.

In this work the high energy end of the spectra was measured for a series of elements covering a wide range of Z-values. A low background in the high energy region was highly desirable and, therefore, policy (ii) was adopted.

The inclusion of at least one proportional counter between sample and E-counter, with a demand of time coincidence, reduced the background further. Indeed, many particles reach the E-counter from the walls, without having an appreciable path in the dE/dx counters.

Experience showed that the inclusion of two proportional counters (and demanding a triple coincidence) is still more effective in reducing the registration of parasitic radiation.

An important requirement of the proportional counter gas mixture was that it should not contribute appreciably to the background. A mixture containing 200 mm Hg of A and 20 mm Hg of CO_2 was selected. The Q-values of the various constituents for (n, α) reactions are:

^{12}C: - 5.70 Mev

^{16}O: - 2.21 Mev

^{40}A: - 2.42 Mev

Thus all alpha particles generated in the counter gas had energies well below 14 Mev.

The cathodes and anodes of the proportional counters were constructed from tungsten wire. The total mass is considerable, but the total surface area presented to the neutron beam is small, and this together with the low cross section for (n, α) reactions (Z = 74) resulted in a small contribution to the total background.

3.2 Design of the counter assembly.

Many features of the experimental arrangement have already been dictated by the general design criteria. The choice of the counter assembly will now be discussed in detail.

3.2.1 The E-detector.

Three types of detectors can be conveniently used for the measurement of the alpha particle spectra.

a) a CsI(Tl) scintillator.

b) a surface barrier silicon detector.

c) a lithium drifted silicon detector.

The main advantage of the scintillation detector lies in the low cross section for alpha particle production in the Cs and I of the crystal. The large gain of the photomultiplier eliminates the need for considerable post amplification of the signals. Several disadvantages should however be noted:

i) the resolution is considerably inferior to the one obtained with a semiconductor detector.

ii) the energy response of CsI(Tl) is nonlinear at low energies. This makes the energy calibration of the spectrum difficult.

iii) great experimental difficulties are encountered in trying to achieve a permanently stable seal between a thin CsI(Tl) crystal and the light pipe coupling it to the photomultiplier, when the pressure in the target chamber is variable.

Surface barrier silicon detectors were tried, but their operation seemed to be seriously impaired by the presence of the proportional counter gas. Often the bias voltage could not be raised high enough to reach the desired depletion depth, without causing electrical breakdown.

Lithium drifted silicon detectors of the type built by Simtec Ltd. operated satisfactorily in a gaseous environment, because of their tough but thin inactive front window.

These detectors are, however, quite sensitive to radiation damage by fast neutrons, considerably more so than surface barrier detectors. In both types of counters the deterioration is due to silicon atoms being knocked out of their crystal sites by incident neutrons. The displaced atoms end up in interstitial positions in the lattice. The resulting vacancy-interstitial pairs, or Frenkel defects, act as carrier trapping sites. These trapping sites reduce both the carrier mobility and carrier lifetime. Lithium drifted detectors are especially sensitive to this effect because of their low internal fields (and consequent short trapping lengths). Moreover, lithium tends to precipitate out in radiation produced vacancies.

In spite of this drawback, a 500 mm^2 silicon lithium drift device having a depletion depth of 500 μ was used in the present work. It was found that the detector could stand a dose of about 10^{12} neutrons before becoming unusable. This corresponds to roughly 100 hours of operation.

3.2.2 The proportional counters.

Several considerations dictated the use of gas filled proportional counters as dE/dx detectors. Totally depleted silicon detectors of the required thickness are expensive, fragile and possess rather short lifetimes. Moreover, many

alpha particles would be generated in the silicon. Fig. 3.1 shows that the cathodes of the proportional counters have an elliptic rather than a circular contour. In this manner, the sensitive volumes of the proportional counters still cover the total active area of the E-counter, while the target semiconductor detector distance can be made considerably smaller than would be possible with cylindrical cathodes having a circular cross section. Tungsten wire of 0.003" diameter was used in the construction of the proportional counters. After much experimenting a gas mixture of 200 mm Hg of A and 20Ø mm Hg of CO_2 was selected.

Using a high voltage of 750 V, a stable spectrum was obtained, indicating that the multiplication factor was not too high. During the first 30 minutes after the counters have been filled with fresh gas, the multiplication factor decreases by about 20%, due to contamination of the initially pure gas. After this initial period it remains virtually constant over a period of 20 hours. Therefore, only minor adjustments were required every two hours.

When 5.47 Mev alpha particles were allowed to traverse both proportional counters along similar paths, it was found that all signals from the gas counters had the same pulse

height with a 14% spread. Fig. 3.2 shows the observed pulse height distribution for the counter adjacent to the source. These measurements were carried out by placing an ^{241}Am source at the location of the sample target and registering the signals of the respective proportional counters in a multi-channel analyser, the latter being gated by the semi-conductor detector. Only the alpha particles which completely traversed both proportional counters were, therefore, included in the pulse height distribution.

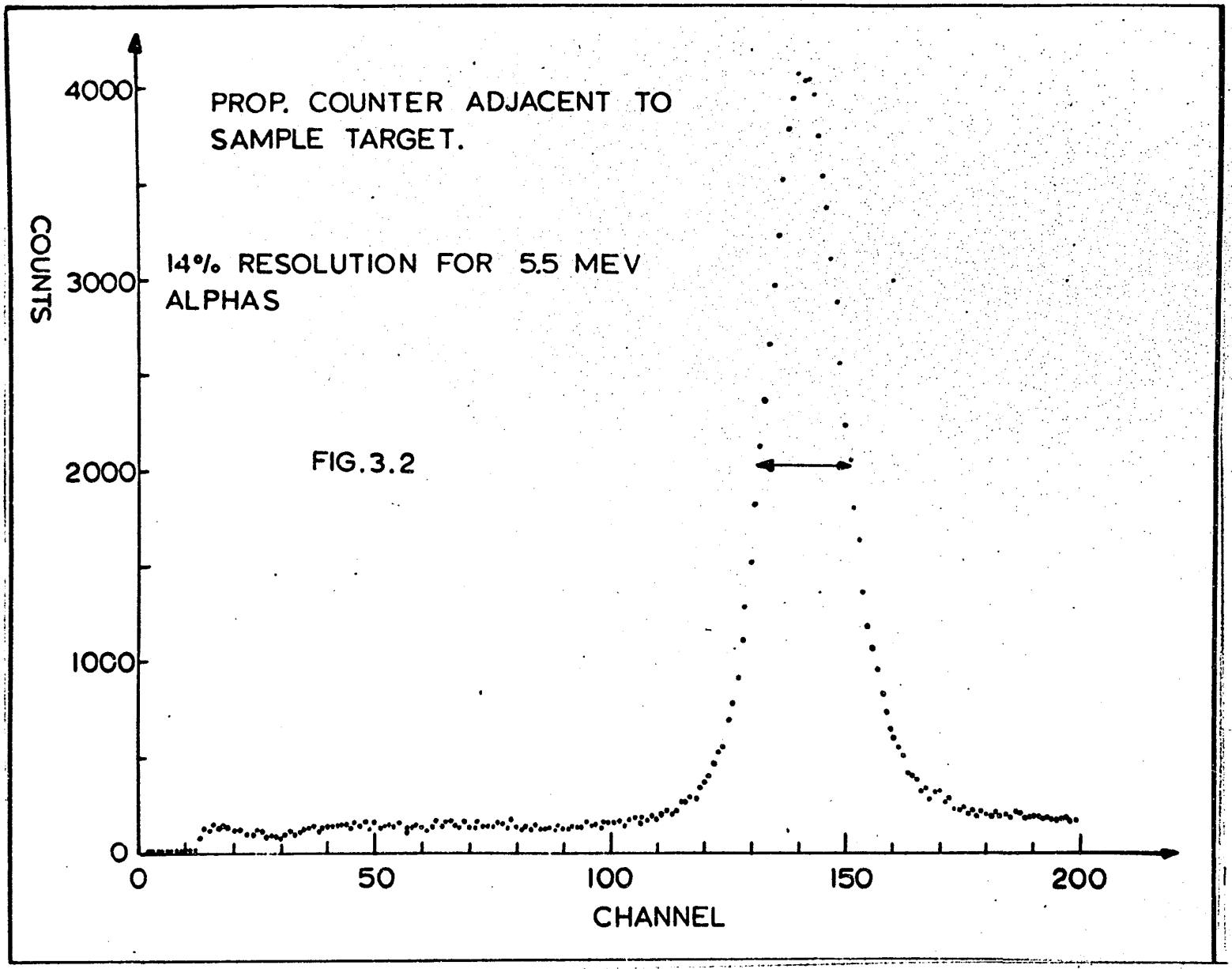

FIG. 3.2

IV - THE NEUTRON MONITOR

4.1 Method.

If one wants to quote absolute (n, α) cross sections, the total number of neutrons produced in each experiment must be known. An alpha particle is associated with each neutron produced in the $^{3}H(^{2}H, n)^{4}He$ reaction. The neutron yield was, therefore, measured by counting the associated alpha particles emitted within a known solid angle. The orientation of the alpha counter (associated particle detector) is not important because the $^{3}H(^{2}H,n)^{4}He$ reaction is virtually isotropic at the low deuteron bombarding energies used in this experiment.

4.2 Experimental arrangement.

The alpha particle detector, which is of the surface barrier type, was mounted eccentrically inside the accelerator tube at a distance of 32-3/4" from the tritium target, in such a way that it would not interfere with the deuteron beam. The detector was mounted inside a metallic case in order to avoid heating by the periphery of the deuteron beam. The case provided at the same time a good protection against electronic pick-up. The front face of the detector, which has a nominal sensitive area of 7 mm^2, was covered with a 150 $\mu g/cm^2$ aluminum foil, in order to absorb stray electrons which might

reduce the useful life of the detector. The experimental set-up is schematically illustrated in Fig. 4.1.

In order to calculate absolute cross sections, the ratio N_{ap}/N_n must be known, where N_n is the total number of neutrons and N_{ap} the corresponding number of counts registered in the associated particle detector. In principle this ratio can be deduced from the geometry. A fraction of the counts N_{ap} is, however, due to coulomb scattering of alpha particles into the associated particle detector by the wall of the beam tube. This effect is difficult to evaluate.

4.3 Measurement of N_{ap}/N_n.

The associated particles emerge with an energy of 3 Mev in the backward direction. A calibrated americium source, having the same diameter as the tritium target was substituted for the latter. Nickel foils were placed in front of the source to degrade the alpha particle energy to 3 Mev. Denoting by C_α and C_{ap} the rate of emission by the source and the corresponding counting rate in the associated particle detector, one may write:

$$\frac{N_{ap}}{N_n} = \frac{C_{ap}}{C_\alpha} \qquad (4.1)$$

THE NEUTRON MONITOR

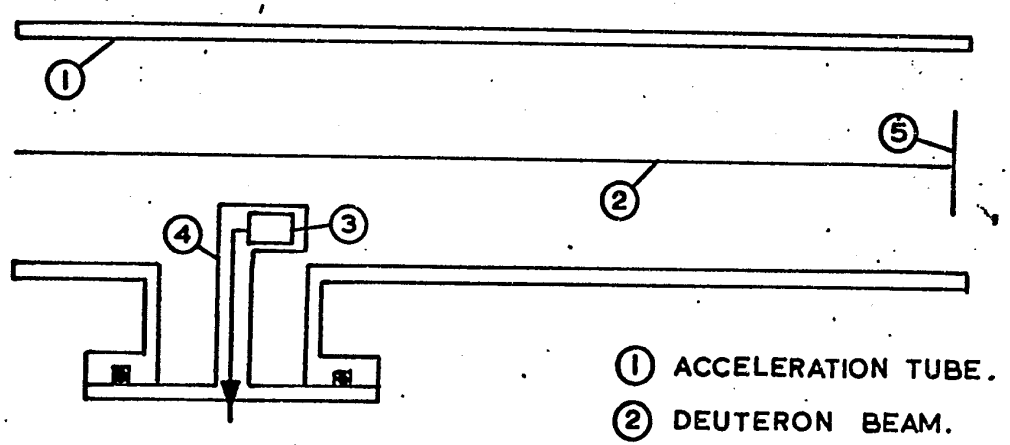

1. ACCELERATION TUBE.
2. DEUTERON BEAM.
3. SURFACE BARRIER DETECTOR.
4. METAL CASING.
5. TRITIUM TARGET.

FIG.4.1

From this it was deduced that:

$$\frac{N_{ap}}{N_n} = (9.4 \pm 1.4) \times 10^{-7} \qquad (4.2)$$

If the sensitive area of the associated particle detector is known, the contribution to N_{ap} by coulomb scattering can be calculated. This turns out to be about 30% of the total number of counts.

V - THE ELECTRONIC SYSTEM

5.1 The proportional counter circuitry.

Fig. 5.1 shows the circuitry associated with each proportional counter. It consisted of a stabilized high voltage supply, a preamplifier and a main amplifier. A window discriminator allowed the selection of pulses which are comprised located between independently adjustable upper and lower levels. The discriminator signal passed through a pulse shaper and then activated one channel of the coincidence system.

5.1.1 The preamplifier.

The final design adopted for the preamplifiers consisted of a tube input stage (Jordan 1947) and two transistorized stages (Waugh 1960). This preamplifier provided the possibility of large gain. (It was not known from the start what multiplication constant would be used in the proportional counters). Figs. 5.4 and 5.5 respectively show the tube stage and one transistor stage.

5.1.2 The main amplifier and the window discriminator.

The main amplifier and the window discriminator were incorporated in a commercial unit. The counting rates in the proportional counters were very high and double delay

line clipping was used to minimize the danger of pile-up.

5.1.3 The pulse shaping circuit.

The pulse shaping circuit consisted of a monovibrator followed by an emitter follower (Fig. 5.6).

5.2 The solid state detector circuitry.

A preamplifier and a main amplifier featuring double delay line clipping were associated with the solid state detector (Fig. 5.2). The output from the integral discriminator was fed into a pulse shaping circuit.

The use of the particle identification system required that the signal from the linear amplifier be delayed for approximately 25 μsec before being presented to the multichannel analyser. The lumped parameter delay line (delay 1) had an impedance of 100 Ohm. An impedance matching circuit separated the output of the main amplifier and the delay line.

5.2.1 The preamplifier.

The preamplifier was a commercial version of the low noise circuit with cascode input stage described by Chase et al. (Chase 1961A).

5.2.2 The main amplifier, the integral discriminator and the pulse shaping network.

The main amplifier and the integral discriminator were incorporated in a commercial unit.

The lithium drifted silicon detector was in principle capable of a resolution better than 1.5% for 5.47 Mev alpha particles. The energy spread due to non-electronic causes gave rise to a much poorer resolution. The extra noise introduced by double delay line clipping was negligible in comparison with the "non-electronic" energy spread.

The pulse shaping circuit was identical to the one in section 5.1.3.

5.3 The neutron monitor circuitry

The neutron monitor equipment is shown in Fig. 5.3. The preamplifier (Chase 1961) was followed by a commercial linear amplifier with single RC shaping and an integral discriminator. The linear output was fed into a 3 μsec delay and then displayed on an oscilloscope. When the latter was triggered externally by the discriminator output, the discriminator level could be adjusted by visual inspection.

5.4 The coincidence system

5.4.1 The random coincidence rate

Completely unrelated signals from the three detectors, which occur within the resolving time of the coincidence circuit, give rise to a random coincidence at the output. A random triple coincidence also takes place when a genuine

coincidence between two counters is followed by an unrelated signal from the third counter within a period shorter than the resolving time.

The counting rates per second are respectively N_1, N_2 and N_3 in the three channels. Each detector activates the coincidence circuit for a time τ after an event has been registered (τ is supposed to be identical for the three channels). It can be shown that the random coincidence rate R is given by

$$R = 3\tau^2 N_1 N_2 N_3 \qquad (5.1)$$

if no correlations exist between the various pairs of channels (De Benedetti 1958).

Let N_i and N_j be the counting rates in channels i and j. A correlation is said to exist between channels i and j if C_{ij} among these counts constitute genuine double coincidences. The presence of these coincidences affects the chance triple coincidence rate considerably. It becomes now (De Benedetti 1958):

$$R = 3\tau^2 N_1' N_2' N_3' + 2\tau (C_{12} N_3 + C_{13} N_2 + C_{23} N_1) \qquad (5.2)$$

with $N_i' = N_i - C_{ij} - C_{ik}$ (i, j and k constitute a combination of the indices 1, 2 and 3).

5.4.2 The choice of τ.

The ratio of genuine to chance coincidences should be as high as possible. R can be reduced by making τ small and by operating at low counting rates. The minimum value for τ is set by the response time of the porportional counters which is considerably longer than that of the solid state detector. A value τ = 1.5 μsec was adopted.

5.4.3 Principle of operation of the coincidence circuit.

Fig. 5.7 shows the triple coincidence circuit. Transistors T_1, T_2 and T_3 which have a common collector load, conduct heavily in the quiescent state. As a result the potential of P is close to ground. If all three transistors are cut off simultaneously, the potential of P is lowered to -10V until at least one input signal disappears. T_4 inverts the signal and T_5 provides a low output impedance.

The output of the coincidence circuit provides the gating pulse for the time to pulse height converter of the particle identification system (Section 6.3.3).

PROPORTIONAL COUNTER CIRCUIT

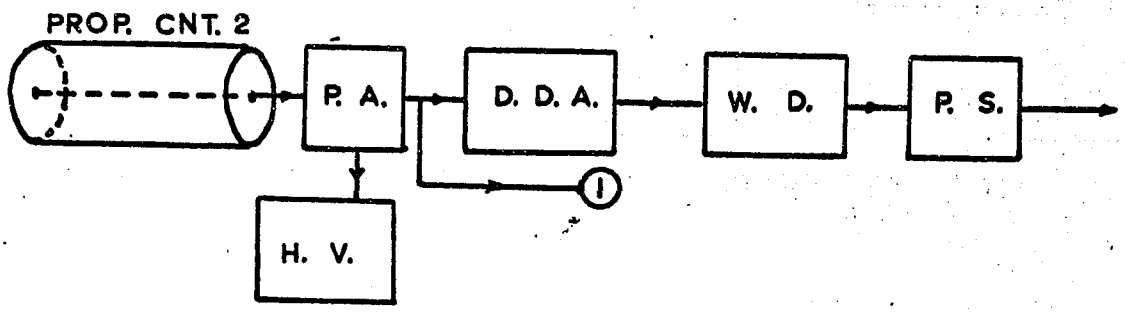

H.V. : HIGH VOLTAGE POWER SUPPLY
PROP. CNT. : PROPORTIONAL COUNTER
P. A. : PREAMPLIFIER
D. D. A. : DOUBLE DELAY LINE CLIPPED AMPLIFIER
W. D. : WINDOW DISCRIMINATOR
P. S. : PULSE SHAPER

FIG.5.1

SEMICONDUCTOR DETECTOR CIRCUIT

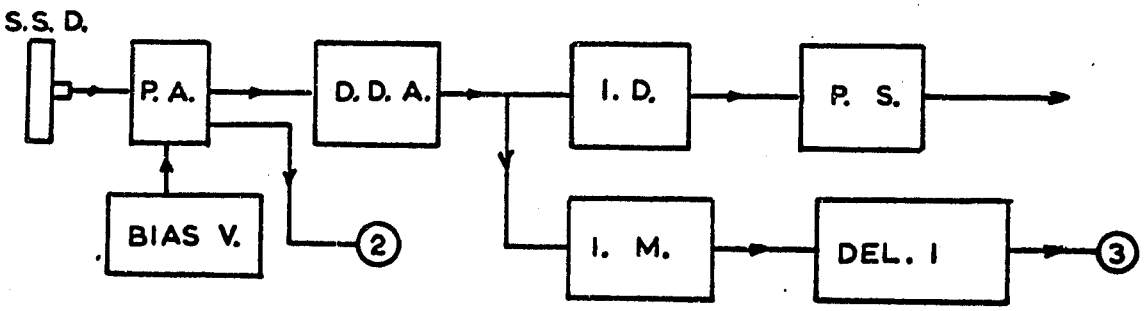

S. S. D. : SOLID STATE DETECTOR
BIAS V. : BIAS VOLTAGE SUPPLY
I. D. : INTEGRAL DISCRIMINATOR
I. M. : IMPEDANCE MATCHING CIRCUIT
DEL. I : LUMPED DELAY LINE

FIG.5.2

ASSOCIATED PARTICLE DETECTOR CIRCUIT

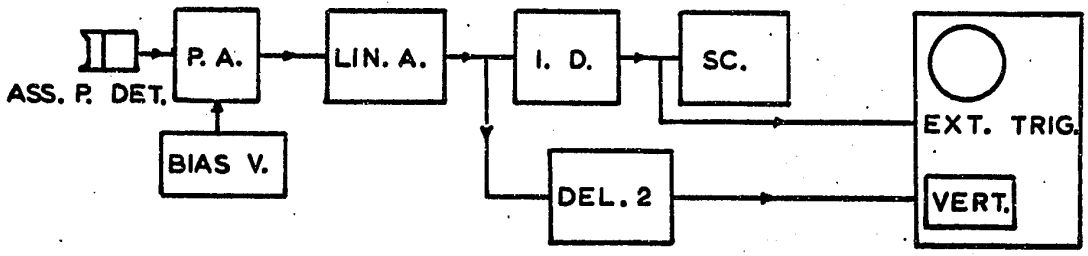

ASS. P. DET. : ASSOCIATED PARTICLE DETECTOR
P. A. : PREAMPLIFIER
LIN.A. : LINEAR AMPLIFIER
I. D. : INTEGRAL DISCRIMINATOR
SC. : SCALER
DEL. 2 : DELAY LINE 2
EXT. TRIG. : EXTERNAL SWEEP TRIGGER
VERT. : VERTICAL AMPLIFIER

FIG.5.3

P. C. PREAMPLIFIER (TUBE STAGE)

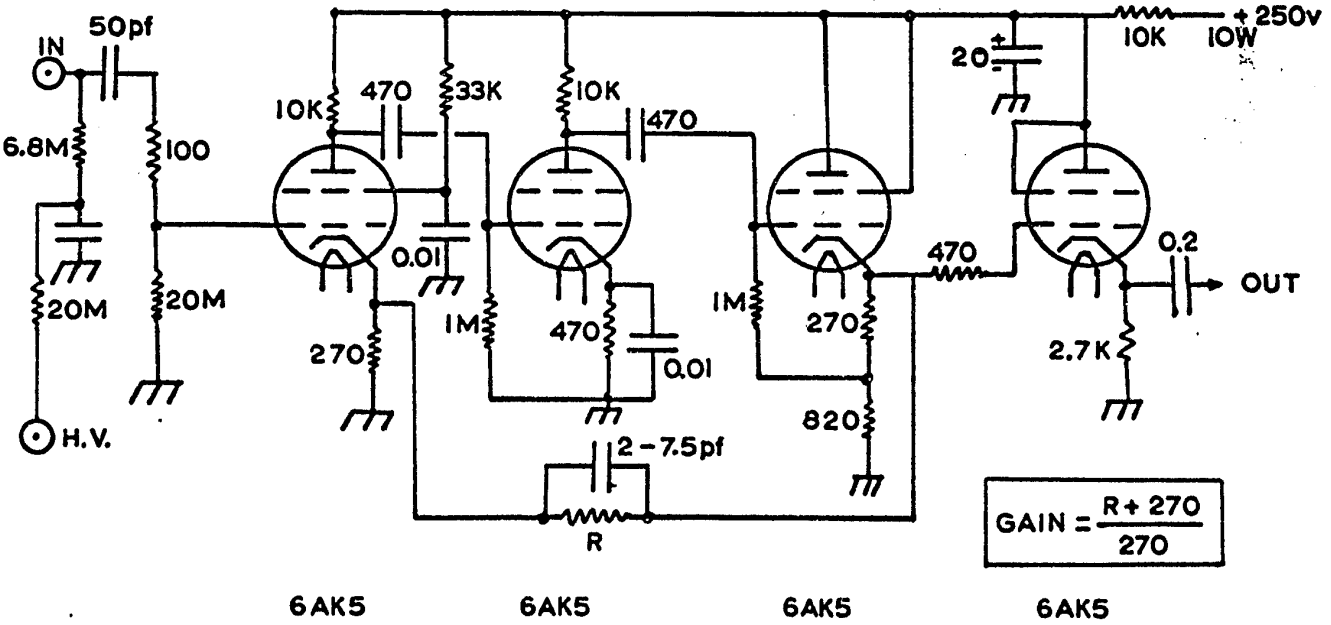

FIG.5.4

P. C. PREAMPLIFIER (TRANSISTOR STAGE)

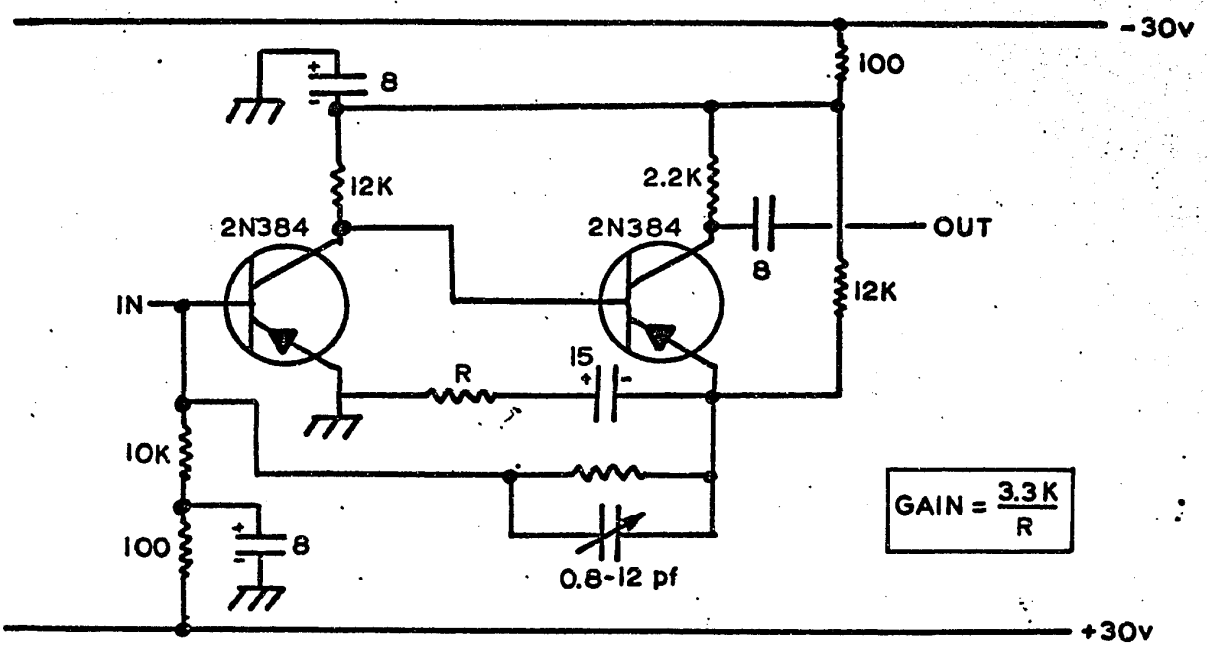

FIG. 5.5

PULSE SHAPING CIRCUIT

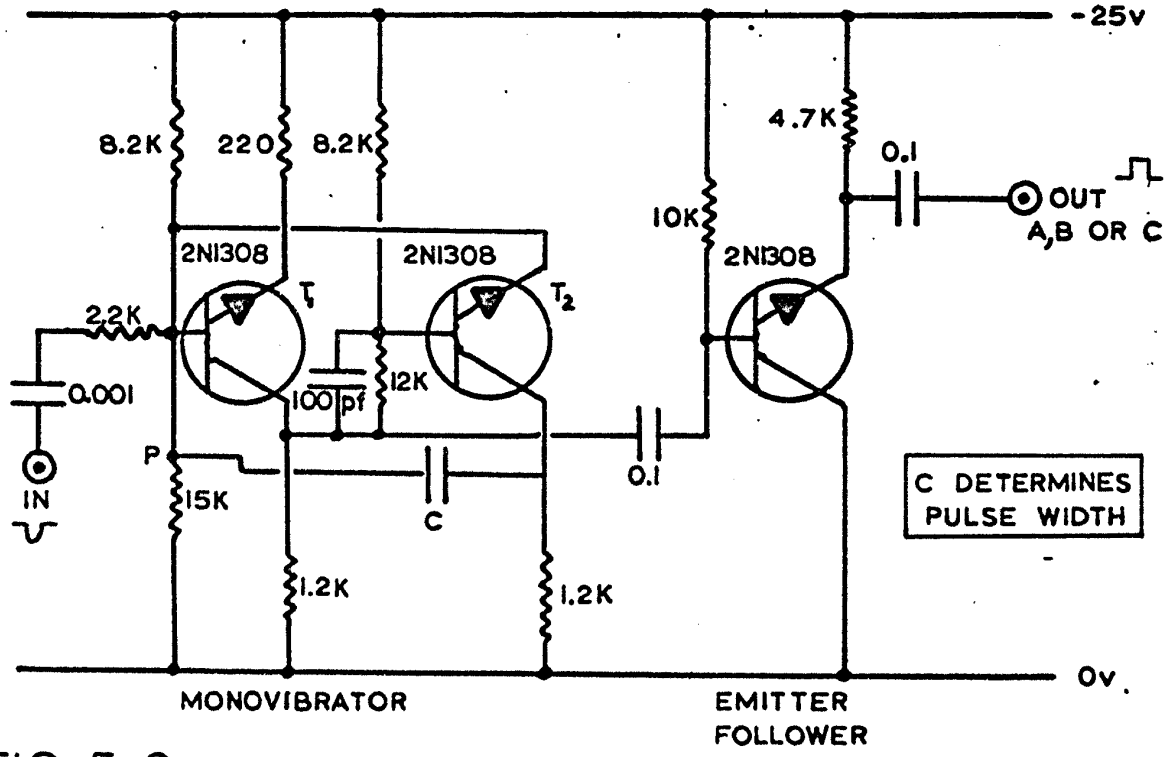

FIG. 5.6

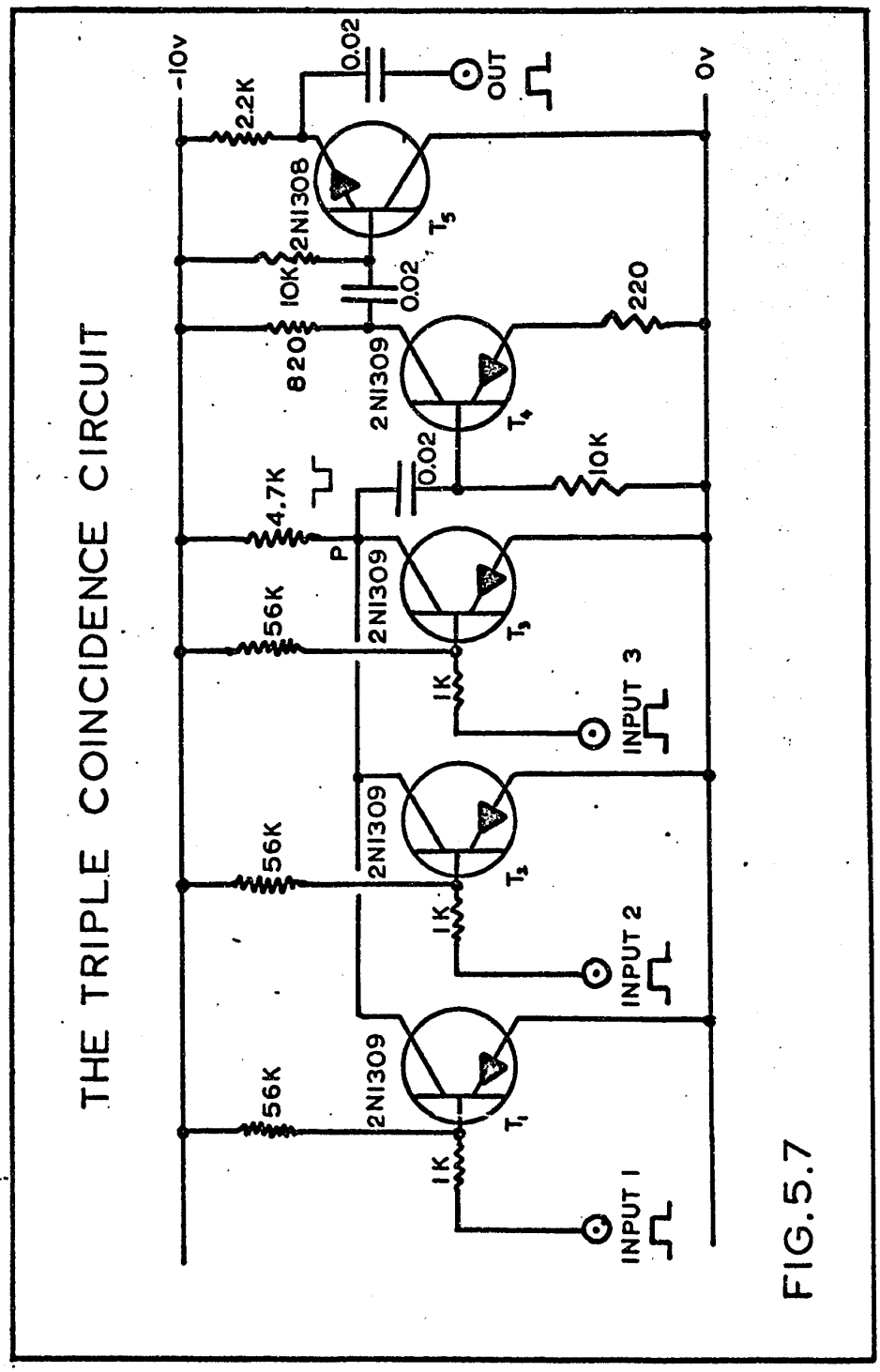
THE TRIPLE COINCIDENCE CIRCUIT
-10v
0v
2.2K
0.02
OUT
2N1308
T5
10K
0.02
220
820
2N1309
T4
0.02
10K
4.7K
P
56K
2N1309
T3
1K
INPUT 3
56K
2N1309
T2
1K
INPUT 2
56K
2N1309
T1
1K
INPUT 1

FIG.5.7

VI - THE PARTICLE IDENTIFICATION SYSTEM

In order to distinguish the alpha particles from the protons and deuterons resulting from neutron interactions in the sample and surrounding materials, a particle identification system was used.

6.1 The principle of particle identification.

All methods for charged particle identification require the simultaneous knowledge of the total energy of the particle, and a quantity related to its rate of energy loss in matter. For non-relativistic velocities Bethe's well-known formula for the rate of energy loss of a charged particle in a material medium reduces to:

$$\frac{dE}{dx} = \frac{4\pi e^4 z^2}{mV^2} NZ \ln \frac{2mV^2}{I} \quad (\text{erg cm}^{-1}) \qquad (6.1)$$

e and m are the charge and mass of the electron.
V and z are the velocity of the charged particle and the number of elementary charges it carries.
N and Z are the number of atoms per unit volume and the atomic number of the material medium.
I is the mean excitation energy of the atomic electrons (Evans 1955).

Expression (6.1) is not universally valid. The range of validity for each type of particle depends on the nature of the absorber through which it travels.

If M and E are the mass and kinetic energy of the charged particle, (6.1) can be written:

$$\frac{dE}{dx} = K_1 \frac{Mz^2}{E} \cdot \ln K_2 \frac{E}{M} \qquad (6.2)$$

with $K_1 = \frac{4\pi e^4 NZ}{2m}$ and $K_2 = \frac{4m}{I}$

K_1 and K_2 are constants for a given absorber.

The product

$$E \frac{dE}{dx} = K_1 Mz^2 . \ln K_2 \frac{E}{M} \qquad (6.3)$$

depends on the nature of the projectile through z and M, but is nearly independent of E within a large energy range. (The logarithmic term $\ln K_2 \frac{E}{M}$ varies only slowly with E).

The product $E \frac{dE}{dx}$ has, therefore, a definite value for each type of particle, irrespective of its energy. Many particle identifiers are based on the evaluation of this product:

e.g., Briscoe 1958, Gianelli 1960, Aitken 1961, Swenson 1964. Some incorporate correction factors in order to account for the effect of the logarithmic term. If the product $E \frac{dE}{dx}$ is put equal to 16 for alpha particles, it will be roughly 2 and 1 for deuterons and protons. Since in this work the identifier is only used to single out alpha particles, the logarithmic term can be safely ignored.

6.2 The present identification system.

The design of the present identifier is similar to that of Aitken (Aitken 1961).

Aitken uses the pulse height to time conversion performed on the E-signal in a multi-channel analyser to provide a start and stop signal to a sawtooth generator producing a signal with a slope proportional to $\frac{dE}{dx}$. The final pulse height of the sawtooth is proportional to $E \frac{dE}{dx}$. The product pulse is then sorted by a single channel analyser, in time to allow an inhibiting pulse to be fed back into the multi-channel analyser, if the product pulse is not of the desired value.

In the present design the need for access to the internal circuitry of the multi-channel analyser has been

eliminated by incorporating a pulse height to time converter in the multiplier. Figs. 6.1 and 6.2 explain how the product $\frac{dE}{dx} E$ is obtained and how gating of the multi-channel analyser is achieved.

E-counter pulses associated with a triple coincidence are transmitted by linear gate 1 to a pulse height to time converter (PTC). They are transformed by the latter into square pulses of constant amplitude with widths proportional to the input amplitudes. Pulses with slow exponential decay from proportional counter 2 are applied to linear gate 2. The latter is gated by the output of the PTC. The pulses at the input of linear gate 2 are, therefore, transmitted during a time interval which is proportional to the amplitude of the corresponding E-counter signals. Square waves modulated in amplitude by $\frac{dE}{dx}$ counter 2 and in width by the E-counter appear behind linear gate 2. Subsequent integration yields pulses with amplitudes proportional to $\frac{dE}{dx} .E$. An integral discriminator allows to select those product pulses which correspond to alpha particles. After having passed through a pulse shaper, the discriminator pulses gate the multi-channel analyser.

It will be noted that E and $\frac{dE}{dx}$ signals are delayed by delay circuits 3 and 4 and amplified by a linear amplifier. The delays are necessary to provide correct time correlation between gating pulses and counter signals.

Fig. 6.2 shows waveforms for two alpha particles with different energies at several points of the block diagram in Fig. 6.1. It can be seen (Fig. 6.2e) that the product pulse reaches full amplitude at different times, depending on the size of the E-counter signal. The logic pulses from the integral discriminator show, therefore, a considerable time jitter with respect to the E-counter pulses which are fed directly into the multi-channel analyser. To insure proper gating of the analyser, the E-counter signals must be delayed by an amount larger than this maximum time spread by means of delay 1. The square waves from the pulse shaper must be wide enough to guarantee overlapping of E-signals and gating pulses at all times. The building blocks enclosed in the dashed rectangle in Fig. 6.1 constitute the heart of the identification system and have been built as a single unit.

THE PARTICLE IDENTIFICATION SYSTEM

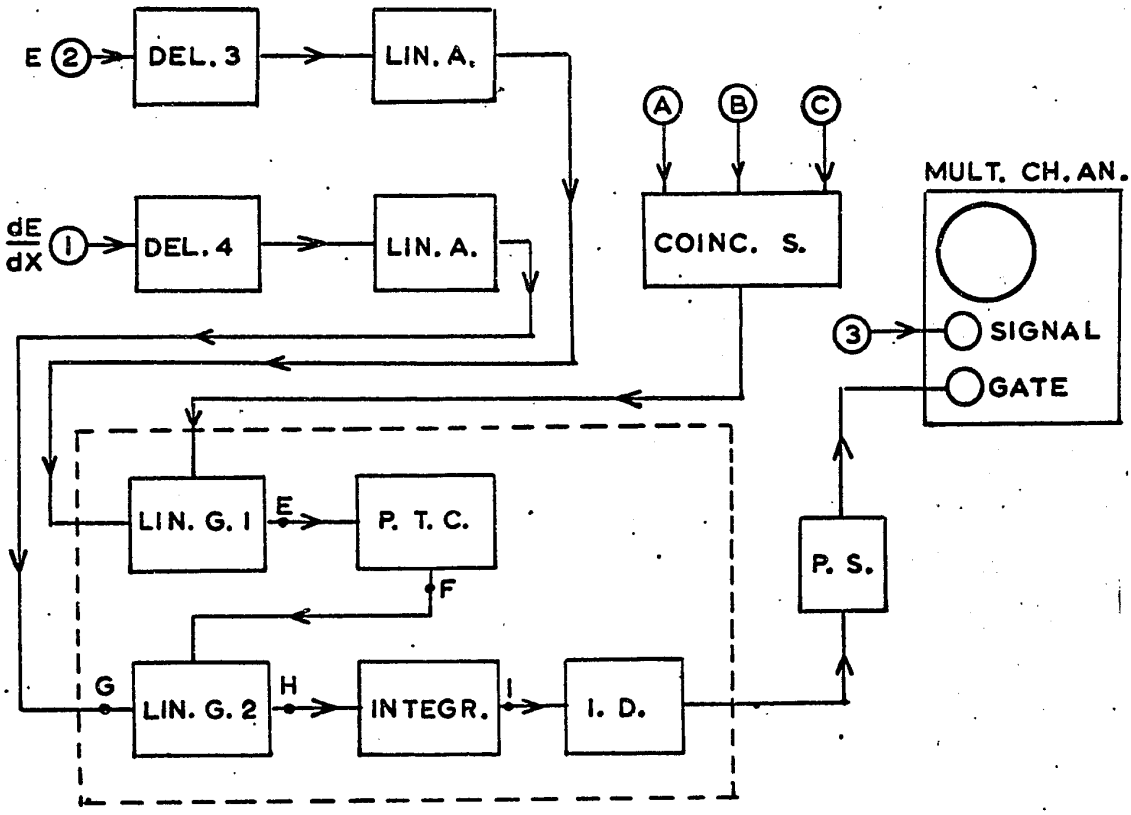

LIN. G. 1,2 : LINEAR GATE 1 AND 2
MULT. CH. AN. : MULTI-CHANNEL-ANALYZER
INTEGR. : INTEGRATOR
P. T. C. : PULSE HEIGHT TO TIME CONVERTER
COINC. S. : COINCIDENCE SYSTEM
① ② ③ Ⓐ Ⓑ Ⓒ : SEE OTHER FIGURES

FIG. 6.1

PULSE PROFILES IN THE P. IDENT. SYSTEM

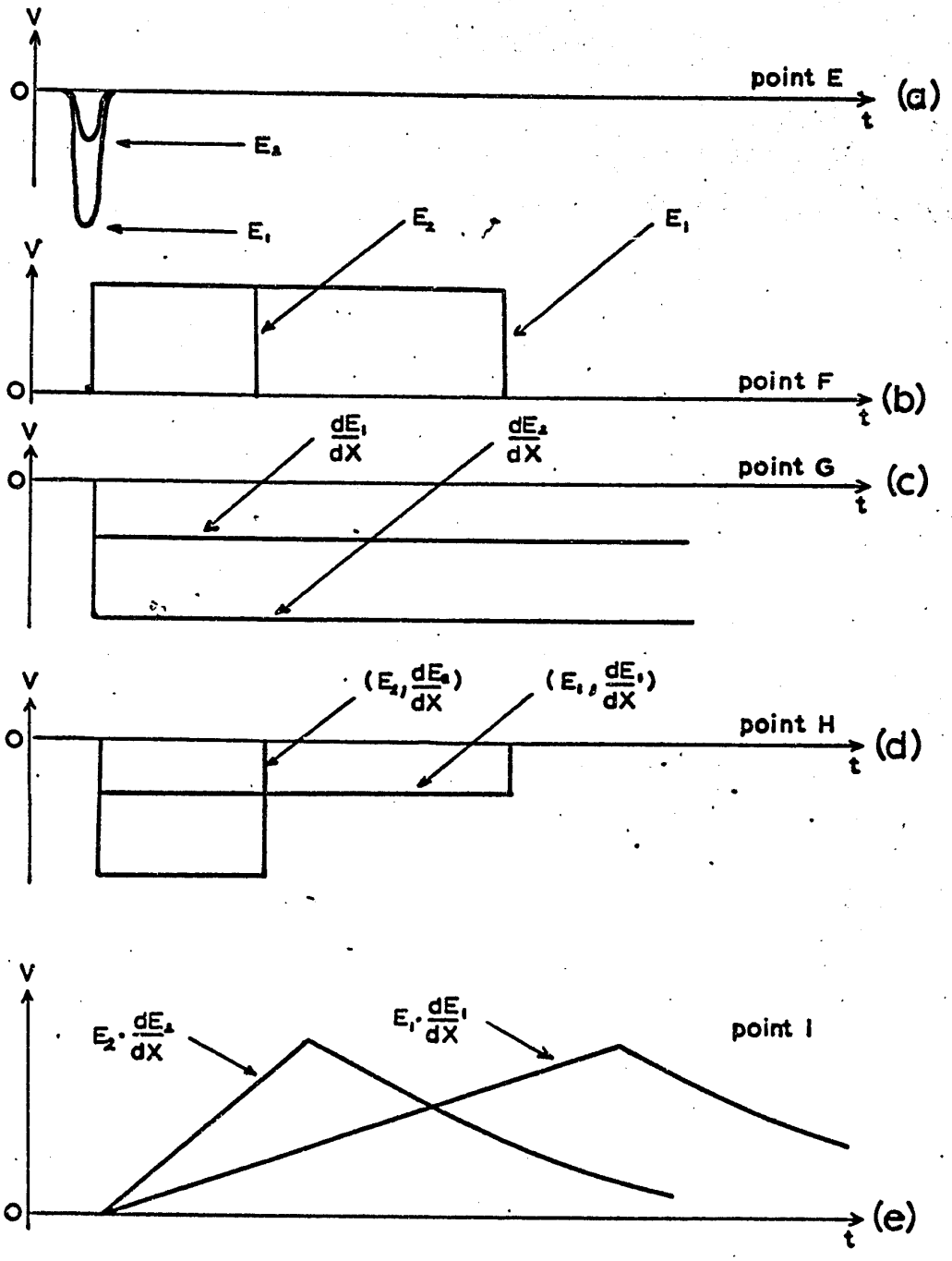

E, F, G, H AND I REFER TO FIG. 6.1

FIG. 6.2

6.3 The circuitry of the identifier .

6.3.1 The delay line circuits .

Delay line circuits 3 and 4 in Fig. 6.1 were 3 μsec delays incorporated in an amplifier. One of the two circuits with a gain of about 4 is shown in Fig. 6.3.

6.3.2 The linear amplifiers .

The linear amplifiers increased the level of the E and dE/dx signals further. One of them is shown in Fig. 6.4.

6.3.3 The pulse height to time converter .

The PTC is shown in Fig. 6.5. The E-counter signal is transformed into a pulse with linear decay. The time taken by the pulse to return to the base line is then porportional to the input amplitude. The linear decay is achieved by letting the input pulse at K charge capacitor C to a negative voltage ΔV. After disappearance of the input signal, both diodes D_1 and D_2 are backbiased and C discharges through R towards the supply voltage Vo (+30V). D_2 prevents the upper plate of C from going positive.

If $\frac{|\Delta V|}{Vo} \ll 1$ the discharge is essentially linear

between ΔV and ground. A cathode follower couples the signal with linear decay to the next stage. Fig. 6.6 a) and b) show the waveforms observed at K and L. The pulses at L are further amplified. The larger pulses exceed the dynamic range of the stage (Fig. 6.6c), but this is of no consequence since the base line recovery time is the quantity of interest. T_2 has a large collector load and the pulses on its base are transformed into square waves having the same width at their base as the signal at M (Fig. 6.6d). After polarity inversion the time analogues of the E-counter signals act as triggers for linear gate 2.

6.3.4 The integrator.

The operational integrator is shown in Fig. 6.7. Chase shows that nearly all of the input charge appears on the feedback capacitor C and that the voltage at the emitter of T_2 is approximately $\frac{Q}{C}$ (Chase 1961 B).

6.3.5 The integral discriminator.

The schematic diagram of the integral discriminator which follows the integrator is shown in Fig. 6.8.

6.3.6 The linear gates.

Linear gates 1 and 2 are nearly identical designs (Gabriel 1961). The schematic diagram is shown in Fig. 6.9.

6.4 The complete electronic system.

In Fig. 6.10 the electronic system is shown in its entirety. The neutron monitor circuitry which is completely self contained has not been included.

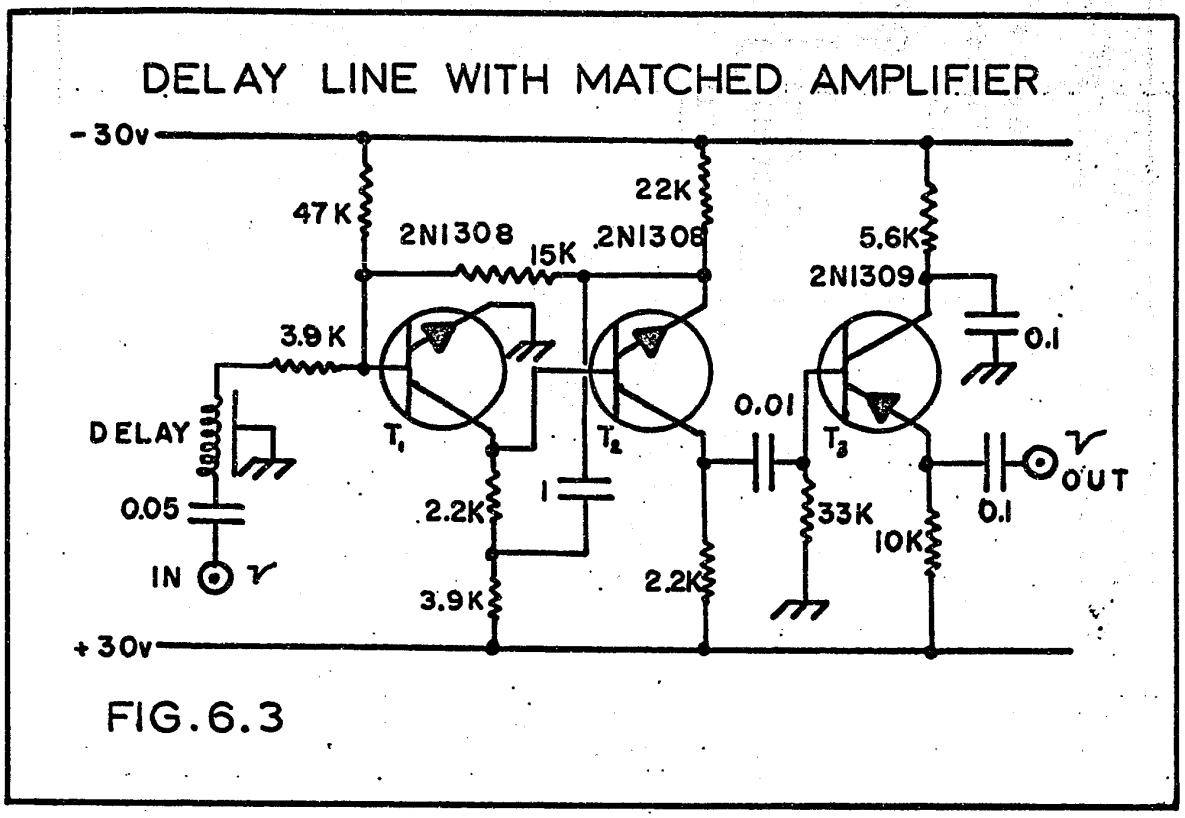
DELAY LINE WITH MATCHED AMPLIFIER
-30v
47K
2N1308
15K
2N1308
22K
5.6K
2N1309
3.9K
0.1
DELAY
T1
T2
T3
0.01
0.05
2.2K
1
33K
0.1
OUT
IN
10K
3.9K
2.2K
+30v

FIG.6.3

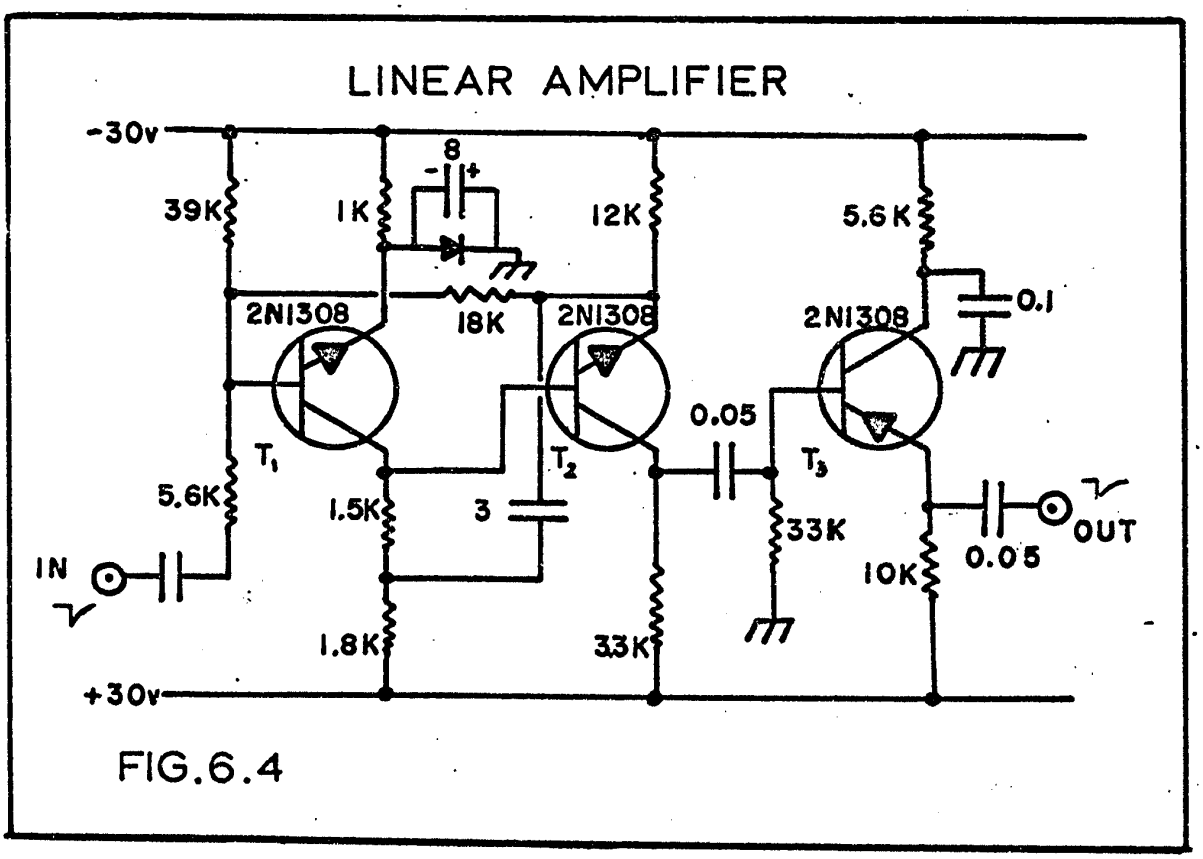
LINEAR AMPLIFIER
-30v
8
39K
1K
12K
5.6K
2N1308
18K
2N1308
2N1308
0.1
T1
T2
T3
0.05
5.6K
1.5K
3
33K
0.05
OUT
IN
10K
1.8K
33K
+30v

FIG.6.4

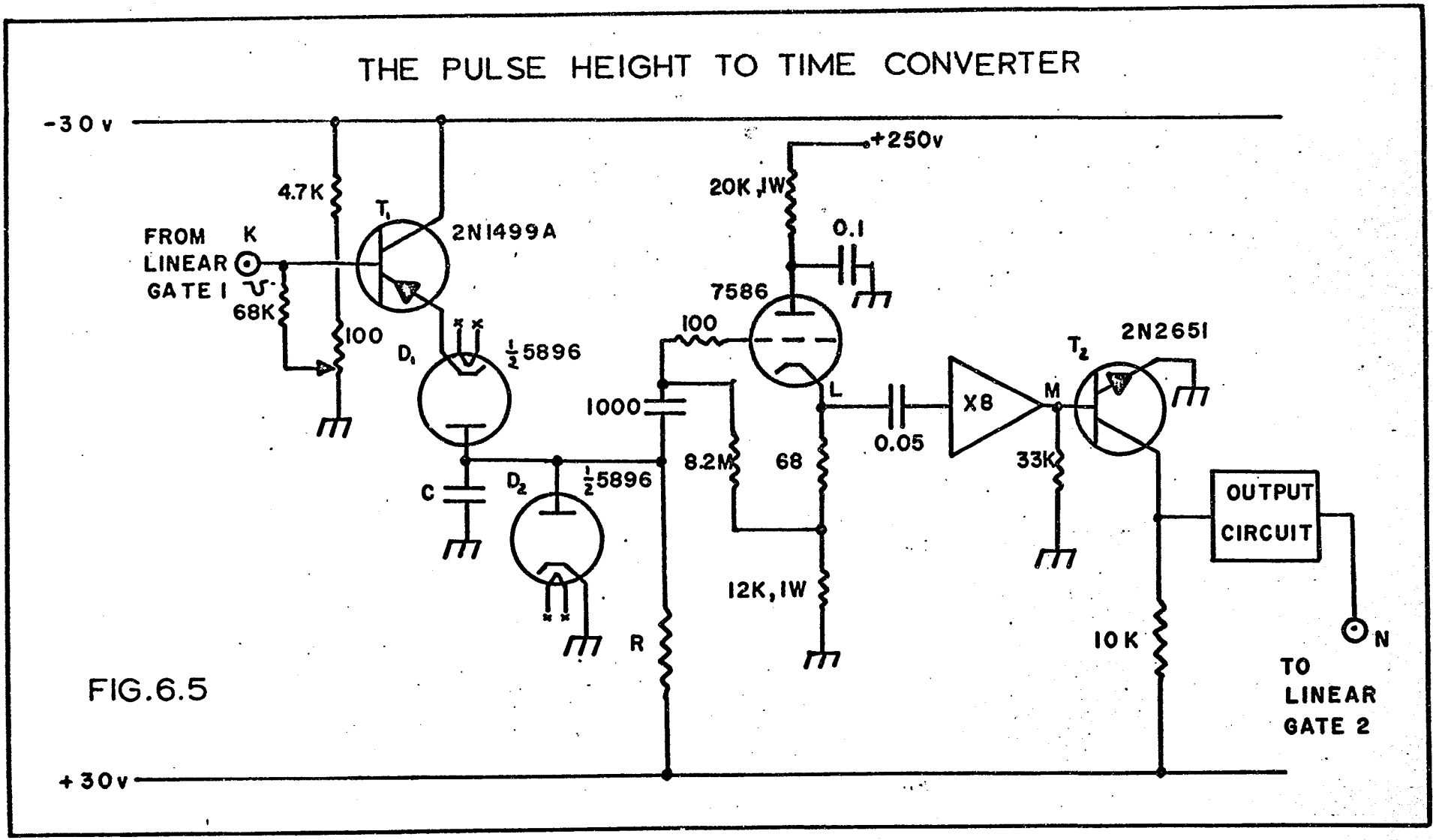
THE PULSE HEIGHT TO TIME CONVERTER
-30 v
+30v
+250v
4.7K
T1
2N1499A
FROM LINEAR GATE 1
K
68K
100
D1
½5896
C
D2
½5896
R
1000
20K, 1W
0.1
7586
100
L
0.05
X8
M
T2
2N2651
8.2M
68
33K
12K, 1W
10K
OUTPUT CIRCUIT
N
TO LINEAR GATE 2

FIG.6.5

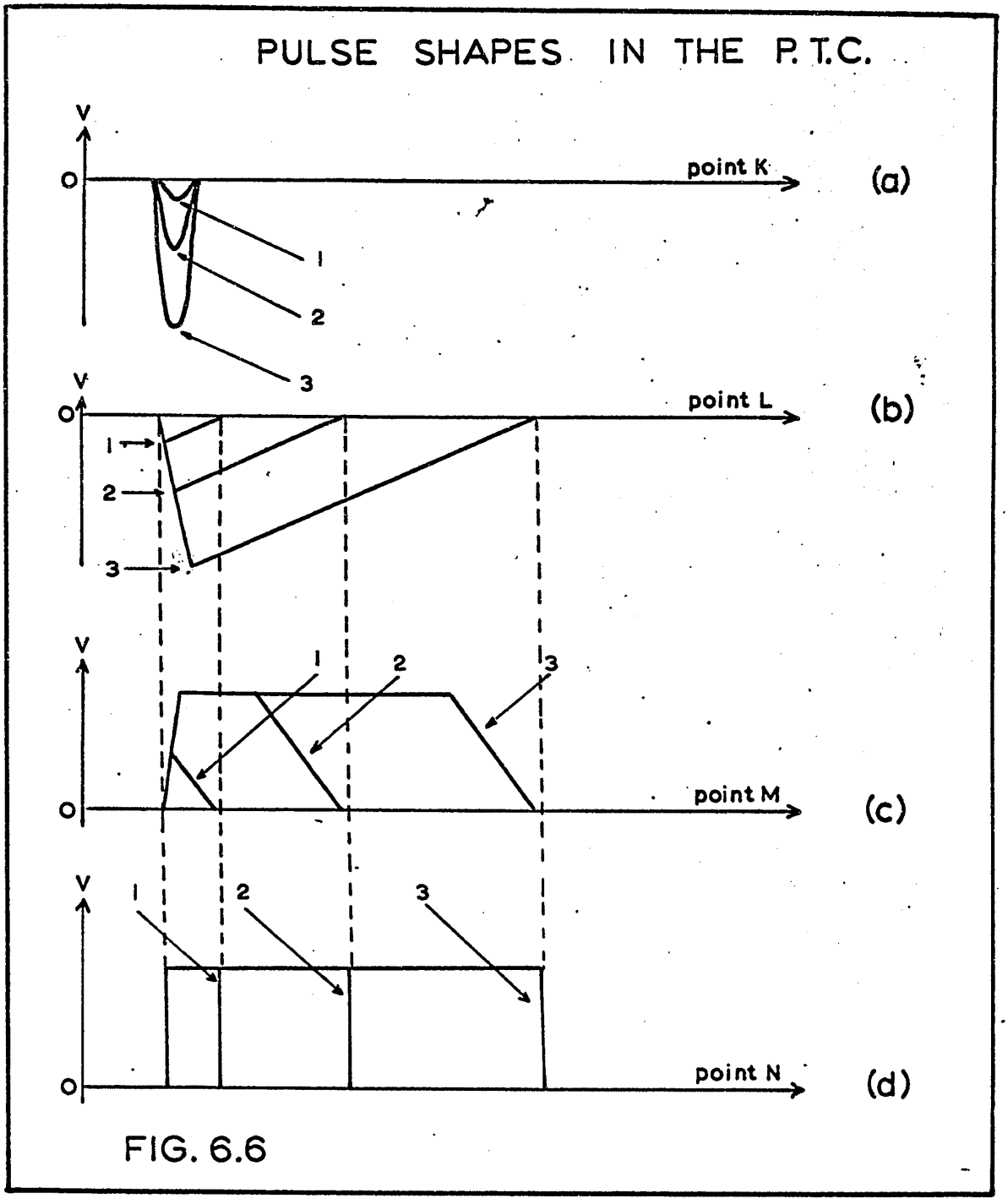
PULSE SHAPES IN THE P.T.C.
V
O
point K
(a)
1
2
3
V
O
point L
(b)
1
2
3
V
O
1
2
3
point M
(c)
V
O
1
2
3
point N
(d)

FIG. 6.6

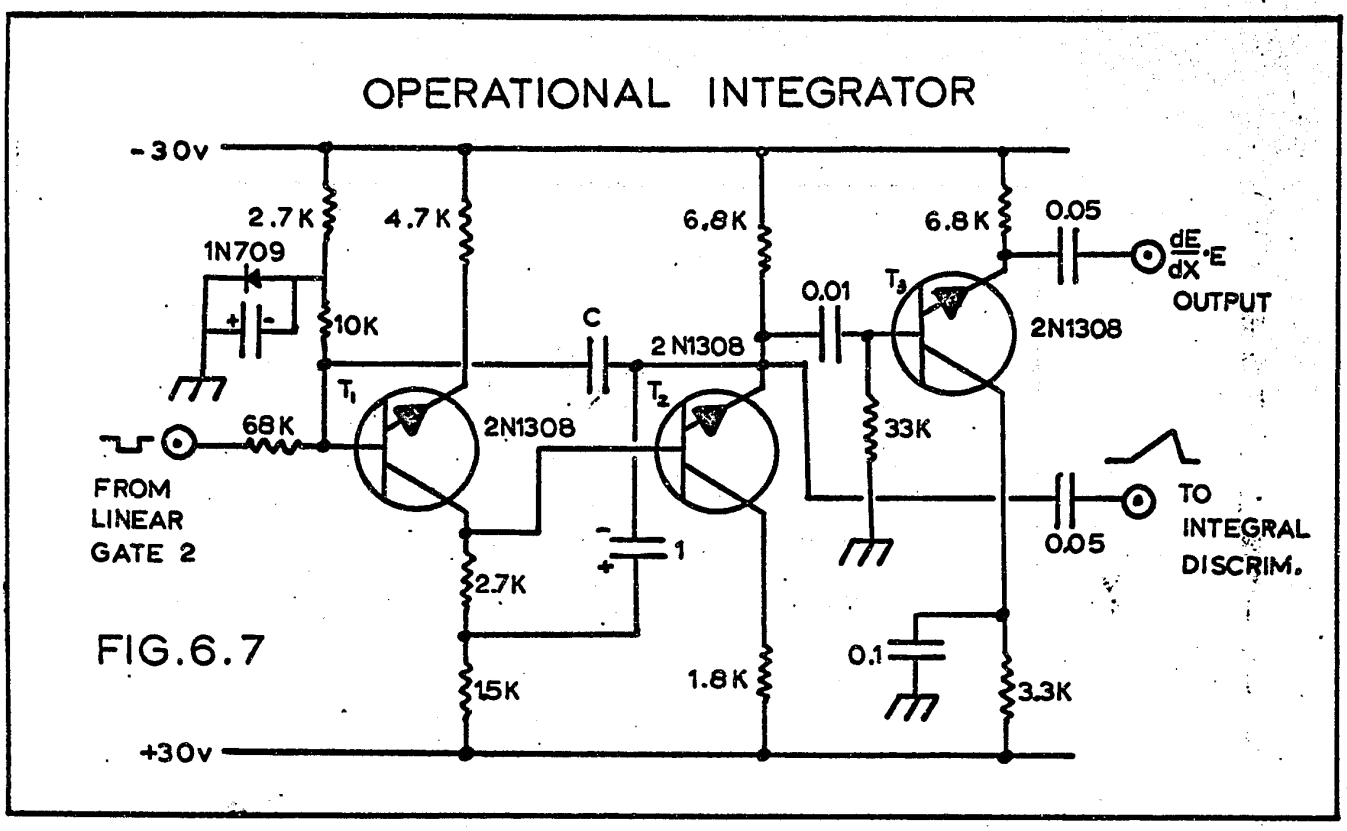
OPERATIONAL INTEGRATOR
-30v
2.7K
4.7K
6.8K
6.8K
0.05
1N709
10K
C
2N1308
0.01
2N1308
OUTPUT
68K
2N1308
33K
FROM
LINEAR
GATE 2
0.05
TO
INTEGRAL
DISCRIM.
2.7K
1
0.1
15K
1.8K
3.3K
+30v

FIG.6.7

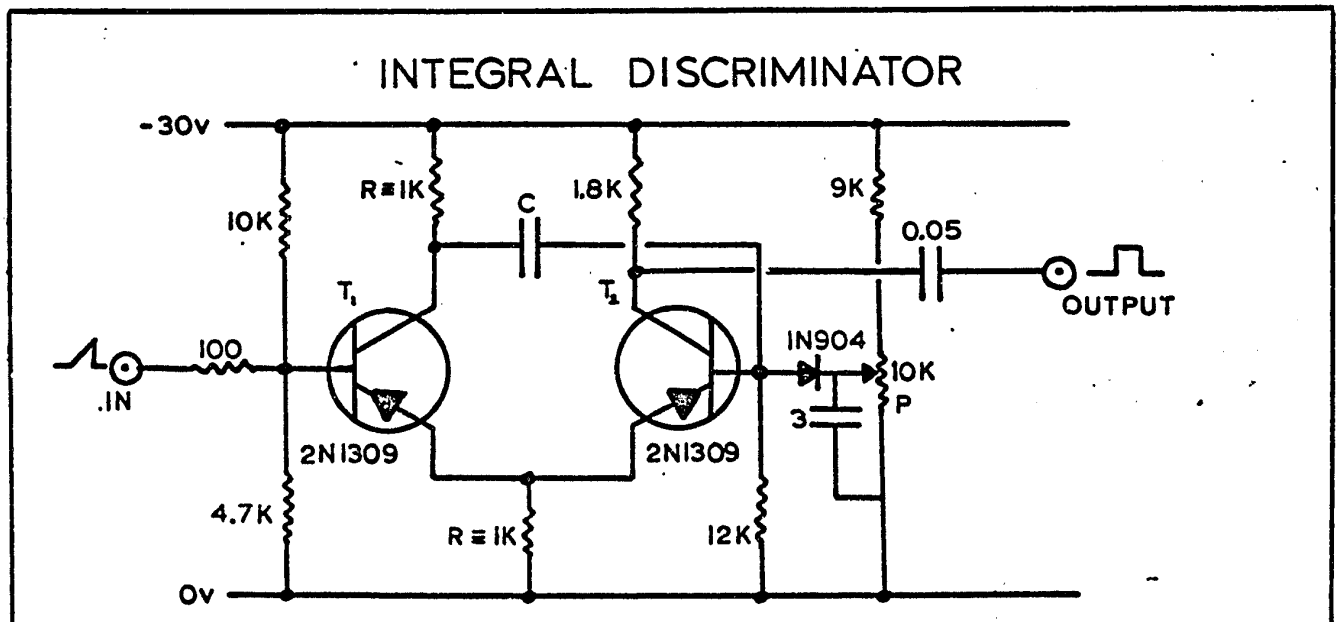
INTEGRAL DISCRIMINATOR
-30v
R=1K
C
1.8K
9K
10K
0.05
OUTPUT
100
IN904
10K
P
.IN
3
2N1309
2N1309
4.7K
R=1K
12K
0v

FIG.6.8

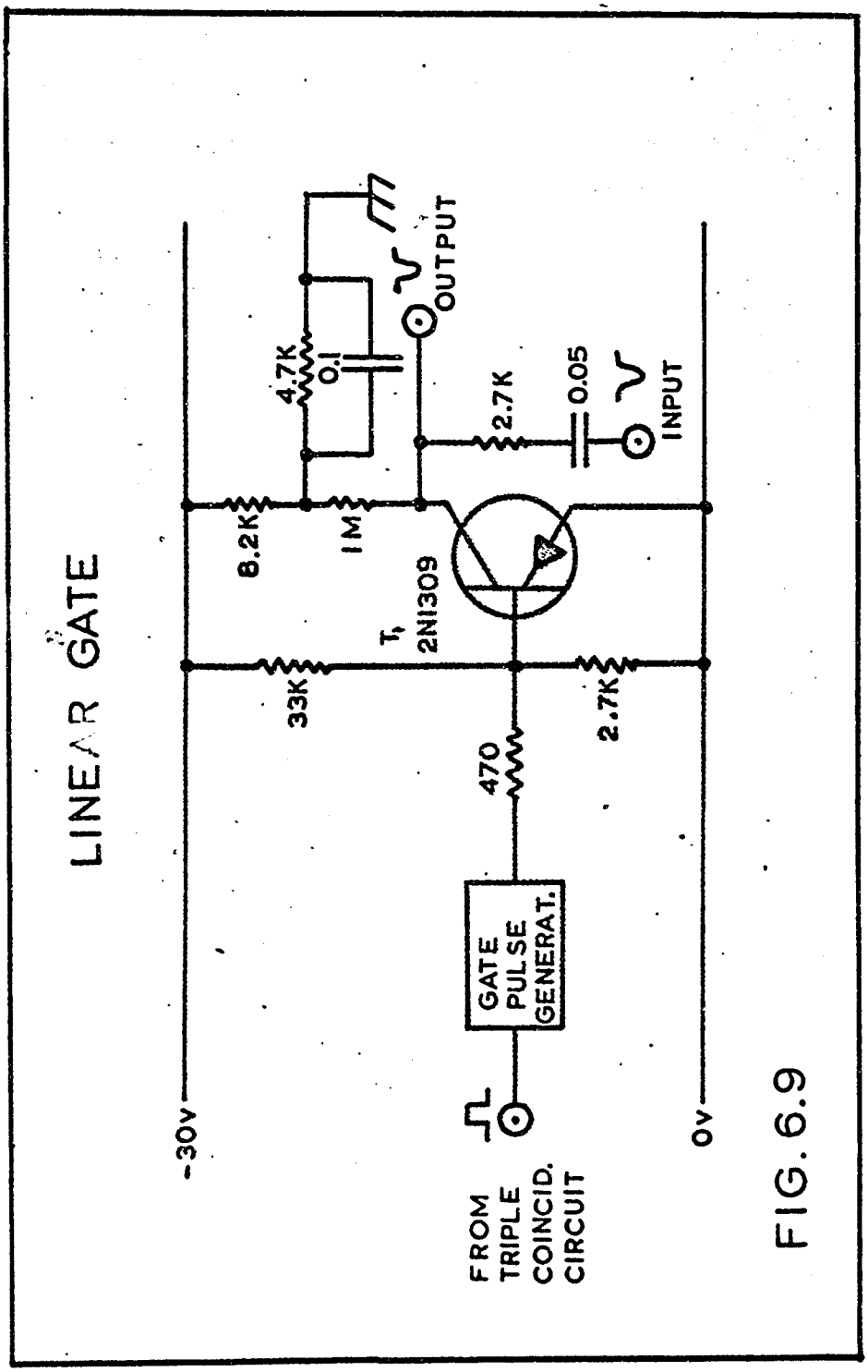
LINEAR GATE
-30v
0v
8.2K
1M
4.7K
0.1
OUTPUT
2.7K
0.05
INPUT
T1
2N1309
33K
2.7K
470
GATE PULSE GENERAT.
FROM TRIPLE COINCID. CIRCUIT

FIG. 6.9

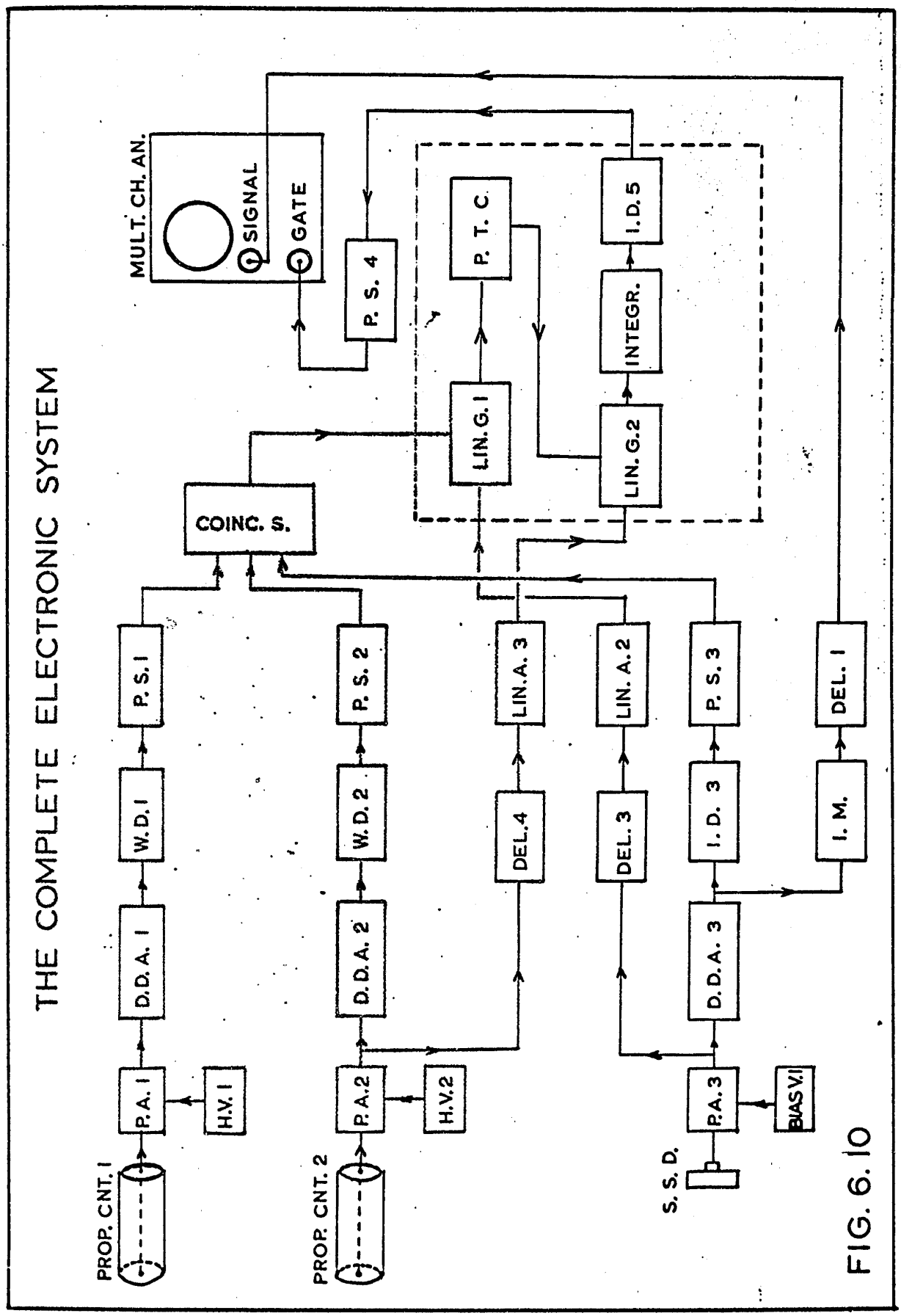
THE COMPLETE ELECTRONIC SYSTEM
MULT. CH. AN.
SIGNAL
GATE
P. S. 4
P. T. C.
I.D.5
INTEGR.
LIN. G.1
LIN. G.2
COINC. S.
P. S. I
W.D. I
D.D.A. I
P.A. I
H.V. I
PROP. CNT. I
P. S. 2
W.D. 2
D.D.A. 2
P.A.2
H.V.2
PROP. CNT. 2
LIN. A. 3
DEL. 4
LIN. A. 2
DEL. 3
P. S. 3
I. D. 3
D.D.A. 3
P.A.3
BIAS V.I
S. S. D.
DEL. I
I. M.

FIG. 6. 10

VII - THE DETERMINATION OF CROSS SECTIONS

The calculation of the cross section from the observed counting rate depends both on geometric factors and on the angular distribution of the reaction. The appropriate expressions are developed below for two cases - an isotropic angular distribution and an arbitrary distribution. The first calculation, for the isotropic distribution, will illustrate the way in which the geometrical factors have been computed and the second calculation will show the natural extension to any arbitrary angular distribution.

This is followed by a discussion in section 7.4 of the inherent energy resolution of the apparatus and of the effect of the geometry and the angular resolution on the peak profile.

7.1 The reaction products are distributed isotropically.

7.1.1 The cross section formula.

From N_n, the total number of neutrons produced in the tritium target and from N_α, the number of alpha particles that have been detected, the cross section σ for the (n, α) reaction can be deduced. Fig. 7.1 a will be helpful in relating these three quantities.

If N_n neutrons are emitted isotropically by the tritium target, the sample target will intercept N_1 of them

$$N_1 = \frac{\omega_1}{4\pi} \cdot N_n \qquad (7.1)$$

ω_1 is the average solid angle subtended by the sample at the tritium target. These N_1 neutrons generate N_2 alpha particles in the sample and

$$N_2 = N_1 \frac{N_A \rho}{M} \cdot \sigma t f \qquad (7.2)$$

where

N_A : Avogadro's number

ρ : density of the sample

M : atomic mass of the sample

t : sample thickness

f : relative abundance of the isotope of interest ($0 < f \leq 1$).

σ : the reaction cross section.

One supposes here that the alpha particles are emitted isotropically from the sample. The number that will reach the semiconductor detector is:

$$N_\alpha = N_2 \frac{\omega_2}{4\pi} \qquad (7.3)$$

where ω_2 is the average solid angle subtended by the semiconductor detector at the sample.

From (7.1), (7.2) and (7.3) one finds:

$$N_\alpha = \frac{\omega_1}{4\pi} \frac{\omega_2}{4\pi} \cdot \frac{N_A \rho}{M} \cdot ft\sigma N_n \qquad (7.4)$$

If one calls $G_1 = \frac{\omega_1}{4\pi}$ and $G_2 = \frac{\omega_2}{4\pi}$ and solves (7.4) for σ :

$$\sigma = \frac{N_\alpha}{N_n} \cdot \frac{M}{G_1 G_2 N_A \rho ft} \qquad (7.5)$$

7.1.2 The choice of G_1 and G_2.

The product G_1G_2 in (7.5) is called the geometry of the experiment. The selected geometry is a compromise between contradictory requirements. If $G_1.G_2$ is large, the detection efficiency of the assembly is high, but its angular resolution becomes poor, which causes a smearing out of the peaks in the alpha spectrum. The product G_1G_2 is also limited by practical considerations.

i) the need for cooling of the tritium target requires a minimum distance between the latter and the sample. This

sets an upper limit to G_1.

ii) two proportional counters must be accommodated between the sample and the semiconductor detector. This sets an upper limit to G_2.

7.1.2 The evaluation of G_1 and G_2.

The calculation of both G_1 and G_2 reduces to the following problem: given two parallel disks of radii a and A (where a denotes the smaller of the two), if one disk emits particles uniformly and isotropically from its entire surface, what fraction of the particles will be intercepted by the other disk? In other words if a is the source and A is the receiver (Fig. 7.1b), the average solid angle subtended by A at a has to be evaluated and vice versa. Garrett has given the solution to this problem (Garrett 1954).

Let Z be the distance between the two disks and $R^2 = A^2 + Z^2$,

$$\frac{A}{R} = \sin\beta \qquad \text{and} \quad \frac{Z}{R} = \cos\beta$$

If a is the source and A the receiver then $G\ (a \rightarrow A) = K$ (7.6)

If A is the source and a the receiver then

$$G\ (A \rightarrow a) = \left(\frac{a}{A}\right)^2 K \qquad (7.7)$$

$$K = \frac{1}{2}\left[1 - \cos\beta + 2\sin^2\beta \sum_{n=2,4,\ldots}^{\infty} \frac{P_n(o)}{n(n+2)} P'_n(\cos\beta)\left(\frac{a}{R}\right)^n\right] \tag{7.8}$$

The P_n and P'_n are the Legendre polynomials and their first derivatives.

The quantities G (a → A) and G (A → a) can in principle be computed from equations (7.6), (7.7), and (7.8). In an appendix (section A1) it is shown, however, that the G's can be correlated with the mutual inductance of a solenoid and a coaxial circular filament. This analogy yields the following simple equations.

$$G(a \to A) = \frac{1}{2}(1 - Q_o \cos\beta) \tag{7.9}$$

$$G(A \to a) = \frac{1}{2}\alpha^2(1 - Q_o \cos\beta) \tag{7.10}$$

where $\alpha = \frac{a}{A}$, $Q_o = Q_o(\alpha, \rho^2)$ and $\rho = \sin\beta$

The values of Q_o are tabulated (Grover 1946) and can be obtained through interpolation. In this way the summation of series (7.8) can be avoided.

7.2 The reaction products are not isotropically distributed.

In general the measured yield of a reaction in an element of solid angle dΩ is given by:

$$\frac{dN_\alpha}{d\Omega} = \frac{N_A \rho}{M} \text{ ft } N_n \frac{d\sigma}{d\Omega} \eta(\theta) \qquad (7.11)$$

where η (θ) is the detection efficiency at an angle θ with respect to the path of the incoming neutron, and $\frac{d\sigma}{d\Omega}$ is the differential cross section. If the distribution of reaction products is not isotropic, the number of particles emitted in various directions is not the same, and they are detected with different efficiencies because η is a function of θ.

Expression (7.5) which is based on the calculation of the average solid angle becomes invalid and (7.11) has to be integrated formally.

In the present geometrical arrangement one has:

$$\begin{aligned} 0 < \eta\ (\theta) < 1 \quad & \text{for } \theta < \theta_1 \\ \eta\ (\theta) = 0 \quad & \text{for } \theta \geq \theta_1 \end{aligned} \qquad (7.12)$$

and the value of θ_1 can be easily deduced from the geometry.

Integrating (7.11) over θ and ϕ one obtains

$$N_\alpha = \frac{N_A \rho}{M} \text{ ft } N_n \int_0^{\pi} d\theta \int_0^{2\pi} d\phi \frac{d\sigma}{d\Omega} \eta\ (\theta) \sin\theta \qquad (7.13)$$

where N_α is the total alpha particle yield.

$$N_\alpha = \frac{N_A \rho}{M} \cdot ftN_n 2\pi \int_0^\pi \frac{d\sigma}{d\Omega} \cdot n(\theta) \sin\theta d\theta \qquad (7.14)$$

To integrate (7.14) further one must either know the angular distribution or assume a plausible distribution

$$\frac{d\sigma}{d\Omega} = k\phi(\theta) \qquad (7.15)$$

where k is a scaling factor.

But $n(\theta) = o$ for $\theta > \theta_1$ and, therefore,

$$N_\alpha = \frac{N_A \rho}{M} ftN_n 2\pi k \int_0^{\theta_1} \phi(\theta) n(\theta) \sin\theta d\theta \qquad (7.16)$$

Solving equation (7.16) for k and substituting into (7.15) yields

$$\frac{d\sigma}{d\Omega} = \frac{N_\alpha \phi(\theta)}{\frac{N_A}{M} \rho ftN_n 2\pi \cdot \int_0^{\theta_1} \phi(\theta)\, n(\theta) \sin\theta d\theta} \qquad (7.17)$$

$$\sigma(\theta)d\theta = \frac{M}{N_A \rho ft} \cdot \frac{N_\alpha}{N_n} \frac{\phi(\theta) \sin\theta d\theta}{\int_0^{\theta_1} \phi(\theta)\, n(\theta) \sin\theta d\theta} \qquad (7.18)$$

If one wants to use the assumed angular distribution only over the range for which the reaction yield is observed experimentally, then:

$$\int_0^{\theta_1} \sigma(\theta)d\theta = \frac{M}{N_A \rho f t} \cdot \frac{N_\alpha}{N_n} \cdot \frac{\int_0^{\theta_1} \phi(\theta) \sin\theta d\theta}{\int_0^{\theta_1} \phi(\theta) n(\theta) \sin\theta d\theta} \qquad (7.19)$$

If the assumed angular distribution is accepted for the full range of θ (from o to π in the laboratory system), then:

$$\sigma = \int_0^{\pi} \sigma(\theta)d\theta = \frac{M}{N_A \rho f t} \frac{N_\alpha}{N_n} \frac{\int_0^{\pi} \phi(\theta) \sin\theta d\theta}{\int_0^{\theta_1} \phi(\theta) n(\theta) \sin\theta d\theta} \qquad (7.20)$$

If the reaction products are distributed isotropically

$\frac{d\sigma}{d\Omega} = k$ and (7.20) becomes

$$\sigma = \frac{M}{N_A \rho f t} \frac{N_\alpha}{N_n} \frac{\int_0^{\pi} \sin\theta d\theta}{\int_0^{\theta_1} n(\theta) \sin\theta d\theta} = \frac{M}{N_A \rho f t}$$

$$\times \frac{N_\alpha}{N_n} \cdot \frac{2}{\int_0^{\theta_1} n(\theta) \sin\theta d\theta} \qquad (7.21)$$

Putting $G = \frac{1}{2} \int_0^{\theta_1} n(\theta)\sin\theta d\theta$ and substituting in (7.21)

yields $$\sigma = \frac{N_\alpha}{N_n} \cdot \frac{M}{N_A \rho f t\, G} \qquad (7.22)$$

(7.22) is identical to (7.5) with $G = G_1 G_2$ as expected.

7.3 The determination of $n(\theta)$.

7.3.1 Introduction.

The problem is the following:

N neutrons are emitted from the source having radius R_1. (Fig. 7.1C). The source emits isotropically and uniformly over its entire surface. In the hypothesis that every neutron which hits the sample target (radius R_2) produces an alpha particle making an angle θ_o with the direction of the incident neutron, what will be the ratio $n(\theta) = \frac{N_1}{N}$, where N_1 is the number of alpha particles that hit the detector having radius R_3. The source to sample and sample to detector distances are d_1 and d_2 respectively.

The analytic solution of this problem presents serious difficulties. No simplifying assumptions can be introduced because the radii of the various apertures are of the same order of magnitude as the distances that separate them.

DETERMINATION OF THE GEOMETRY

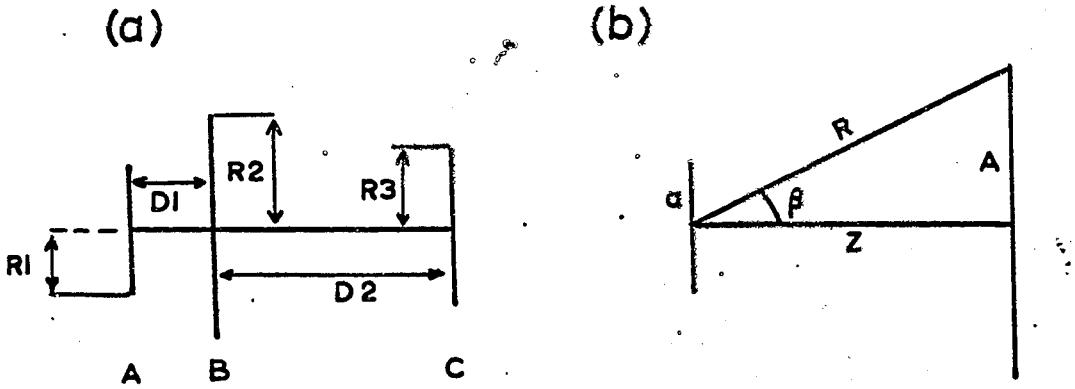

A : TRITIUM TARGET

B : SAMPLE TARGET

C : SEMICONDUCTOR DETECTOR

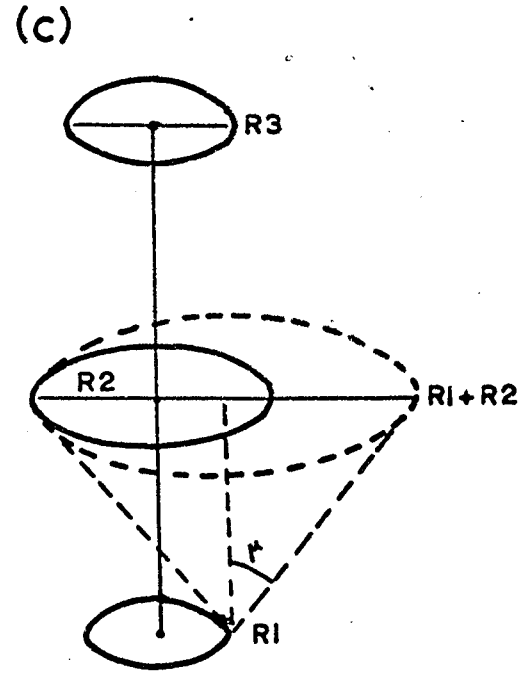

FIG. 7.1

It was, therefore, decided to solve the problem by means of a Monte Carlo type calculation. This is equivalent to carrying out an imaginary experiment.

7.3.2 The Monte Carlo procedure.

By means of a random number generating subroutine in the computer, a point is selected on the disk of radius R_1 from which a neutron is supposed to be emitted. Two random numbers are needed to fix the coordinates (x_1, y_1, o) of that point. The neutron emission being isotropic, two new random numbers are needed to fix the three direction cosines (u_1, v_1, w_1) of that neutron. Next one checks whether the neutron hits or misses the sample. If it misses it is abandoned and a new source neutron is selected. If it hits one generates a line passing through the impact point (x_2, y_2, d_1), making an angle θ_o with the incident neutron direction, but otherwise randomly oriented. The latter is the most difficult step in the procedure. An elegant solution is suggested by Cashwell and Everett (Cashwell 1959). One random number is needed to find the direction cosines (u_2, v_2, w_2). One has to verify finally that the line through (x_2, y_2, d_1) with the aforementioned direction cosines strikes the detector aperture. If N is the total number of

source neutrons processed and N_1 the number of alpha particles that strike the detector, $\eta(\theta) = \frac{N_1}{N}$ is the desired quantity.

A lot of computer time will be wasted in letting the neutron source be isotropic in all space. Clearly, neutrons proceeding towards the hemisphere pointing away from the detector cannot hit the sample. Closer examination of Fig. 7.1C shows that the only neutrons that can possibly hit the sample are those comprised within the solid angle of aperture μ, perpendicular to the source and pointing towards the detector. The apex of this cone can of course be any point of the neutron source. Actually, any neutron emitted in this solid angle has a good chance of hitting the sample, and this results in a tremendous economy of computer time. If $(\frac{N_1}{N})_R$ is the ratio for all space and $(\frac{N_1}{N})_o$ the ratio for source neutrons which are restricted to the solid angle μ (expressed in steradians), then

$$(\frac{N_1}{N})_R = (\frac{N_1}{N})_o \frac{\mu}{4\pi} \qquad (7.23)$$

and $$\frac{\mu}{4\pi} = \frac{1}{2}\left(1 - \frac{d_1}{\sqrt{(R_1+R_2)^2 + d_1^2}}\right)$$

Fig. 7.2 shows the graph for $\eta(\theta)$ versus θ which is obtained by repeating the above procedure for various values of θ_o. 10^5 source neutrons were processed for each point.

7.3.3 Verification of the result.

Monte Carlo programs are notoriously difficult to check for errors. The validity of the present calculation was checked in two ways:

a) When $\theta = o$, $\eta(\theta)$ is the average solid angle subtended by the semiconductor detector at the neutron source. This quantity can be calculated by the method of section 7.1.3, which yields $\eta(o) = 6.58 \times 10^{-3}$. The Monte Carlo procedure gives $\eta(o) = 6.47 \times 10^{-3}$, the agreement being better than 2%.

b) When the integral $G = \frac{1}{2} \int_o^{\theta_1} \eta(\theta) \sin\theta \, d\theta$ from section 7.2 is evaluated, the result should be identical to that obtained by the method described in section 7.1.3. Numerical integration yields $G = 1.00 \times 10^{-3}$, whereas the product of the two average solid angles yielded the same numerical value up to 3 significant figures.

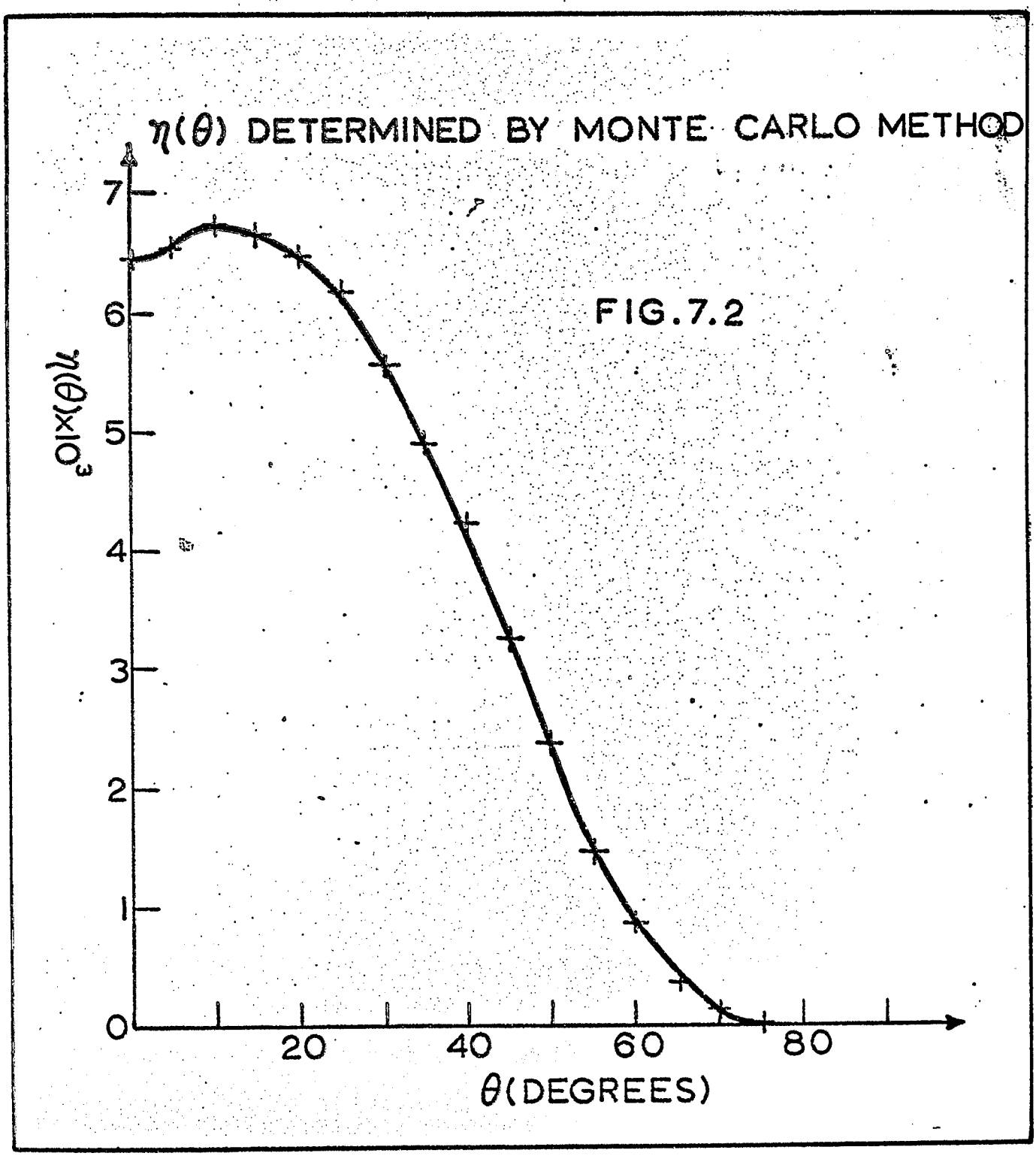
η(θ) DETERMINED BY MONTE CARLO METHOD
FIG. 7.2
ε Ω I × (θ) μ
0
1
2
3
4
5
6
7
20
40
60
80
θ (DEGREES)

7.4 The process of peak formation.

7.4.1 Factors determining the pulse profile.

Definite line widths are associated with the various peaks in the experimental spectra. The factors contributing to the line profile will be examined and the theoretical line width will be calculated for a specific case. The results will show whether useful information can be extracted from the observed line profiles.

In a "good geometry" experiment three factors account for the line profile:

i) counter resolution

ii) target thickness

iii) different path lengths of the alpha particles in the counter gas.

In a "bad geometry" experiment two other causes of energy spread have to be added:

iv) the energy of the alpha particle is a function of the angle of deviation θ between incoming and outgoing projectiles.

v) the detection efficiency of the system is a function of θ.

Through iv) and v) the observed line shape depends in a complex manner on the geometry. The effect of iv) is important

for lighter nuclei.

7.4.2 Calculation of the line profile for the ground state transition in the reaction $^{58}Ni\ (n, \alpha)^{55}Fe$.

The Monte Carlo method provides a convenient tool for calculating the line shape. The calculation is carried out assuming an isotropic distribution of the reaction products. The energy spread due to geometry, kinematics and finite target thickness is calculated first. In the program a series of random numbers (R_1, R_2, ..., R_n) is generated. R_1 selects the angle of deviation between alpha and neutron, which at the same time fixes the energy of the former. The curve $n(\theta)$ versus θ determined in section 7.3.2, is a probability distribution for the detection of alpha particles as a function of θ. By means of R_2 and this distribution, one decides whether the alpha particle is detected or not. If not, it is immediately discarded. If yes, the value of R_3 decides from which depth in the target it was emitted and the energy loss in the target is calculated (one supposes for this calculation that all paths are parallel to the symmetry axis of the apparatus). The final energy of the particle is recorded in 150 "counters" which are set up in the computer each covering a 20 keV interval. The result is presented as a multi-channel

analyser spectrum. Fig. 7.3 shows this energy distribution, which will be referred to as Spectrum 1. Spectrum 1 is used as input to a new random walk program which will calculate the energy loss in the proportional counter gas and evaluate the contribution of the semiconductor noise to the total line width. For each alpha particle which is selected from Spectrum 1 by means of a random number, the energy loss in the counter gas is computed and by means of a second random number, a noise pulse is added to the "signal". The noise pulse is extracted from a normal distribution stored in the computer memory. The standard deviation of this distribution was obtained from an actual semiconductor detector spectrum corresponding to the ground state transition of the $^{28}Si\ (n,\ \alpha)^{25}Mg$ reaction, which exhibits a peak at 12.0 Mev. The width was extrapolated to the energy associated with the $^{58}Ni(n,\ \alpha)^{55}Fe$ ground state transition by assuming a $E^{-1/2}$ dependence of the detector resolution. The result of this calculation (Spectrum 2) must be compared with the experimental line shape.

The second random walk calculation was repeated assuming that all alpha particles are emitted with $\theta = 0^{\circ}$. This corresponds to an extremely forward peaked direct interaction.

The resultant energy distribution (Spectrum 3) should be compared with Spectrum 2. If the line width in Spectrum 3 is considerably less than in the other, some information on the angular distribution might be extracted from the peak profile. Figs. 7.4 and 7.5 show spectra 2 and 3. Table 7.1 gives the full widths at half maximum for the experimental distribution and Spectra 2 and 3.

Table 7.1

Energy distribution	FWHM (keV)
Experimental	650
Spectrum 2	685
Spectrum 3	620

The agreement between the experimental and theoretical values of the FWHM is excellent. The values for Spectra 2 and 3 are too close together to be able to draw any conclusions regarding the angular distribution.

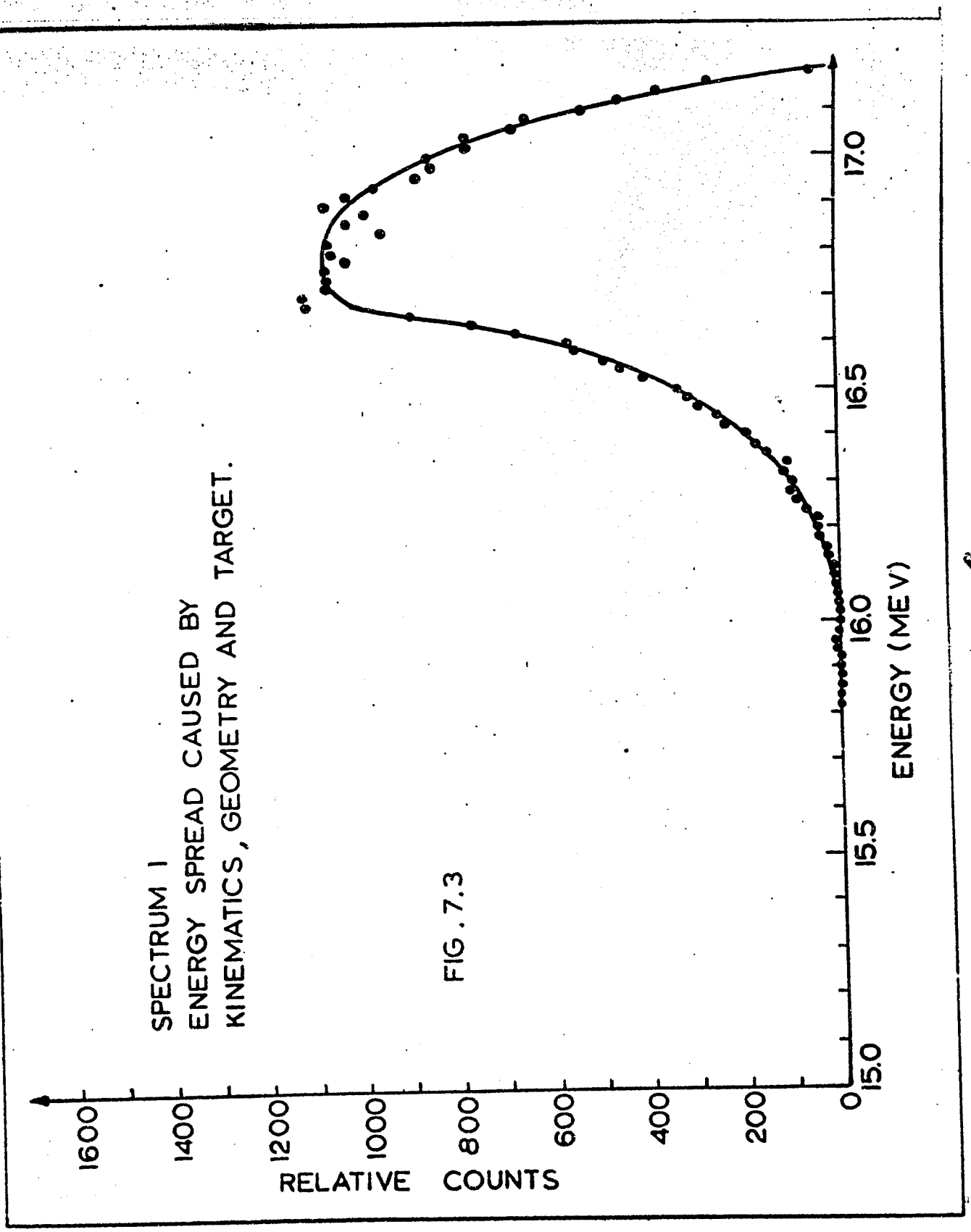
SPECTRUM 1
ENERGY SPREAD CAUSED BY
KINEMATICS, GEOMETRY AND TARGET.
RELATIVE COUNTS
ENERGY (MEV)
0
200
400
600
800
1000
1200
1400
1600
15.0
15.5
16.0
16.5
17.0

FIG. 7.3

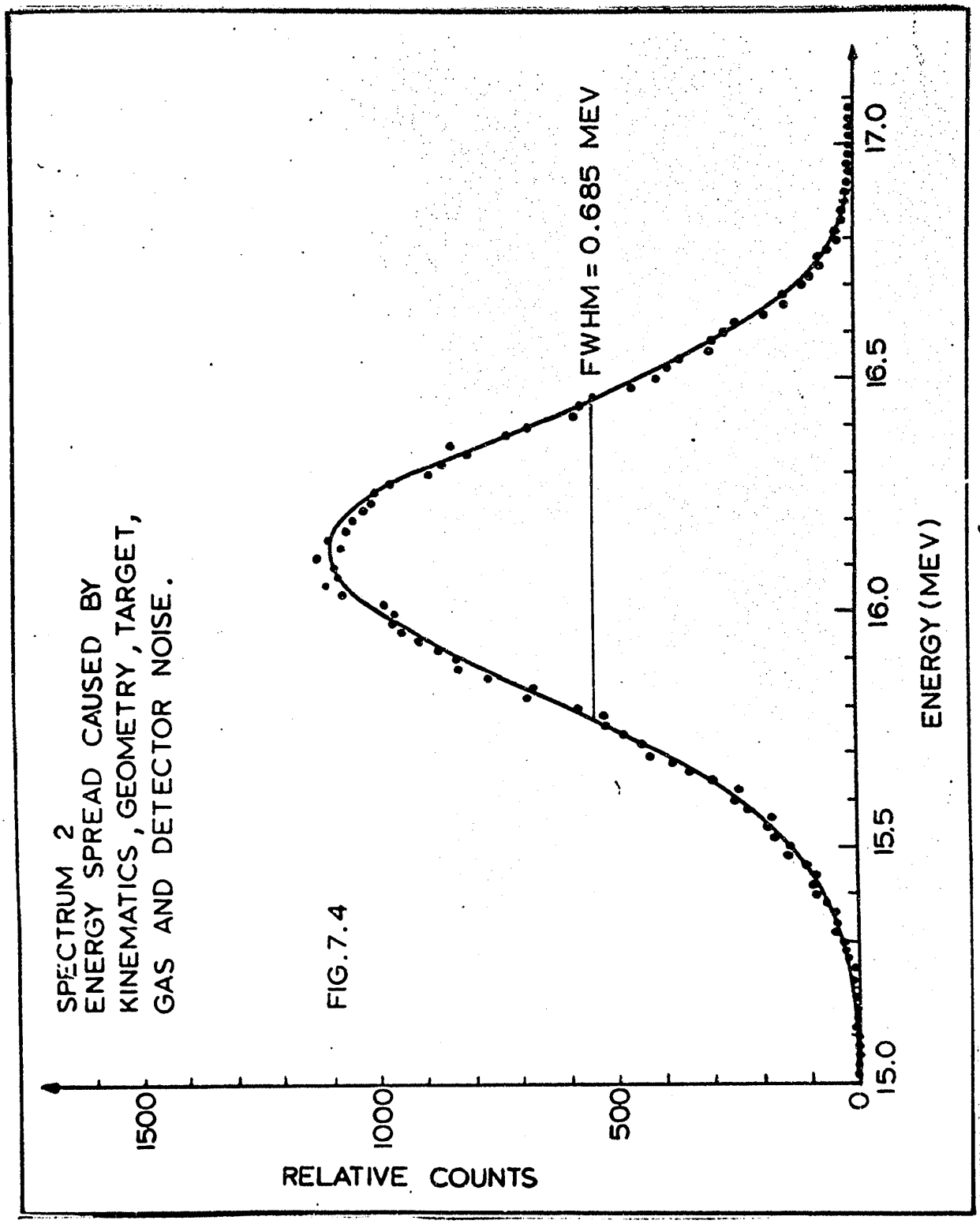
SPECTRUM 2
ENERGY SPREAD CAUSED BY
KINEMATICS, GEOMETRY, TARGET,
GAS AND DETECTOR NOISE.
FWHM = 0.685 MEV
RELATIVE COUNTS
ENERGY (MEV)
0
500
1000
1500
15.0
15.5
16.0
16.5
17.0

FIG. 7.4

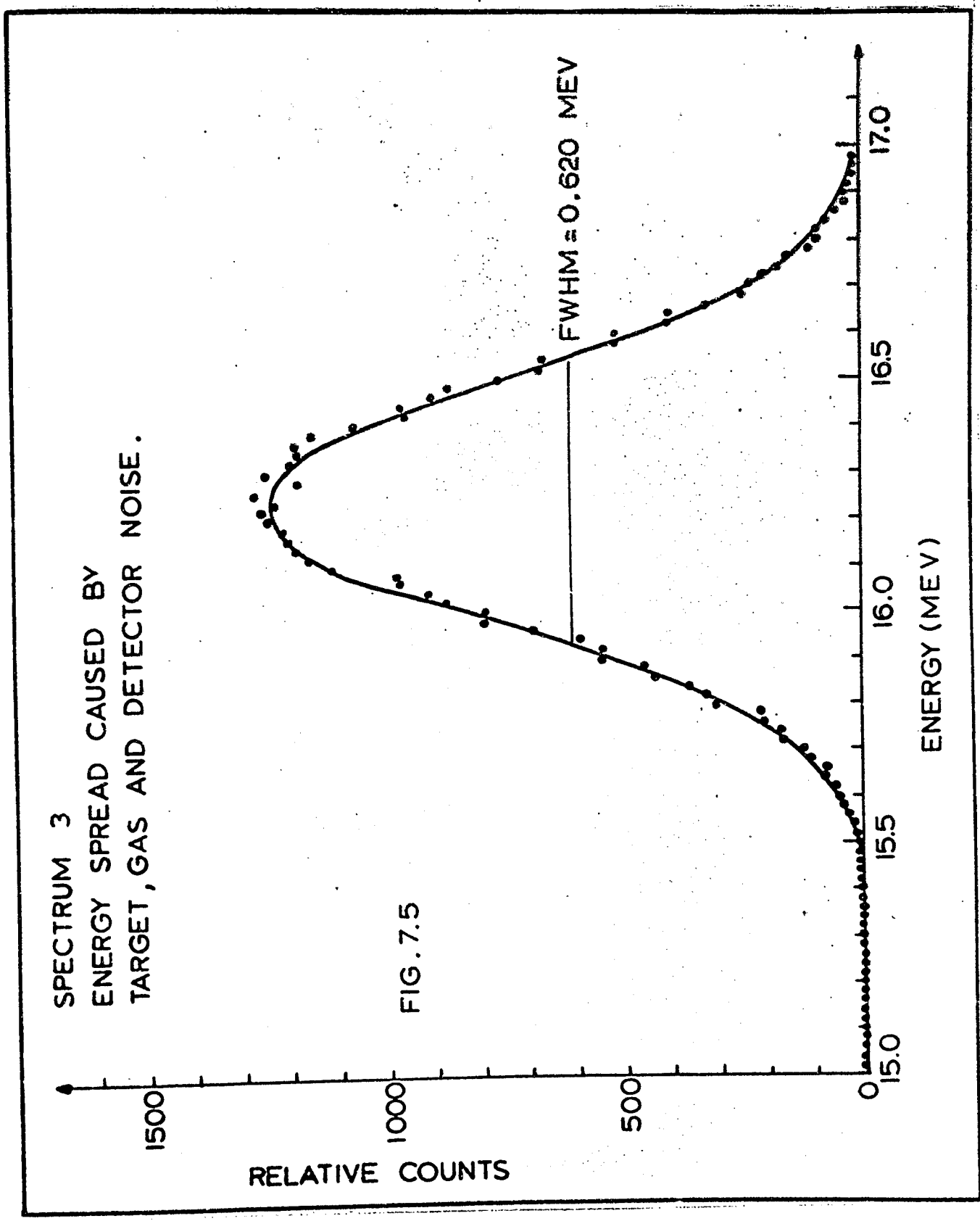
SPECTRUM 3
ENERGY SPREAD CAUSED BY
TARGET, GAS AND DETECTOR NOISE.
FWHM = 0.620 MEV
RELATIVE COUNTS
1500
1000
500
0
15.0
15.5
16.0
16.5
17.0
ENERGY (MEV)

FIG. 7.5

VIII - EXPERIMENTAL PROCEDURE

8.1 Selecting the operating conditions of the system.

Before an experiment can be carried out, the gains and bias levels in the electronic system must be adjusted such that the signals from the alpha particles of interest are properly processed. Alpha particles having energies between 12 and 25 Mev are not available in the laboratory for testing purposes. One can, however, use a 5.47 Mev ^{241}Am source for testing and work out what the behaviour of the system will be at higher energies.

8.1.1 Calibration and choice of bias levels in the proportional counter channels.

The following method was adopted to ensure that the window discriminators of the proportional counter channels were set to accept alpha particles between 12.5 and 25 Mev. An experimental chamber in which the distance between an ^{241}Am source and a solid state detector can be adjusted at will, was filled with 200mm A and 20 mm CO_2. The pulse height was recorded as a function of source detector distance. From these data and from the well known positions and dimensions of the proportional counters, it was possible to

determine the average energy loss of a 5.47 Mev alpha particle in the dE/dx counters. The results were respectively 0.400 and 0.450 Mev for the detector closest to and farthest from the source. The energy loss of 12.5, 17.0, 20.0 and 25.0 Mev alpha particles in the proportional counters has been calculated from Bethe's formula (eq.6.1). Table 8.1 shows the result. (The data measured at 5.47 Mev are also included. The 5.47 Mev values could not be calculated because Bethe's formula becomes unreliable at low velocities).

Table 8.1

Energy of alpha particle (Mev)	Energy loss in counter 1A (Mev)	Energy loss in counter 2 (Mev)
5.47	0.40	0.45
12.5	0.22	0.22
17.0	0.18	0.18
20.0	0.15	0.15
25.0	0.12	0.12

A - counter 1 is encountered first by the incident radiation.

If the pulse amplitudes in the proportional counters for 5.47 Mev alpha particles which completely traverse both counters are observed experimentally, the expected amplitudes for 12.5, 17.0, 20.0 and 25.0 Mev alpha particles can be immediately deduced from Table 8.1. The upper and lower discriminators in the proportional counter channels are set relying on Table 8.1. Conservative bias settings are nevertheless adopted, so that possible inaccuracies in the table cannot result in the loss of part of the alpha spectrum.

8.1.2 Calibration and choice of bias level in the E-counter channel.

Two convenient calibration points allow to establish an unambiguous relationship between channel number in the multichannel analyser and alpha particle energy. The first point is given by the 5.47 Mev alpha particles from a ^{241}Am source which is introduced in the vacuum chamber. The second point is obtained from the sharp peak at 12.0 Mev corresponding to the ground state transition of the ^{28}Si (n, α) ^{25}Mg reaction. This peak is easily observed when the semiconductor detector is exposed to 14.6 Mev neutrons and the multichannel analyser is allowed to accumulate the spectrum without gating precautions.

It is worth noting that the peak at 12.0 Mev is not only due to the alpha particles which leave ^{25}Mg in the ground state, but that the recoil energy of the latter nuclei also is included in the signal.

The integral discriminator of the E-counter amplification channel was set such as to cut off all alpha particles below 12.5 Mev. In this way the numerous alpha particles from the $^{28}Si(n, \alpha)^{25}Mg$ reaction do not contribute to the counting rate in the corresponding channel of the coincidence system. This reduces the random coincidence rate drastically.

8.2 The data collection.

Each experimental run consists of typically 4 spectra accumulated with the target in place, and 2 spectra with a background blank. Between successive spectra (each representing about 2 hours of irradiation), the energy calibration of the semiconductor detector and the proportional counters was checked.

8.3 The processing of data.

After completion of the experiment the spectra accumulated with the target in place were summed, and the normalized

sum of the background runs was subtracted. This was done by computer. The computer program allowed unsatisfactory spectra to be discarded.

The alpha particles that are recorded have lost energy both in the target and in the proportional counter gas. Their original energy is the quantity of interest. A computer program using Bethe's formula (equation 6.1) for the rate of energy loss of a charged particle through ionization, allowed the original energy of each group of alphas to be calculated from their observed energy. In this calculation a simplifying assumption was made: all alpha particles were supposed to originate from a depth d/2 in the target (where d is the total target thickness), and they were supposed to travel parallel to the symmetry axis of the apparatus. These energy loss calculations were checked for several isotopes and for various energies against the values predicted by the tables of Williamson and Boujot (Williamson 1966). The agreement was excellent.

IX - EXPERIMENTAL RESULTS

9.1 The alpha particle spectra.

Plots of the yield versus original alpha particle energy (in the laboratory coordinate system) are shown in Figs. 9.1 to 9.13 for 13 different targets. The following targets were also attempted, but either the yield was extremely low, or the statistical scatter of the points was so large that no structure could be seen in the high energy part of the spectrum: natural Ag, natural Sn, natural Sb, natural Pb. No plots are presented for these elements.

The alpha particle spectra will now be discussed individually by means of the figures:

Fig 9.1 natural Ni.

The ground state transition and the yield to the $7/2^-$ states at 1.322 Mev and 1.412 Mev in ^{55}Fe are clearly resolved. The latter peak is also contaminated by the ground state transition of the $^{60}Ni\ (n, \alpha)^{57}Fe$ reaction. The peak positions agree well with the locations predicted from the known Q-value of the reaction, as indicated by the arrows.

Fig. 9.2 : enriched ^{58}Ni

The counting statistics is more favorable than for the natural Ni target. Appreciable scatter can, however, be seen

in the experimental points. This is attributed to the fact that the semiconductor detector had already suffered appreciable radiation damage at the time of this experiment.

Fig. 9.3 : enriched ^{60}Ni

The peak which appears at the location of the ground state transition may also contain contributions to low lying levels in ^{57}Fe.

Fig. 9.4 : enriched ^{61}Ni

The ground state transition and the transition to the 0.810 Mev 2^+ state in ^{58}Fe are partially resolved. The peaks appear in the expected locations.

Fig. 9.5 : enriched ^{47}Ti

The ground state transition is not observed. The 2^+ state at 1.156 Mev in ^{44}Ca gives rise to a clearly resolved peak in the expected location.

Fig. 9.6 : natural Zn

The high yield from this target allowed the ground state transitions corresponding to ^{64}Zn, ^{66}Zn and ^{68}Zn to be observed. The first is totally and the other two are partially resolved. Cross section values will only be quoted for ^{64}Zn, since the peaks corresponding to ^{66}Zn and ^{68}Zn are contaminated respectively

by alpha particles from ^{64}Zn and $^{64}Zn + ^{66}Zn$. The Q-value equation again predicts the correct position of the peaks.

Fig. 9.7 : ^{103}Rh

A broad, partially resolved peak is observed, at slightly too low energy to fit the predicted location of the ground state transition. No information is available on the excited states of ^{100}Tc. If the Q-value from the 1964 Mattauch and Wapstra tables (Mattauch 1965) is correct, the observed peak could be attributed to several low lying excited states in ^{101}Tc.

Fig. 9.8 ^{59}Co

Not withstanding the small Q-value of the ^{59}Co (n, α)^{56}Mn reaction, the transition to the ground state and the first excited levels of ^{56}Mn (3^+ at o Mev, 2^+ at 0.026 Mev and 1^+ at 0.109 Mev, etc...) are distinguishable as a single unresolved peak from the line due to the ^{28}Si (n, α)^{25}Mg reaction. The participation of the excited states in ^{56}Mn is suggested by the disagreement between predicted and observed position of the ground state transition. It is interesting to note that the peak corresponding to the ^{28}Si (n, α)^{25}Mg reaction with the silicon of the semiconductor

detector appears at 13 instead of 12 Mev. The computer program which corrected the alpha particle energies for loss through ionization in the target and the gas, applied the same procedure to the alphas generated in the silicon and assigned an "original" energy of 13 Mev to them.

Fig. 9.9 : natural Fe

The ground state transition is partially resolved and appears in the right place.

Fig. 9.10 : ^{197}Au

The experimental points show appreciable scatter and the ground state transition does not appear as an individual peak. The general shape of the spectrum can, however, still be recognized.

Fig. 9.11 : natural Ba

A broad peak is observed corresponding rather well to the expected location of the ground state transition. The partially resolved peak at 16.8 Mev cannot be taken too seriously in view of the appreciable scatter of the experimental points below 16.5 Mev.

Fig. 9.12 : natural Cu

The peak corresponding to the ground state transition is partially resolved. (arrows 1 and 2 correspond to ^{65}Cu and ^{63}Cu).

Fig. 9.13 : ^{209}Bi

The considerable scatter of the data only allows the general shape of the spectrum to be drawn. There is no indication of a peak corresponding to the ground state transition.

Table 9.1 lists for each target its thickness and physical construction: F stands for foil, EA for evaporated on aluminum and EG for evaporated on graphite. The thicknesses were measured by weighing and the accuracy is usually 5% or better. The last column lists the percentage enrichment for the enriched isotopes.

9.2 The cross section values assuming an isotropic angular distribution .

If the alpha particles are supposed to be emitted isotropically, equations 4.2 and 7.5 can be combined to yield

$$\sigma = 1.57 \times 10^{-30} \frac{1}{\epsilon_1 G_2} \cdot \frac{M}{\rho f t} \cdot \frac{N_\alpha}{N_{ap}} \qquad (9.1)$$

Table 9.1

Target	Thickness (μ)	Construction	% enrichment
natural Ni	2.6	F	
enriched ^{58}Ni	2.3	F	99.95
enriched ^{60}Ni	2.3	F	99.1
enriched ^{61}Ni	2.2	F	92.11
enriched ^{47}Ti	4.5	F	80.1
natural Zn	2.8	EA	
^{103}Rh	3.3	F	
^{59}Co	2.6	EA	
natural Fe	2.4	F	
^{197}Au	3.0	F	
natural Ba	18.1	EG	
natural Cu	2.3	F	
^{209}Bi	4.9	EA	

If N_α is the number of counts under an isolated peak, the (n, α) cross section to the corresponding level in the residual nucleus is given by (9.1).

If N_α is the number of alpha particles having an energy greater than E_o, (9.1) yields the cross section for producing alpha particles having energies $E > E_o$.

In some cases when the ground state transition is not completely resolved, an estimated value is given for the corresponding cross section.

The results are tabulated in Table 9.2

σ (g.s.) stands for the cross section to the ground state of the residual nucleus, or to a group of unresolved levels to which the ground state belongs.

σ (exc.) stands for the cross section to an excited level, or to a group of unresolved excited levels in the residual nucleus. If the target contains various isotopes with comparable abundances, cross sections are quoted provided the contributions from the various isotopes could be separated.

The error limits were calculated by estimating the uncertainties on G_1, G_2, N_{ap}/N_r and the target thickness. The uncertainty on N_α was taken to be $\sqrt{N_\alpha}$.

Table 9.2 (*)

Isotope	σ(g.s.) mb	σ(exc.) mb	E_o MeV	σ(E > E_o) mb
^{58}Ni	1.7 ± 0.5	5.4 ± 2	14.5	9.4 ± 3
^{60}Ni	5.3 ± 2		14.5	6.9 ± 2
^{61}Ni	0.8 ± 0.3	1.4 ± 0.5	15.5	4.1 ± 1
^{64}Zn	6.2 ± 2		17.1	9.9 ± 3
^{47}Ti		2.0 ± 0.7	14.6	2.3 ± 0.8
^{56}Fe	2.9 ± 0.9		14.0	3.9 ± 1
^{59}Co	1.4 ± 0.5		13.7	1.5 ± 0.5
^{63}Cu	3.5 ± 1		15.0	6.5 ± 2
^{103}Rh	3.7 ± 1		15.2	6.8 ± 2
^{197}Au			15.8	1.6 ± 0.5
^{138}Ba			15.6	5.1 ± ?
^{209}Bi			17.7	2.6 ± 0.8

(*) See pages 162 Band C.

9.3 Cross section values for anisotropic angular distributions.

In this case the results of section 7.2 must be used. The procedure will be illustrated by an example. Seebeck and Borman (Seebeck 1965) have fitted the angular distribution of the total alpha particle yield from ^{58}Ni (n, α)^{55}Fe with an expression of the form:

$$y(\theta_c) = a + b\cos^2\theta_c \qquad (9.3)$$

where a = 10.1 mb/ster. and b = 6.30 mb/ster. (θ_c is the centre of mass angle between the neutron and the alpha particle). The ground state transition cross section will now be calculated from the spectrum of Fig. 9.2 assuming that the shape of the angular distribution is given by (9.3). This is done by applying eg. 7.19 keeping in mind that θ is the laboratory system angle in that formula:

$$\int_0^{\theta_{1L}} \sigma(\theta_L)d\theta_L = \frac{M}{N_A\rho ft} \cdot \frac{N_\alpha}{N_n} \cdot \frac{\int_0^{\theta_{1L}} (a + b\cos^2\theta_c)\sin\theta_L d\theta_L}{\int_0^{\theta_{1L}} (a + b\cos^2\theta_c)n(\theta_L)\sin\theta_L d\theta_L} \qquad (9.4)$$

θ_L is the laboratory angle between neutron and alpha particle and

$$\tan\theta_L = \frac{\sin\theta_c}{\gamma + \cos\theta_c} \qquad (9.5)$$

where

$$\gamma = \left[\frac{m_n m_\alpha E_n}{M_R(m_\alpha + M_R)Q + M_R(M_R + m_\alpha - m_n)E_n} \right]^{1/2} \qquad (9.6)$$

m_n, m_α and M_R are the masses of the neutron, the alpha particle and the residual nucleus; E_n and Q are the neutron energy in the laboratory system and the Q-value of the reaction. (9.4) must be integrated in the centre of mass system and, therefore, a change of variable must be effected:

$$d\theta_L = f(\theta_c)d\theta_c \quad \text{with} \quad f(\theta_c) = \frac{\gamma \cos\theta_c + 1}{\gamma^2 + 2\gamma\cos\theta_c + 1} \qquad (9.7)$$

$$\sin\theta_L = \frac{s}{\sqrt{1+s^2}} \quad \text{with} \quad s = \frac{\sin\theta_c}{\gamma + \cos\theta_c} \qquad (9.8)$$

$$\int_0^{\theta_{lc}} \sigma(\theta_c)d\theta_c = \frac{M}{N_A \rho f t} \cdot \frac{N_\alpha}{N_n} \cdot \frac{\int_0^{\theta_{lc}} (a + b\cos^2\theta_c)\frac{s}{\sqrt{1+s^2}} f(\theta_c)d\theta_c}{\int_0^{\theta_{lc}} (a + b\cos^2\theta_c)n(\theta_c)\frac{s}{\sqrt{1+s^2}} f(\theta_c)d\theta_c} \qquad (9.9)$$

Equation (9.9) yields the ground state transition cross section integrated over the angular range that the reaction products are observed in the experiment. If one wants to calculate the

total ground state cross section, θ_{1c} should be put equal to π in (9.9) and this requires of course that eq. 9.3 be considered valid over the full range $\theta_c = o$ to π. Equation (9.9) was integrated numerically and the results are compared with the cross section corresponding to an isotropic distribution, in Table 9.3.

The cross section for the anisotropic distribution is about 20% smaller than for the isotropic case. The angular distribution of the global spectrum will in general be different from that of the alpha group leading to the ground state. This will be even more true if considerable direct effects contribute to the ground state transition. The present calculation should be considered as an estimate of the influence of anisotropy on cross section values.

Table 9.3

Type of calculation	cross section (mb)
σ(g.s.) (isotropy)	1.7 mb
σ(g.s.) (anisotropy)	1.4 mb
$\int_o^{\theta_{1c}} \sigma(g.s.)d\theta$	0.4 mb

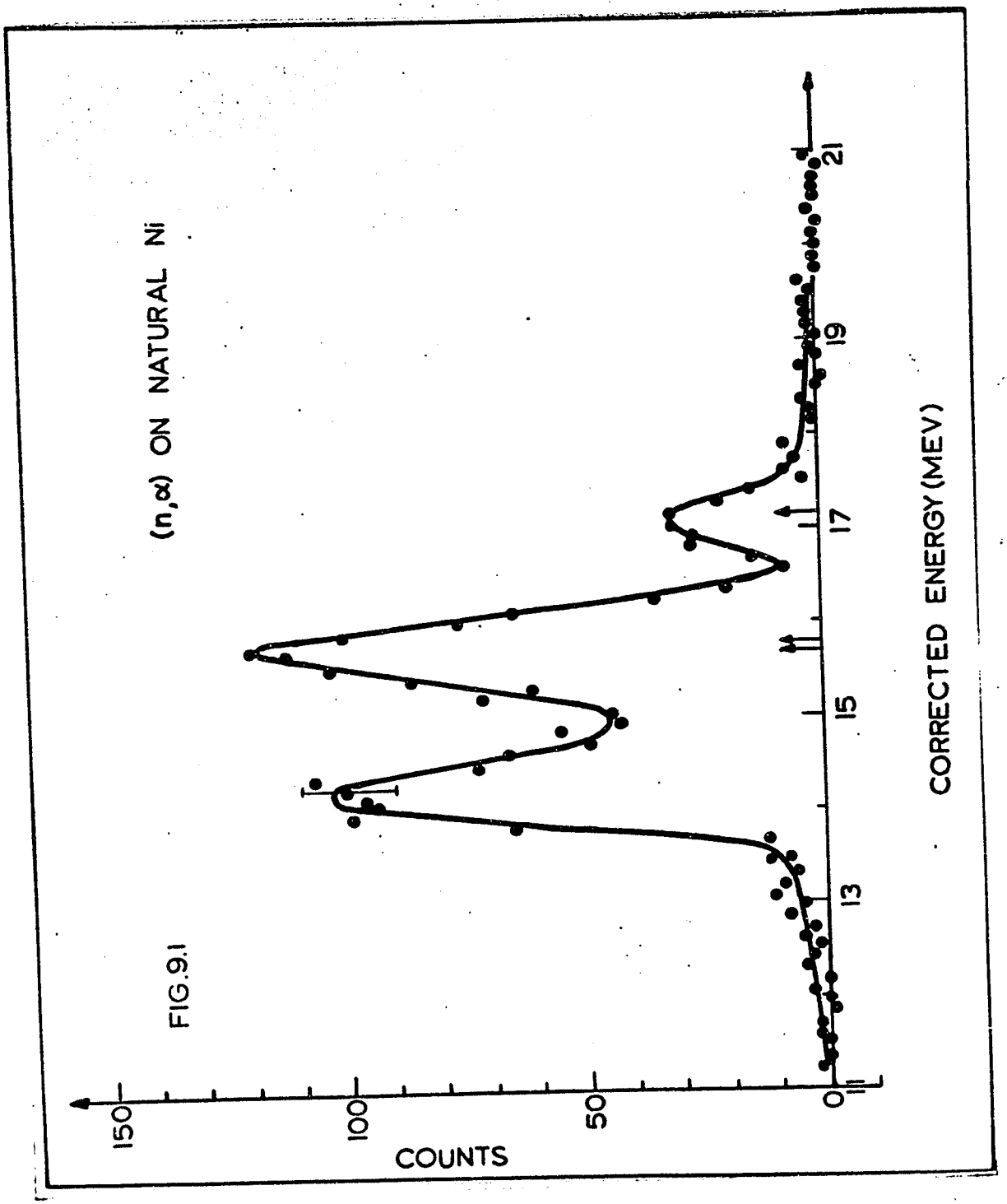
(n,α) ON NATURAL Ni
FIG.9.1
COUNTS
150
100
50
0
13
15
17
19
21
CORRECTED ENERGY (MEV)

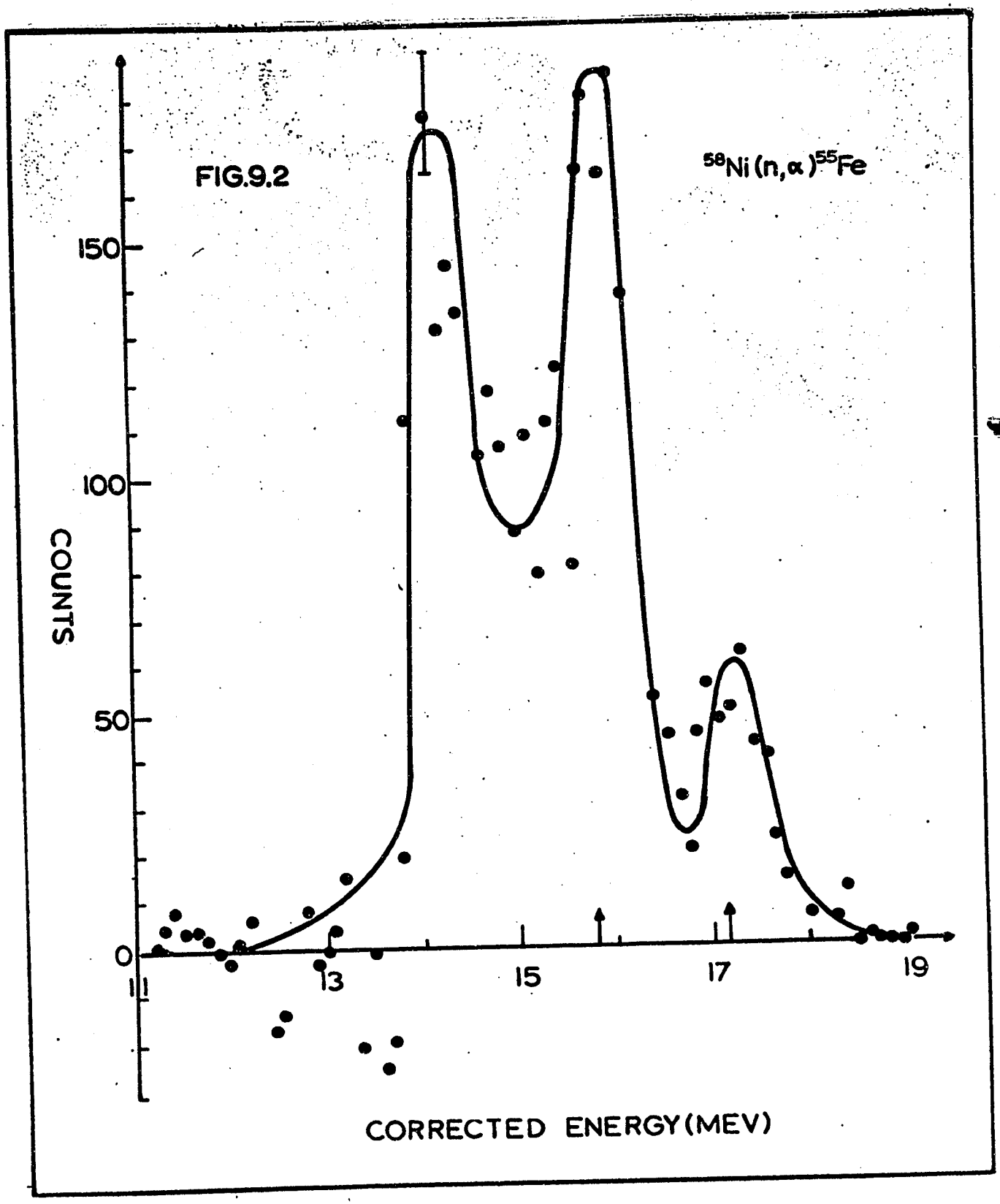
FIG.9.2
$^{58}Ni(n,\alpha)^{55}Fe$
150
100
50
0
COUNTS
11
13
15
17
19
CORRECTED ENERGY(MEV)

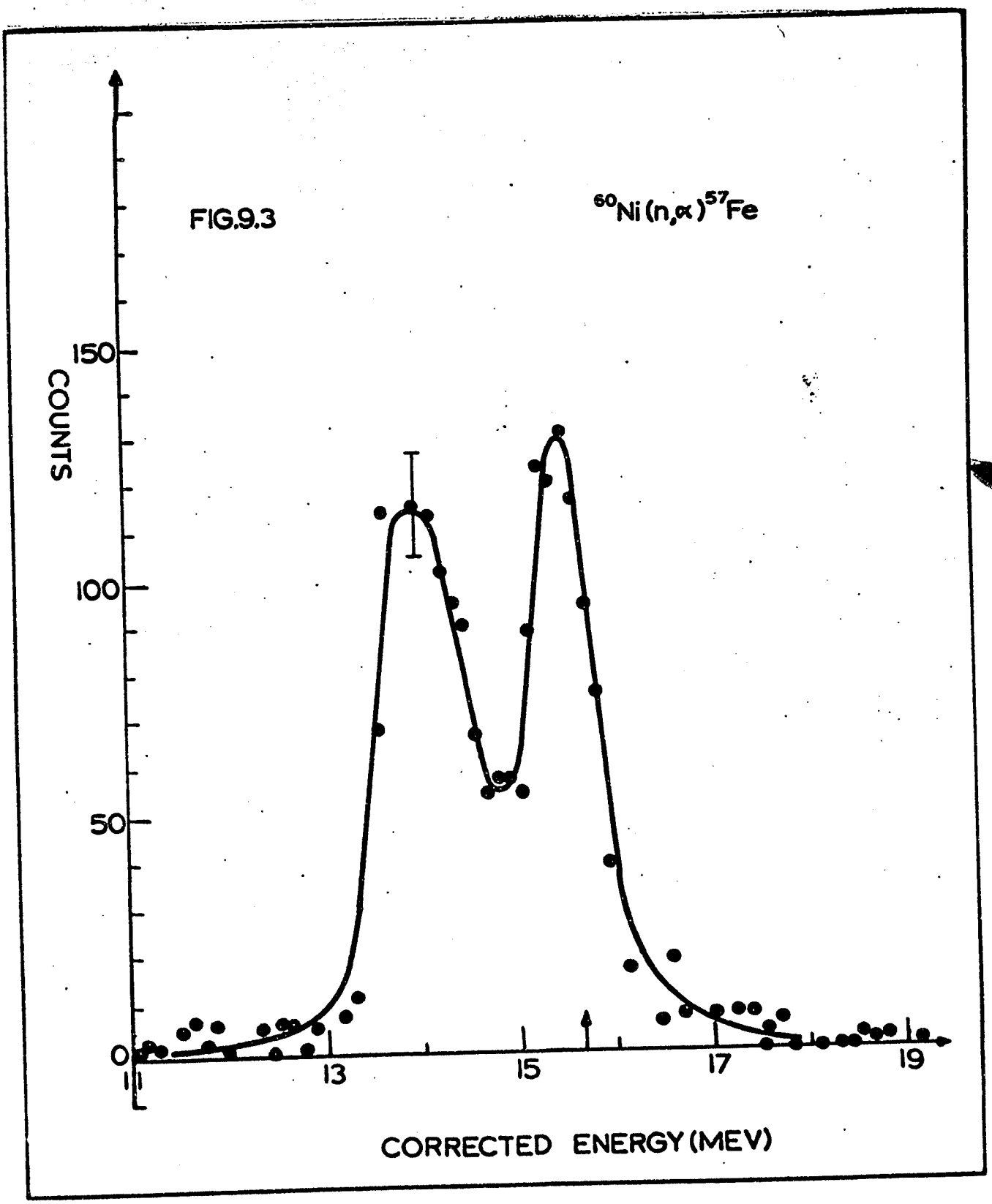
FIG.9.3
$^{60}Ni(n,\alpha)^{57}Fe$
COUNTS
150
100
50
0
13
15
17
19
CORRECTED ENERGY (MEV)

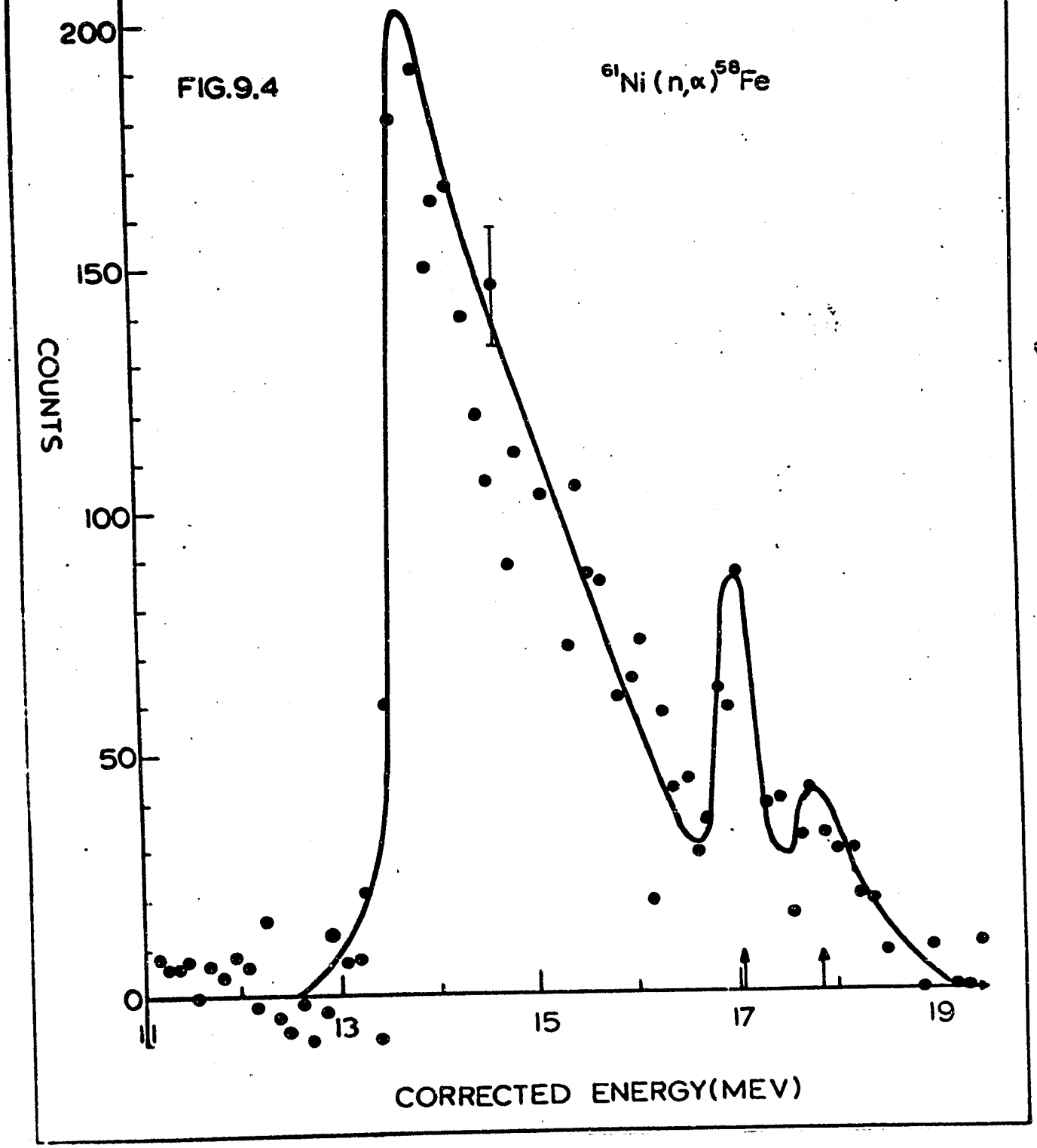
FIG.9.4
$^{61}Ni\,(n,\alpha)^{58}Fe$
COUNTS
200
150
100
50
0
13
15
17
19
CORRECTED ENERGY(MEV)

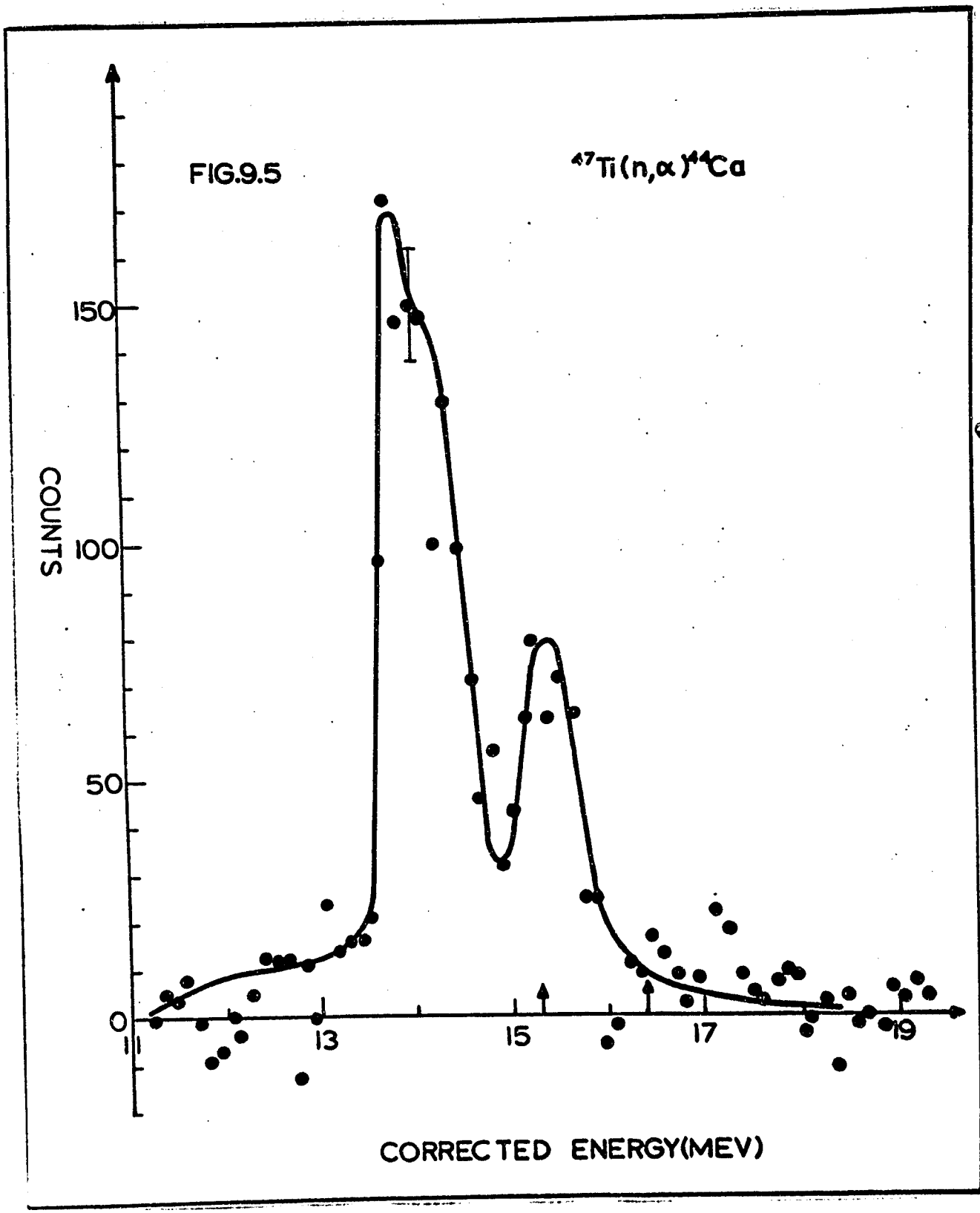
FIG.9.5
$^{47}Ti(n,\alpha)^{44}Ca$
150
100
50
0
COUNTS
13
15
17
19
CORRECTED ENERGY(MEV)

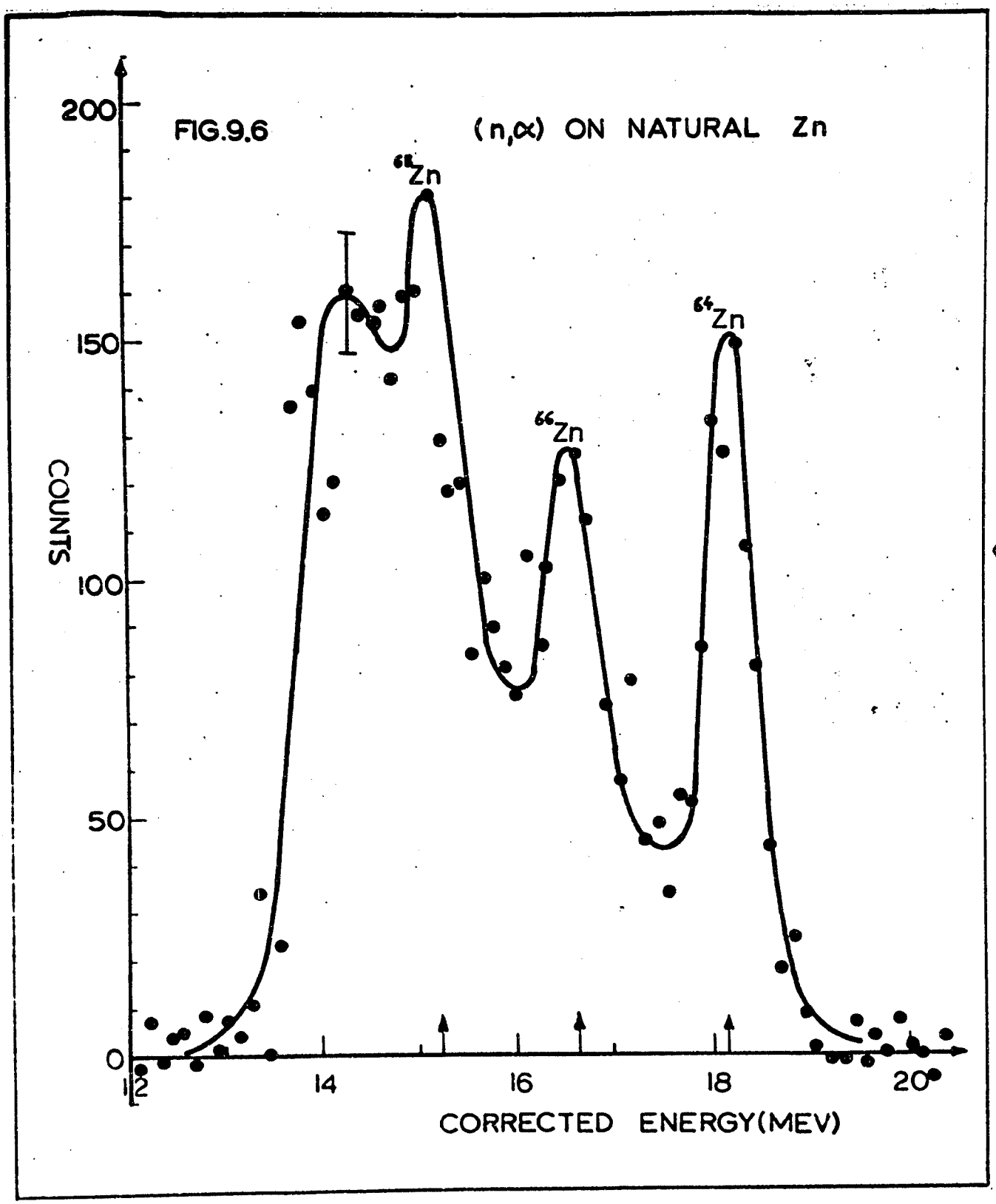
FIG.9.6
(n,α) ON NATURAL Zn
66Zn
66Zn
66Zn
200
150
100
50
0
COUNTS
12
14
16
18
20
CORRECTED ENERGY(MEV)

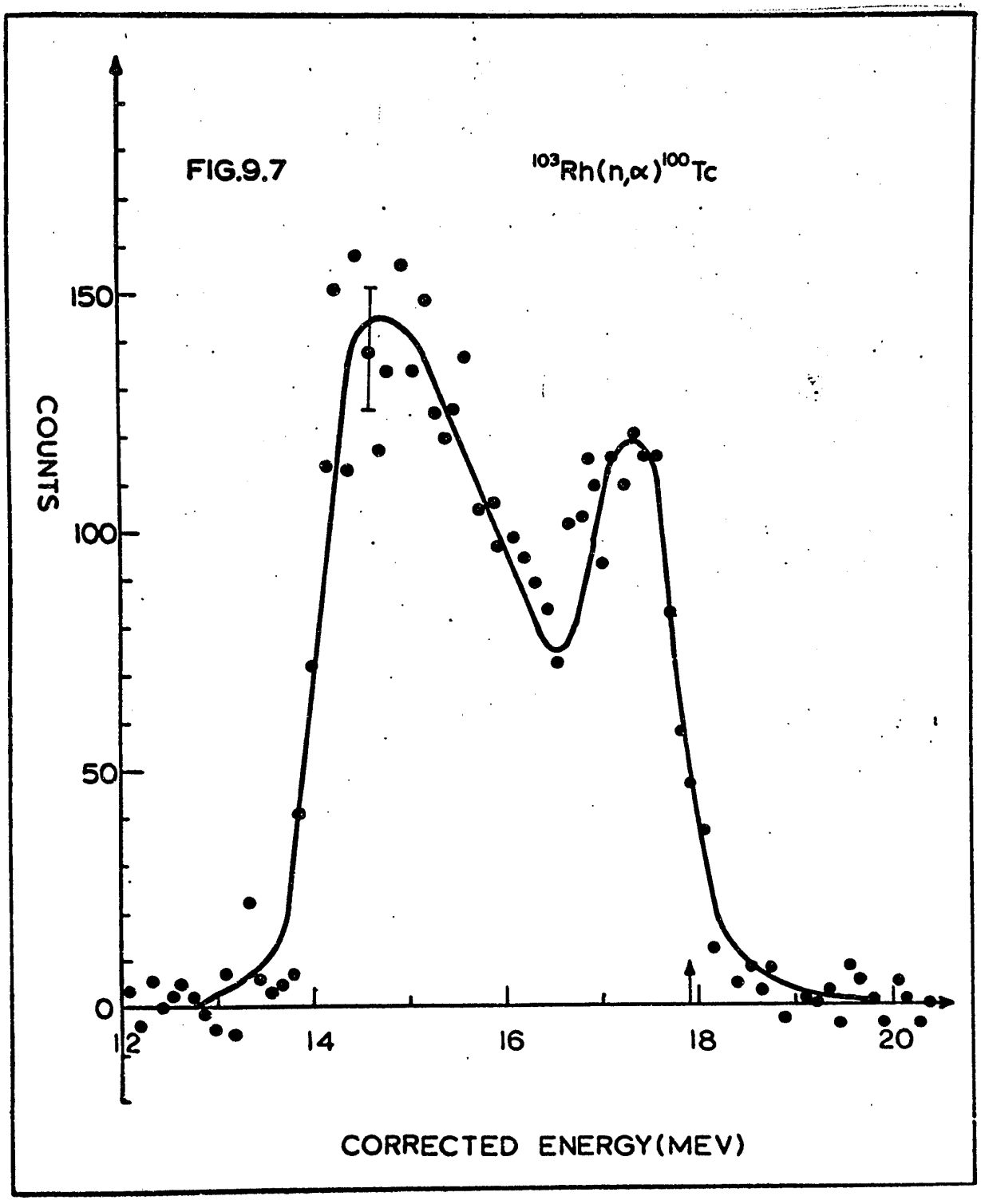
FIG.9.7
$^{103}Rh(n,\alpha)^{100}Tc$
COUNTS
150
100
50
0
12
14
16
18
20
CORRECTED ENERGY(MEV)

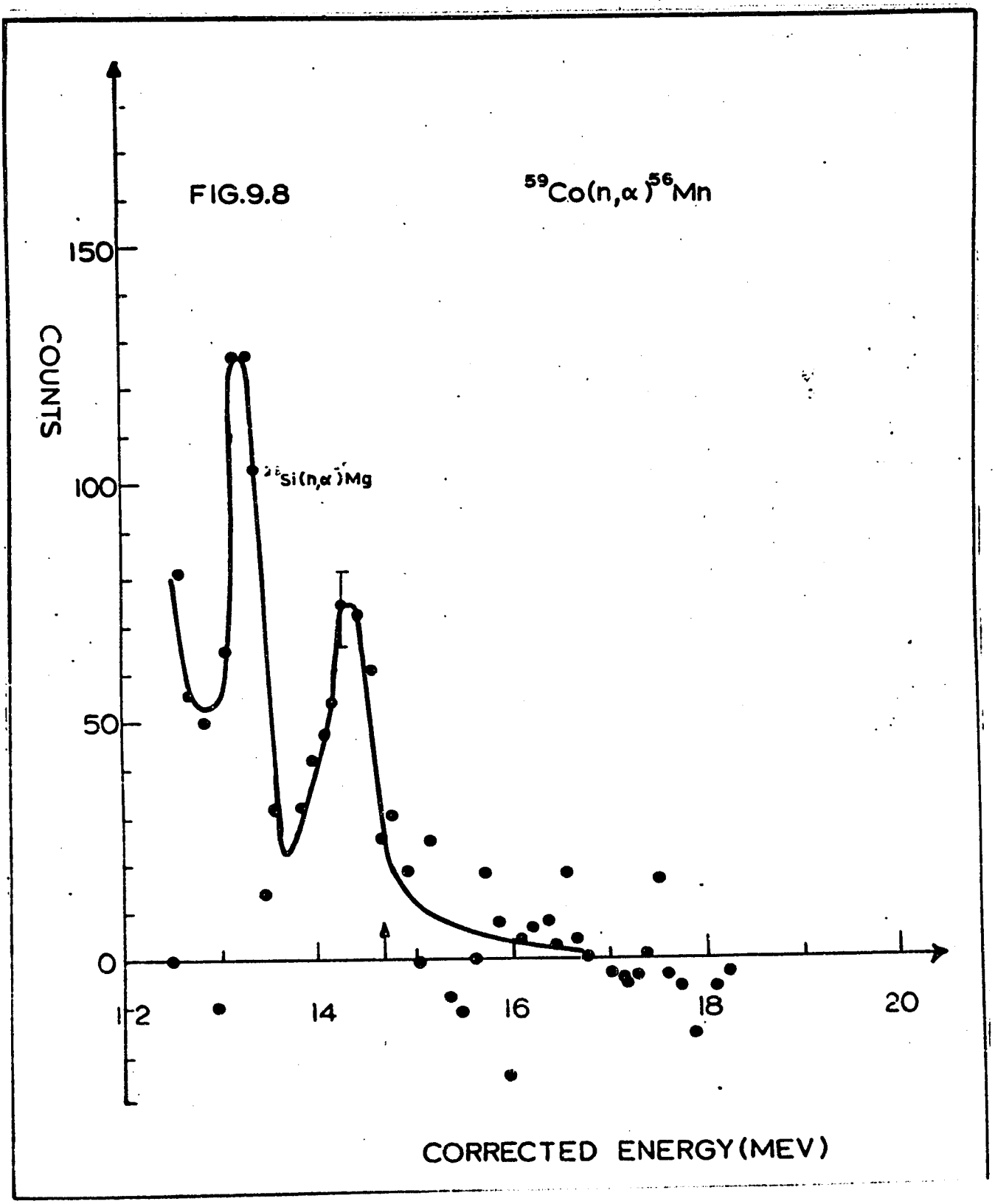
FIG.9.8
$^{59}Co(n,\alpha)^{56}Mn$
150
100
50
0
COUNTS
$^{28}Si(n,\alpha)^{25}Mg$
12
14
16
18
20
CORRECTED ENERGY(MEV)

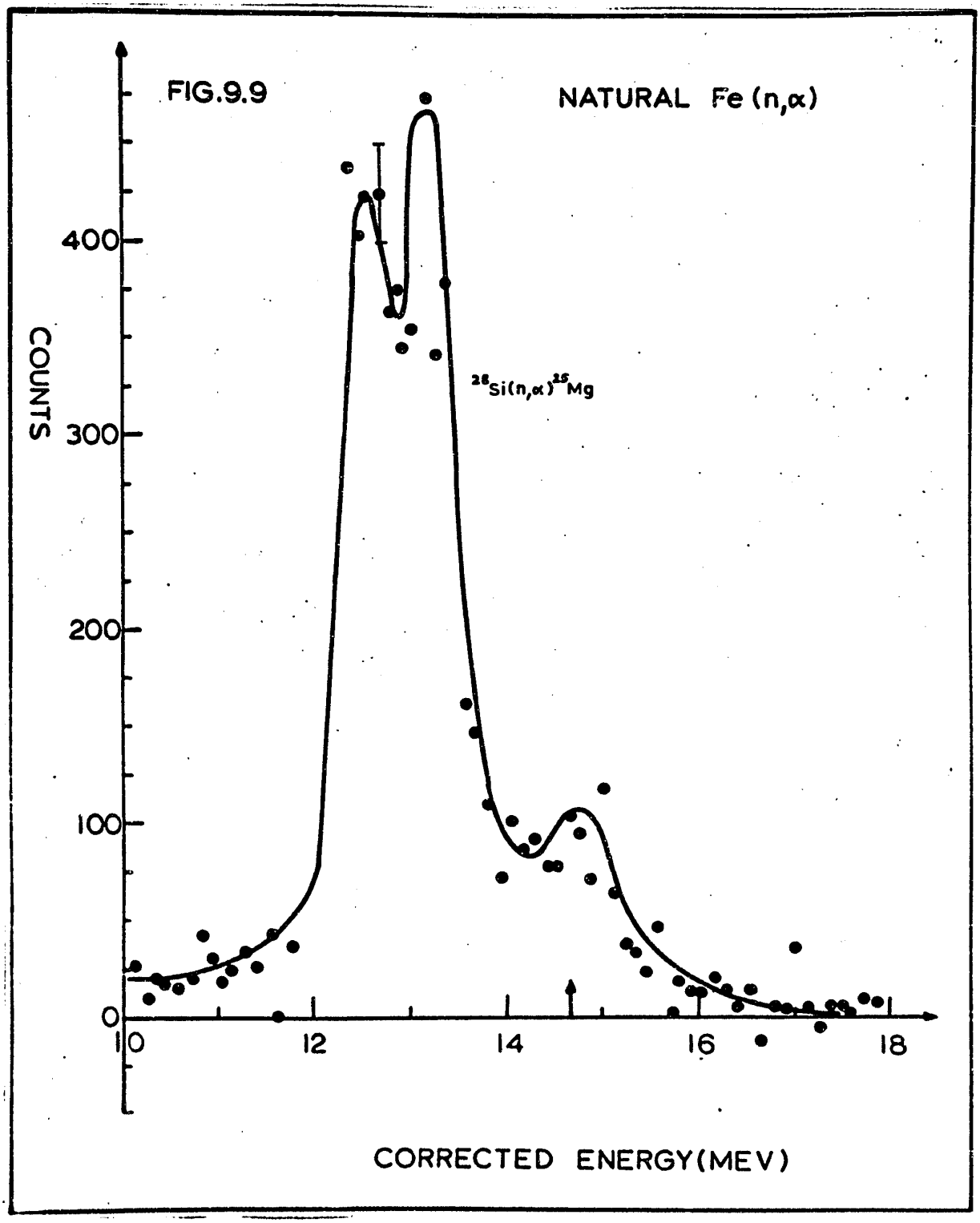
FIG.9.9
NATURAL Fe (n,α)
COUNTS
400
300
200
100
0
$^{28}Si(n,\alpha)^{25}Mg$
10
12
14
16
18
CORRECTED ENERGY(MEV)

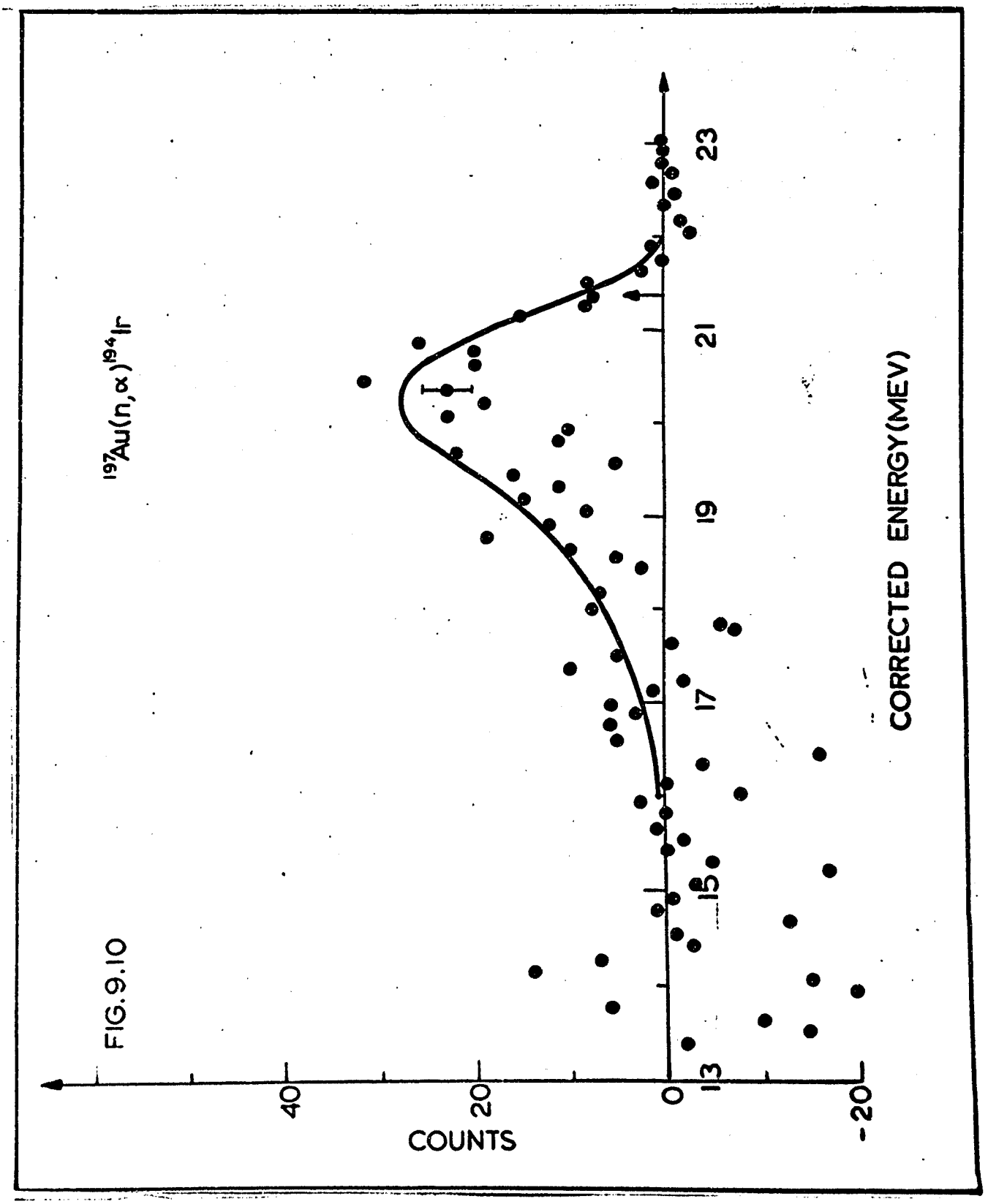
$^{197}Au(n,\alpha)^{194}Ir$
COUNTS
40
20
0
-20
13
15
17
19
21
23
CORRECTED ENERGY(MEV)

FIG.9.10

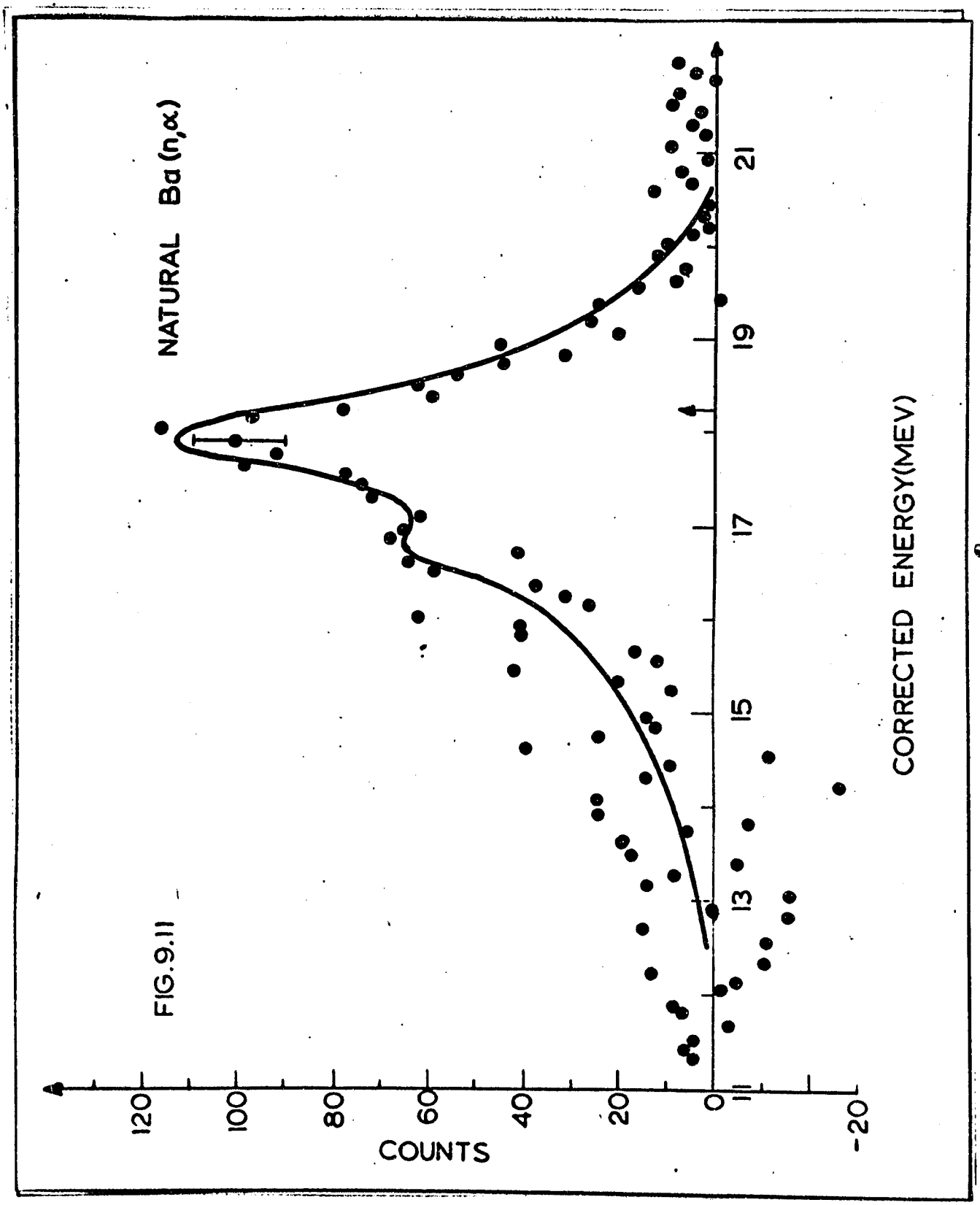
NATURAL Ba (n,α)
COUNTS
120
100
80
60
40
20
0
-20
11
13
15
17
19
21
CORRECTED ENERGY(MEV)

FIG. 9.11

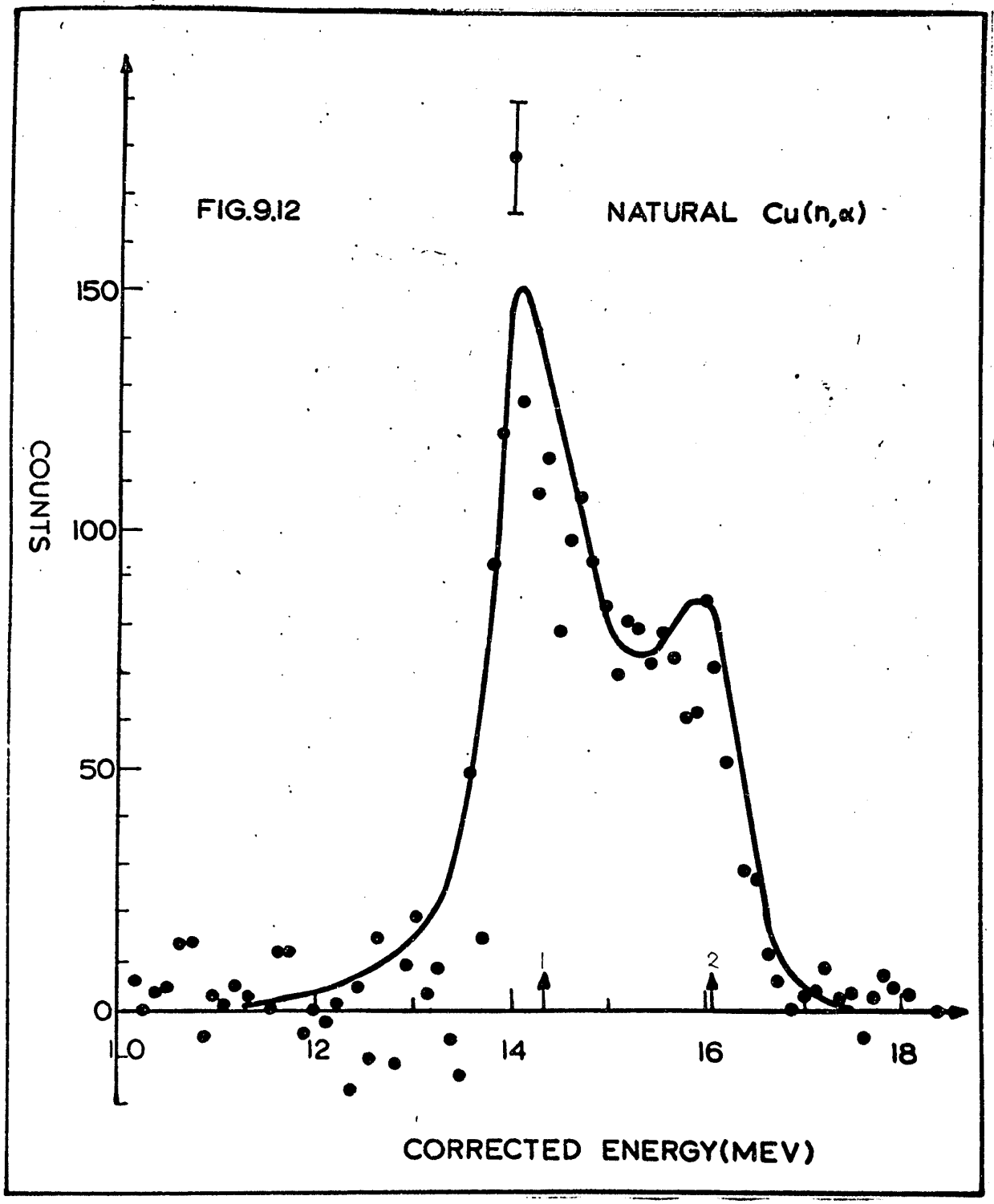
FIG.9.12
NATURAL Cu(n,α)
150
100
50
0
COUNTS
1
2
10
12
14
16
18
CORRECTED ENERGY(MEV)

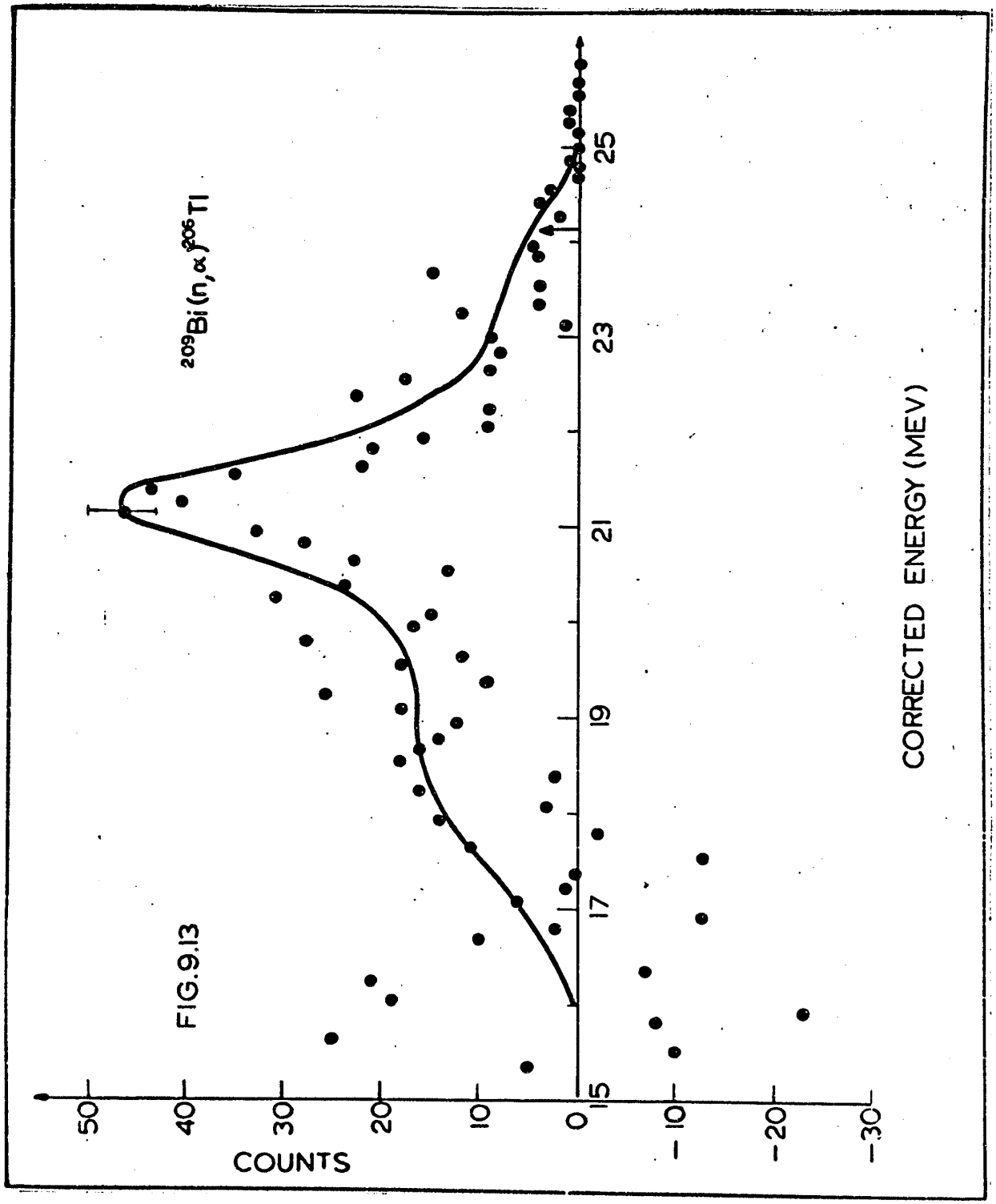
$^{209}Bi(n,\alpha)^{206}Tl$
COUNTS
50
40
30
20
10
0
-10
-20
-30
15
17
19
21
23
25
CORRECTED ENERGY (MEV)

FIG.9.13

X - COMPARISON OF THE RESULTS WITH THE STATISTICAL THEORY OF NUCLEAR REACTIONS.

10.1 Introduction.

In this chapter the statistical theory of nuclear reactions is briefly reviewed and its results applied to the particular case of reactions leading to isolated individual levels in the residual nucleus. The approach of Weisskopf and Ewing is considered first, and its development into the $(2I + 1)$ - rule is stressed. Then the approach of Hauser and Feshbach is discussed.

The experimental data is compared with those two forms of the statistical theory. It is found that the two theoretical procedures agree well with each other, but that both are in very poor agreement with the experimental data.

The theory is presented here in a rather abridged form and is only included for completeness. Fuller treatments can be found in the various references given in the text.

10.2 General cross section formulae

Several assumptions have to be made in order that a reaction of the type X(a, b)Y can be described by the statistical theory (Goldstein 1963):

a) A compound nucleus must actually be formed and its life time should be long compared to the transit time of the incident particle through the nucleus.

b) The excitation of the compound nucleus should be in the region of strongly overlapping levels.

c) Except for the requirement of conservation of total energy, total angular momentum and parity, the decay of the compound nucleus should be independent of its mode of formation.

Under these conditions the total cross section can be written

$$\sigma(a, b) = \sigma_{ca}(\varepsilon_a) \cdot \eta_b(E) \qquad (10.1)$$

$\sigma_{ca}(\varepsilon_a)$ describes the formation of the compound system by the incident particle with channel energy ε_a; $\eta_b(E)$ represents the probability of decay of the compound nucleus by emission of a particle of type b. η_b is the ratio of the probability of decay of the compound nucleus by emission of particle b, to the total decay probability through all possible channels. It can be readily expressed as a function of the various widths for particle emission

$$\eta_b = \frac{\Gamma_b}{\sum_\nu \Gamma_\nu} \qquad (10.2)$$

10.3 The reciprocity theorem for nuclear reactions.

One can show by means of a general argument (Weisskopf 1937), that the width Γ_a for decay of a compound nucleus A by means of emission of particle a is related to the cross section of formation of the same compound nucleus by association of a and the residual nucleus B of the former process:

$$\Gamma_a^{(\ell)}(\varepsilon_a) = \sigma_{ca}^{(\ell)}(\varepsilon_a) \frac{(2s_a + 1)m_a\varepsilon_a}{\pi^2\hbar^2\omega_A(E_A)} \omega_B(E_B) \qquad (10.3)$$

s_a and m_a are the intrinsic spin and mass of a. $\omega_A(E_A)$ and $\omega_B(E_B)$ are the densities of states of A and B at excitation energies E_A and E_B.

The superscript ℓ indicates that the expression is valid for the partial wave ℓ. By summing over all possible ℓ values, Γ_a can be related to σ_{ca}.

10.4 The total cross section for the X(a,b)Y reaction:

When (10.3) is applied to the outgoing particle b in the X(a,b)Y reaction, one gets:

$$\Gamma_b^{(\ell)}(\varepsilon_b) = \frac{2s_b+1}{\omega_c(E)} \cdot \frac{m_b\varepsilon_b}{\pi^2\hbar^2} \cdot \sigma_{cb}^{(\ell)}(\varepsilon_b)\omega_Y(E-E_b-\varepsilon_b) \qquad (10.4)$$

ω_c and ω_Y are the level densities respectively in the coumpound nucleus and the residual nucleus at the indicated excitation energies. E_b is the binding energy of b in the compound nucleus. Summation over all contributing ℓ-values and integration over all possible energies of particle b yields:

$$\Gamma_b = \frac{(2s_b + 1)m_b}{\pi^2 \hbar^2 \omega_c (E)} \int_0^{E-E_b} \varepsilon_b \sigma_{cb}(\varepsilon_b) \omega_Y (E - E_b - \varepsilon_b) d\varepsilon_b \qquad (10.5)$$

From (10.1), (10.2), and (10.5) it follows that

$$\sigma(a,b) = \sigma_{ca}(\varepsilon_a) \frac{(2s_b + 1)m_b \int_0^{E-E_b} \varepsilon_b \sigma_{cb}(\varepsilon_b) \omega_Y (E-E_b-\varepsilon_b) d\varepsilon_b}{\sum_\nu (2s_\nu + 1)m_\nu \int_0^{E-E_\nu} \varepsilon_\nu \sigma_{c\nu}(\varepsilon_\nu) \omega_{Y_\nu} (E-E_\nu-\varepsilon_\nu) d\varepsilon_\nu} \qquad (10.6)$$

where Y_ν is the residual nucleus associated with the outgoing particle ν. This is the Weisskopf-Ewing formula.

10.4.1 The level density formula.

The search for adequate expressions describing the variation of nuclear level density as a function of excitation energy has developed into an independent field. The description proposed by Gilbert and Cameron has been adopted in this

work. (Gilbert 1965). These authors divide the excitation energy of a nucleus into two regions, the dividing line depending on the nucleus under consideration.

In the lower excitation region, the dependence of the total level density (summed over the angular momenta) and including all levels degenerate in M) is given by

$$\omega(E) = \sqrt{2\pi}\,\sigma\,\frac{1}{T}\,\exp\left[(E-E_o)/T\right] \qquad (10.7)$$

σ is the spin cut-off parameter, E_o and T are constants, the latter being referred to as the nuclear temperature.

In the second region the dependence on E is given by

$$\omega(E) = \frac{\sqrt{\pi}}{12}\cdot\frac{\exp(2\sqrt{aU})}{a^{1/4}\,U^{5/4}}$$

$$U = E - \delta \qquad (10.8)$$

In (10.8) E is replaced by an effective excitation energy U, which is equal to or smaller than E, depending on the value of the positive constant δ (the pairing energy). a is called the level density parameter.

The introduction of δ can be justified by noting that (10.8) was derived under the assumption that the nucleus is a

a projection of angular momenta on axes.

gas of independent fermions. Since there are considerable interactions in a real nucleus between nucleons of one kind, some of the excitation energy E must be expended in breaking the links between the partners of the various pairs. The parameter δ reflects the difference of this contribution for even-even, odd-even, and odd-odd nuclei.

10.4.2 The inverse cross sections

The inverse cross sections $\sigma_{c\nu}(\varepsilon_\nu)$ play an important role in (10.6). One should note that $\sigma_{c\nu}(\varepsilon_\nu)$ is the cross section for capture of particle ν by the residual nucleus Y_ν, the latter being at excitation energy $E - E_\nu - \varepsilon_\nu$. Virtually nothing is known, both theoretically and experimentally about the dependence of the compound nucleus formation cross section on the excitation energy of the target nucleus. One is forced through the circumstances to insert ground state cross sections in (10.6), hoping that the approximation will not introduce serious errors.

Several authors have calculated compound nucleus formation cross sections:

Shapiro has evaluated compound nucleus formation cross sections by means of the "schematic theory of nuclear

reactions" and quotes results for protons, alpha particles and deuterons (Shapiro 1953). Results for neutrons based on the same theory are given by Blatt and Weisskopf (Blatt 1952). Huizenga and Igo have obtained the compound nucleus formation cross section by alpha particles for a large number of nuclei by means of optical model calculations (Huizenga 1962). Dostrovsky **et** al. have proposed an empirical formula which gives a good fit to Shapiro's calculations for charged particles (Dostrovsky 1959):

$$\sigma_c = \pi R^2 (1 + c_j)(1 - k_j V_j / E_c) \qquad (10.9)$$

R is the nuclear radius and E_c is the centre of mass energy of the incident particle.

The barrier height is given by

$$V_j = \frac{z\, Ze^2}{R + \rho_j} \qquad (10.10)$$

z and Z are the atomic number of the projectile and the nucleus being bombarded, e is the charge of the electron. ρ_j is zero for protons and positive for alpha particles. A table gives values for c_j and k_j which depend on z and Z.

A similar formula fits the data of Blatt and Weisskopf for neutrons

$$\sigma_c = \pi R^2 \alpha (1 + \beta/E_c) \qquad (10.11)$$

with $\alpha = 0.76 + 2.2\ A^{-1/3}$ and $\beta = (2.12\ A^{-2/3} - 0.050)/\alpha$, where A is the mass number of the target.

10.5 Cross sections for events leading to individual levels in the residual nucleus.

By slightly modifying the results of section 10.4, the cross section for the reaction X(a,b)Y such that Y is left in a definite state, can be obtained.

To indicate that a definite level β is involved in the residual nucleus, (10.1), (10.2) and (10.4) are rewritten:

$$\sigma(a,b\beta) = \sigma_{ca}(\epsilon_a) \cdot \eta_{b\beta}(E) \qquad (10.12)$$

$$\eta_{b\beta} = \frac{\Gamma_{b\beta}}{\sum_\nu \Gamma_\nu} \qquad (10.13)$$

$$\Gamma_{b\beta}^{(\ell)} = \frac{2s_b + 1}{\omega_c(E)} \cdot \frac{m_b \epsilon_{b\beta}}{\pi\, 2\hbar^2}\ \sigma_{cb}^{(\ell)}(\epsilon_{b\beta})\left[\omega_Y(E - E_b - \epsilon_{b\beta})\right]_\beta \qquad (10.14)$$

where $\epsilon_{b\beta}$ is the channel energy of b which leaves Y in level β. If one makes the assumption that the spin distribution of levels in a given nucleus is independent of its excitation

energy, the expression for the total density of levels at excitation energy E can be factorised

$$\omega(E) = \omega_o(E) \sum_J (2J+1)\, \omega_1(J) \qquad (10.15)$$

$\omega_o(E)$ is the level density dependence on E (the same for every J-value), and $\omega_1(J)$ the dependence on J.

$\omega_Y(E-E_b-\varepsilon_{b\beta})_\beta$ in (10.14) involves a single level and from (10.15) one can see that

$$\omega_Y(E-E_b-\varepsilon_{b\beta})_\beta = 2I_\beta + 1 \qquad (10.16)$$

where I_β is the angular momentum associated with level β

On substitution of (10.16) into (10.14) and after summation over all allowed ℓ values (10.12) and (10.13) yield:

$$\sigma(a,b\beta) = \sigma_{ca}(\varepsilon_a)\, \frac{(2s_b+1)m_b\varepsilon_{b\beta}\sigma_{cb}(\varepsilon_{b\beta})(2I_\beta+1)}{\sum_\nu (2s_\nu+1)m_\nu \int_o^{E-E_\nu} \varepsilon_\nu \sigma_{c\nu}(\varepsilon_\nu)\omega_{Y\nu}(E-E_\nu-\varepsilon_\nu)d\varepsilon_\nu} \qquad (10.17)$$

10.6 The (2I + 1)- rule

Suppose that the cross section $\sigma(a,b\,\xi)$ has been calculated, level ξ lying close to β. From (10.17)

$$\frac{\sigma(a,b\beta)}{\sigma(a,b\xi)} = \frac{\varepsilon_{b\beta}\sigma_{cb}(\varepsilon_{b\beta})(2I_\beta+1)}{\varepsilon_{b\xi}\sigma_{cb}(\varepsilon_{b\xi})(2I_\xi+1)} \qquad (10.18)$$

One is tempted to say since β and ξ are close together that

$$\varepsilon_{b\beta} \simeq \varepsilon_{b\xi} \qquad (10.19)$$

$$\sigma_{cb}(\varepsilon_{b\beta}) \simeq \sigma_{cb}(\varepsilon_{b\xi}) \qquad (10.20)$$

and therefore

$$\frac{\sigma(a,b\beta)}{\sigma(a,b\xi)} = \frac{2I_\beta + 1}{2I_\xi + 1} \qquad (10.21)$$

This is the well known (2I + 1)-rule (MacDonald 1962) which states that in a reaction which can be described by the statistical model, the probability for decay of the compound nucleus to a level of spin I in the residual nucleus is proportional to (2I + 1).

One should however be very cautious in applying (10.21).

The summations

$$\Gamma_{b\beta} = \sum_\ell \Gamma_{b\beta}^{(\ell)} \qquad (10.22)$$

$$\Gamma_{b\xi} = \sum_\ell \Gamma_{b\xi}^{(\ell)} \qquad (10.23)$$

which are necessary to evaluate (10.13) are not necessarily extended over the same range of ℓ values and therefore (10.20) can be invalid. The ranges

of ℓ values entering in (10.22) and (10.23) are governed by the conservation of angular momentum. The ranges are different because $I_\beta \neq I_\xi$

At 14.6 Mev incident energy the maximum ℓ-value associated with an incoming neutron, which still can initiate a reaction is $\ell \simeq 6$. This can be seen from a semi-classical argument by putting

$$\ell_{max}\hbar = m_n v_n r \qquad (10.24)$$

and

$$\pi r^2 = \sigma_{cx}(\varepsilon_n) \qquad (10.25)$$

$m_n v_n$ is the momentum of the incoming neutron and r is the maximum impact parameter which still can initiate a reaction. $\sigma_{cx}(\varepsilon_n)$ is the total compound nucleus formation cross section for target nucleus X bombarded by 14.6 Mev neutrons.

When the summations in (10.22) and (10.23) involve about 6 terms, it is anticipated that the resultant sums will not be very sensitive to the values of I_β and I_ξ and (10.21) will be well satisfied.

10.7 Practical expressions for the cross section formulae.

Expressions (10.6) and (10.17) will be slightly modified and presented in a form suitable for numerical work.

E_a is the binding energy of a in the compound nucleus. The excitation energy of the latter is given by

$$E = \varepsilon_a + E_a \tag{10.26}$$

The Q-value of the X(a, b)Y reaction is given by

$$Q_{ab} = E_a - E_b \tag{10.27}$$

and
$$E-E_b = \varepsilon_a + E_a - E_b = \varepsilon_a + Q_{ab} \tag{10.28}$$

The pairing energy correction of section 10.4.1 must also be introduced in the cross section formulae. From (10.28) it follows that

$$\omega_{Y\nu}\,(E - E_\nu - \varepsilon_\nu) \longrightarrow \omega_{Y\nu}\,(\varepsilon_a + Q_{a\nu} - \delta_\nu - \varepsilon_\nu)$$

The upper limits of the integrals must be changed because of the introduction of δ, otherwise one runs into negative excitation energies in $\omega_{Y\nu}$:

$$E - E_\nu = \varepsilon_a + Q_{a\nu} \longrightarrow \varepsilon_a + Q_{a\nu} - \delta_\nu$$

One more change has to be made in (10.6). If after emission of particle b the excitation energy of the residual nucleus is higher than the binding energy B_n of the last neutron, neutron emission will take place and the quantity $[\,\sigma(a,b) + \sigma(a,b,n)\,]$ rather than $\sigma(a,b)$ will be obtained from (10.6). To avoid this contamination the lower limit of the integral in the numerator is chosen

to be

$$\varepsilon_o = \varepsilon_a + Q_{ab} - \delta - B_n \qquad (10.29)$$

All lower integration limits remain zero in the denominators of (10.6)and(10.17). Multiple emission is indeed a valid decay mode of the compound nucleus, causing a decrease of the branching ratio for the phenomenon of interest. The final formulae can now be written:

$$\sigma(a,b) = \sigma_{ca}(\varepsilon_a) \times \frac{(2s_b + 1)m_b \int_o^{\varepsilon_a + Q_{ab} - \delta_b} \varepsilon_b \sigma_{cb}(\varepsilon_b)\omega_Y(\varepsilon_a + Q_{ab} - \delta_b - \varepsilon_b)d\varepsilon_b}{D} \qquad (10.30)$$

$$\sigma(a,b\beta) = \sigma_{ca}(\varepsilon_a) \frac{(2s_b + 1)m_b \varepsilon_{b\beta} \sigma_{cb}(\varepsilon_{b\beta})(2I_\beta + 1)}{D} \qquad (10.31)$$

$$D = \sum_{\nu} (2s_\nu + 1)m_\nu \times \int_o^{\varepsilon_a + Q_{a\nu} - \delta_\nu} \varepsilon_\nu \sigma_{c\nu}(\varepsilon_\nu)\omega_{Y\nu}(\varepsilon_a + Q_{a\nu} - \delta_\nu - \varepsilon_\nu)d\varepsilon_\nu \qquad (10.32)$$

It should be noted that in the region of excitation where level density expression (10.7) is used, δ should be put equal to zero. (At those energies

no pairing corrections have to be made).

10.8 Agreement of the predictions of the (2I + 1)-rule with experiment.

Computer programs were written to calculate expressions (10.31) and (10.32) for the various target nuclei. The level density parameters and the pairing energies given by Gilbert and Cameron were adopted (Gilbert 1965). Also Dostrovsky's formula for inverse cross sections was used (Dostrovsky 1959). The latter yields values of $\sigma_c(\varepsilon_b)$ which correspond to a summation of $\sigma_{cb}^{(\ell)}(\varepsilon_b)$ from 0 to ∞ with respect to ℓ. This is equivalent to assuming the validity of the (2I + 1)-rule. The $\sigma_{ca}(\varepsilon_a)$, the total compound nucleus formation cross sections, were taken from the compilation by Pearlstein (Pearlstein 1965). Table 10.1 gives the (n,α) cross sections to individual levels in the residual nucleus for various target nuclei. The first four columns name the target, the residual nucleus (R.N.), the excitation energy and spin of the residual nucleus at that excitation. Column 5 gives the expected cross section to the level on the basis of the (2I + 1)-rule. Column 6 will

Table 10.1

Targ.	R.N.	Exc.En. (MeV)	Spin R.N.	σ (2I+1)r. (mb)	σ H.F. (mb)	σ Exp. (mb)
^{58}Ni	^{55}Fe	0.000	3/2	0.244	0.200	1.7
		0.413	1/2	0.115	0.103	
		0.933	5/2	0.321	0.285	
		1.322	7/2	0.395	0.361	
		1.412	7/2	0.395	0.360	
^{60}Ni	^{57}Fe	0.000	1/2	0.0570	0.0718	5.3
		0.0144	3/2	0.114	0.139	
		0.136	5/2	0.171	0.197	
^{61}Ni	^{58}Fe	0.000	0	0.0105	0.0104	0.8
		0.810	2	0.0475	0.0528	
^{47}Ti	^{44}Ca	0.000	0	0.0334	0.0538	
		1.156	2	0.144	0.228	
^{64}Zn	^{61}Ni	0.000	3/2	0.0273	0.0230	8.2
		0.0674	5/2	0.0409	0.0324	
		0.284	1/2	0.0121	0.0118	
^{63}Cu	^{60}Co	0.000	5	0.0121	0.0140	3.5

Table 10.1 (con'd)

Targ.	R.N.	Exc.En. (MeV)	Spin R.N.	σ (2I+1)r. (mb)	σ H.F. (mb)	σ Exp. (mb)
		0.0586	2	0.00550	0.0081	
^{59}Co	^{56}Mn	0.000	3	0.0151	0.033	1.4
		0.026	2	0.0108	0.0239	
		0.109	1	0.00648	0.0153	
^{56}Fe	^{53}Cr	0.000	3/2	0.109	0.129	2.9
^{103}Rh	^{100}Tc	0.000	1	0.000	0.000	3.7

be discussed in section 10.10. Column 7 gives the experimentally observed cross sections for the ground state transitions, assuming isotropic emission of the alpha particles. (These values are extracted from Table 9.2 and repeated for convenience). The experimental results should be compared with the sum of the cross sections to all levels which lie close enough to the ground state for not being resolved from the latter. A graphic comparison of the predictions of the (2I + 1)-rule with experiment is shown in Fig. 10.1. The 5 nuclides shown were selected in order that Figs. 10.1 and 11.2 could be easily compared.

The agreement between theory and experiment is poor, both in the absolute magnitudes and the variation of the cross sections for various nuclides.

10.9 Description of the Hauser-Feshbach method.

Hauser and Feshbach have calculated the differential and total cross sections for the inelastic scattering of neutrons (Hauser 1952). Their formalism can be readily extended to nuclear reactions in which charged particles are produced, by introducing the appropriate spins and transmission factors.

AGREEMENT OF (2I+1)-RULE WITH EXPERIMENT

FIG. 10.1

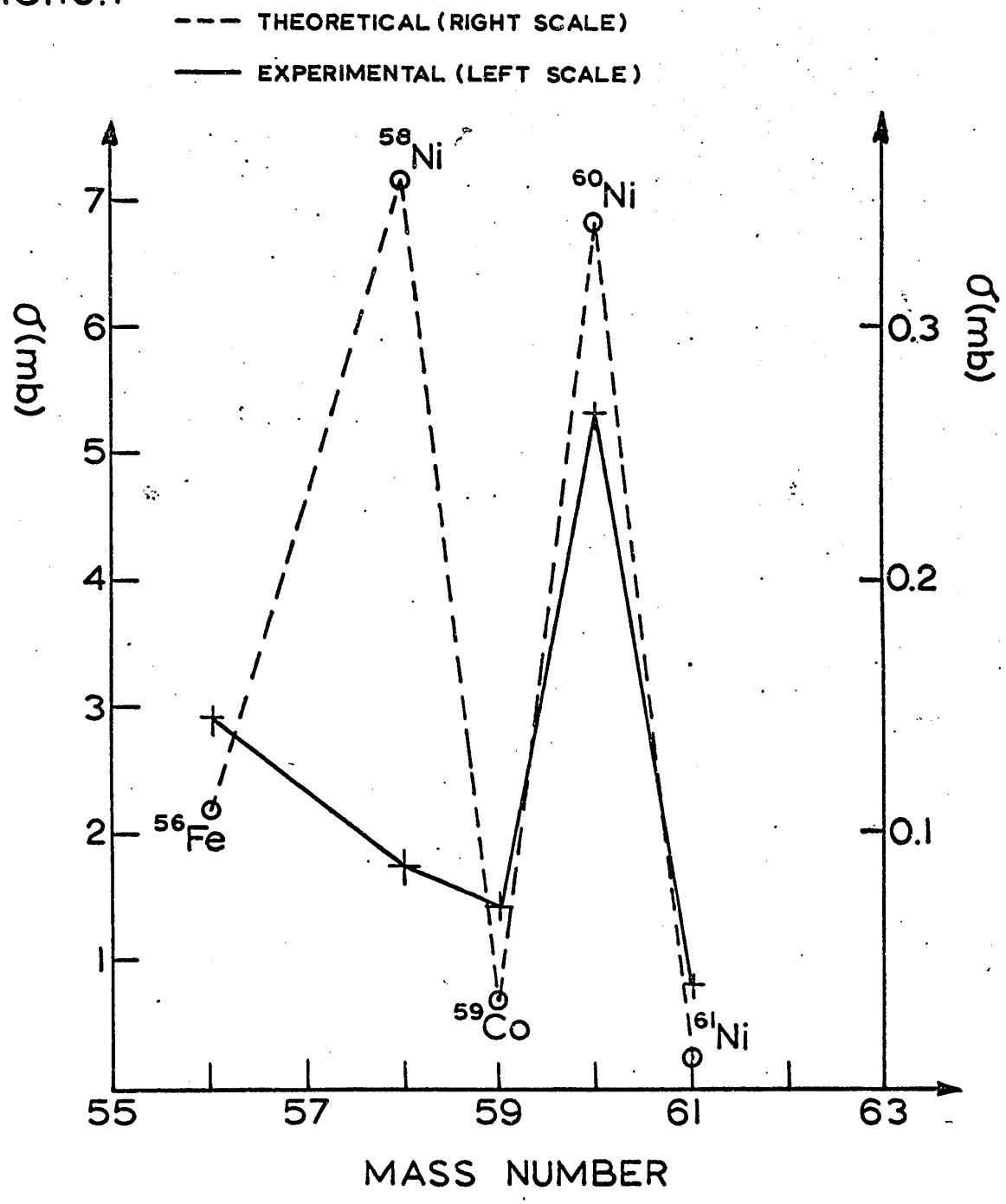

These transmission factors, $T_\ell(\varepsilon)$, which are the most important quantities entering into the calculation are closely related to the inverse cross sections discussed in section 10.4.2:

$$\sigma_c(\varepsilon) = \sum_\ell \sigma_c^{(\ell)}(\varepsilon) = \frac{\pi}{k^2} \sum_\ell (2\ell + 1) T_\ell(\varepsilon) \tag{10.33}$$

where k is the wave vector of the incident (or emitted) particle and the summation is extended over the allowed values of ℓ.

One supposes that the compound nucleus is sufficiently excited, so that the statistical model may be applied to it. The cases where the statistical theory does and does not also apply to the residual nucleus are envisaged separately. In the latter event, cross sections are calculated to isolated levels in the residual nucleus.

In the Hauser Feshbach method summations over particle energies, intrinsic and orbital angular momenta are carried out properly in the region of non overlapping energy levels. No level density expression is needed and no simplified assumptions are made with regard to the ranges of allowed angular momentum values. (In the region of over-

lapping levels a level density formula is of course needed).

In view of what has been said it may be anticipated that this method will yield more accurate results than the calculations based on the (2I + 1)-rule.

10.10 Comparison of the predictions of the Hauser Feshbach method with the (2I + 1)-rule data and the experimental results.

A computer program has been written at the Chalk River Nuclear Laboratories for cross section calculations by means of the Hauser Feshbach method. Transmission factors are computed using the optical model. Column 6 of Table 10.1 shows the (n,α) cross sections to individual levels in the residual nucleus, obtained for various target nuclides by means of this program. The optical model parameters were taken from the following papers:
Rosen et al. for protons and neutrons (Rosen 1965), Huizenga and Igo for alpha particles (Huizenga 1962). In the continuum region the level density parameters of Gilbert and Cameron were used. (Gilbert 1965).

In Fig. 10.2 Hauser Feshbach and (2I + 1)-rule predictions for the "ground state transition cross sections" are compared. The ordinates in this graph are the sums of the cross sections to the various levels which cannot be resolved experimentally from the ground state. (See also Fig. 10.1). The quotation marks are there to remind us that states different from the ground state may be involved. From both Fig. 10.2 and Table 10.1 it is apparent that the predictions of the (2I + 1)-rule and the Hauser Feshbach theory are in excellent agreement with very few exceptions. This is an encouraging result, especially since the Hauser Feshbach results were obtained without fiddling with the optical model parameters. It seems that the underlying assumptions for the validity of the (2I + 1)-rule are well satisfied.

Already from Table 10.1 and Figs. 10.1 and 10.2 one can conclude that the agreement between the Hauser Feshbach theory and the experimental data is poor. A much firmer conclusion will be drawn in section 10.11.

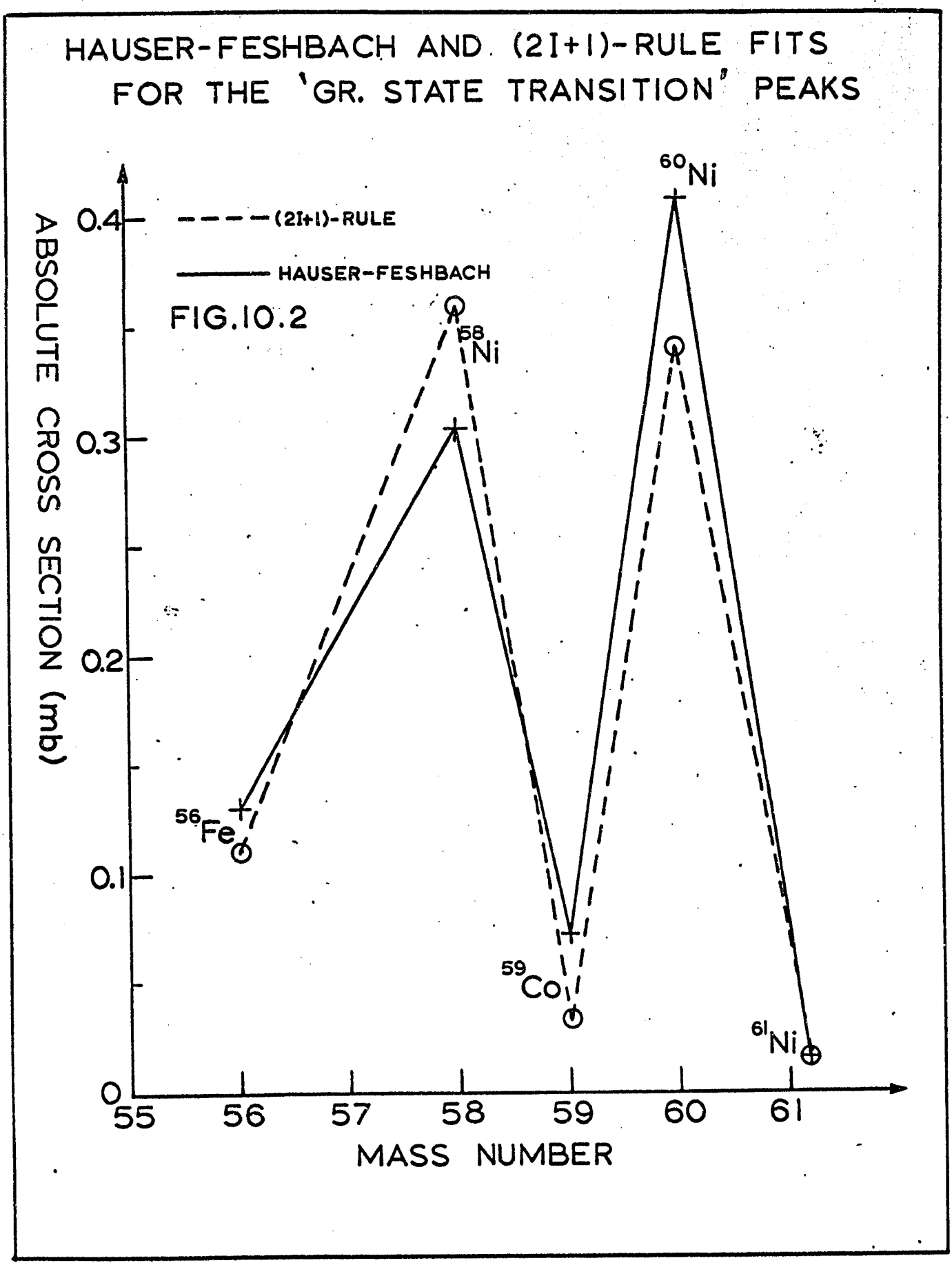
HAUSER-FESHBACH AND (2I+1)-RULE FITS
FOR THE 'GR. STATE TRANSITION' PEAKS
(2I+1)-RULE
HAUSER-FESHBACH
FIG.10.2
ABSOLUTE CROSS SECTION (mb)
0.4
0.3
0.2
0.1
0
55
56
57
58
59
60
61
MASS NUMBER
56Fe
58Ni
59Co
60Ni
61Ni

10.11 Calculation of the alpha particle yields by means of the Hauser-Feshbach theory.

The Hauser Feshbach treatment also yields a detailed angular distribution for the alpha particle group to each level in the residual nucleus. This permits a truly meaningful comparison of this theory with experiment.

The (2I + 1)-rule did not provide information on angular distributions and the comparison of theory and experiment had to be carried out assuming isotropy. Any serious departure from isotropy results in considerable errors in the data of column 7 in Table 10.1.

For each target that has been measured, the thickness and total neutron production are known. It follows from section 7.2 that the total number of alpha particles leading to a definite state in the residual nucleus that will be detected with this experimental arrangement is:

$$N_\alpha = 2\pi N_A \frac{\rho f t N_n}{M} \int_0^\pi \phi(\theta_c) n(\theta_c) \frac{s}{\sqrt{1+s^2}} f(\theta_c) d\theta_c \qquad (10.34)$$

θ_c is the centre of mass angle of deviation between

incoming neutron and outgoing alpha particle and $\eta(\theta_c)$, s and $f(\theta_c)$ have the same meaning as in section 9.3. $\phi(\theta_c)$ is the angular distribution obtained from the Hauser Feshbach calculation.

Introducing in (10.34) the number of counts N_{ap} registered in the associated particle detector, one finally obtains

$$N_\alpha = 3.99 \times 10^3 \frac{\rho f t}{M} N_{ap} \int_0^\pi \phi(\theta_c)\eta(\theta_c)\frac{s}{\sqrt{1+s^2}} f(\theta_c) d\theta_c \qquad (10.35)$$

The quantities N_α are calculated for the individual levels in the residual nucleus of each reaction. The contributions to levels which can give rise to a single peak in the spectrum are summed. These various sums are then compared to the observed number of alpha particles under each peak. Table 10.2 summarizes the results of the calculation. The first four columns are identical to the corresponding ones in Table 10.1. Column 5 gives the theoretical alpha particle yield $N_\alpha(th)$ to the level under consideration. In column 6, labeled $\Sigma N_\alpha(th)$, the yield from levels which might contribute to the same experimental peak are summed. (The

terms of the sums are grouped by means of accolades in column 5). In column 7 one finds the number of alpha particles under the ground state transition peaks in the experimental spectra. In three instances (^{58}Ni, ^{61}Ni and ^{47}Ti) contributions to a resolved peak corresponding to one or more excited states in the residual nucleus are also given. These cases are identified by asterisks in columns 6 and 7. Experiment and theory are also graphically compared by means of a semi-logarithmic plot in Fig. 10.3. The points on the theoretical curve for ^{56}Fe, ^{58}Ni, ^{59}Co, ^{60}Ni and ^{61}Ni follow the same behaviour as in Fig. 10.1. Agreement between theory and experiment is poor, the theoretical yields being in some cases two orders of magnitude too small. ^{103}Rh does not appear on this graph, but it can be seen from the table that the theoretical yield for the ground state transition is catastrophically low. It could not be verified whether low lying excited states in ^{100}Tc contribute to the experimental yield, since no information is available on the level scheme of ^{100}Tc.

Table 10.2

Targ.	R.N.	Exc.En. (MeV)	Spin R.N.	Nα (th)	ΣNα (th)	Nα (exp.)
^{58}Ni	^{55}Fe	0.000	3/2	91		
		0.413	1/2	49	140	475
		0.933	5/2	119		
		1.322	7/2	137		
		1.412	7/2	137	393*	1447*
^{60}Ni	^{57}Fe	0.000	1/2	23		
		0.0144	3/2	42		
		0.136	5/2	55		
		0.368	3/2	42	162	989
^{61}Ni	^{58}Fe	0.000	0	4	4	
		0.810	2	23	23*	469*
^{47}Ti	^{44}Ca	0.000	0	28	28	
		1.156	2	113	113*	588*
^{64}Zn	^{61}Ni	0.000	3/2	3		
		0.0674	5/2	5		

Table 10.2 (con'd)

Targ.	R.N.	Exc.En. (MeV)	Spin R.N.	Nα (th)	ΣNα (th)	Nα (exp.)
		0.284	1/2	2	10	957
^{63}Cu	^{60}Co	0.000	5	2		
		0.0586	2	1	3	509
^{59}Co	^{56}Mn	0.000	3	14		
		0.026	2	10		
		0.109	1	7	31	479
^{56}Fe	^{53}Cr	0.000	3/2	70	70	831
^{103}Rh	^{100}Tc	0.000	1	0	0	1358

EXPERIMENTAL AND THEORETICAL ALPHA PARTICLE YIELDS

FIG.10.3

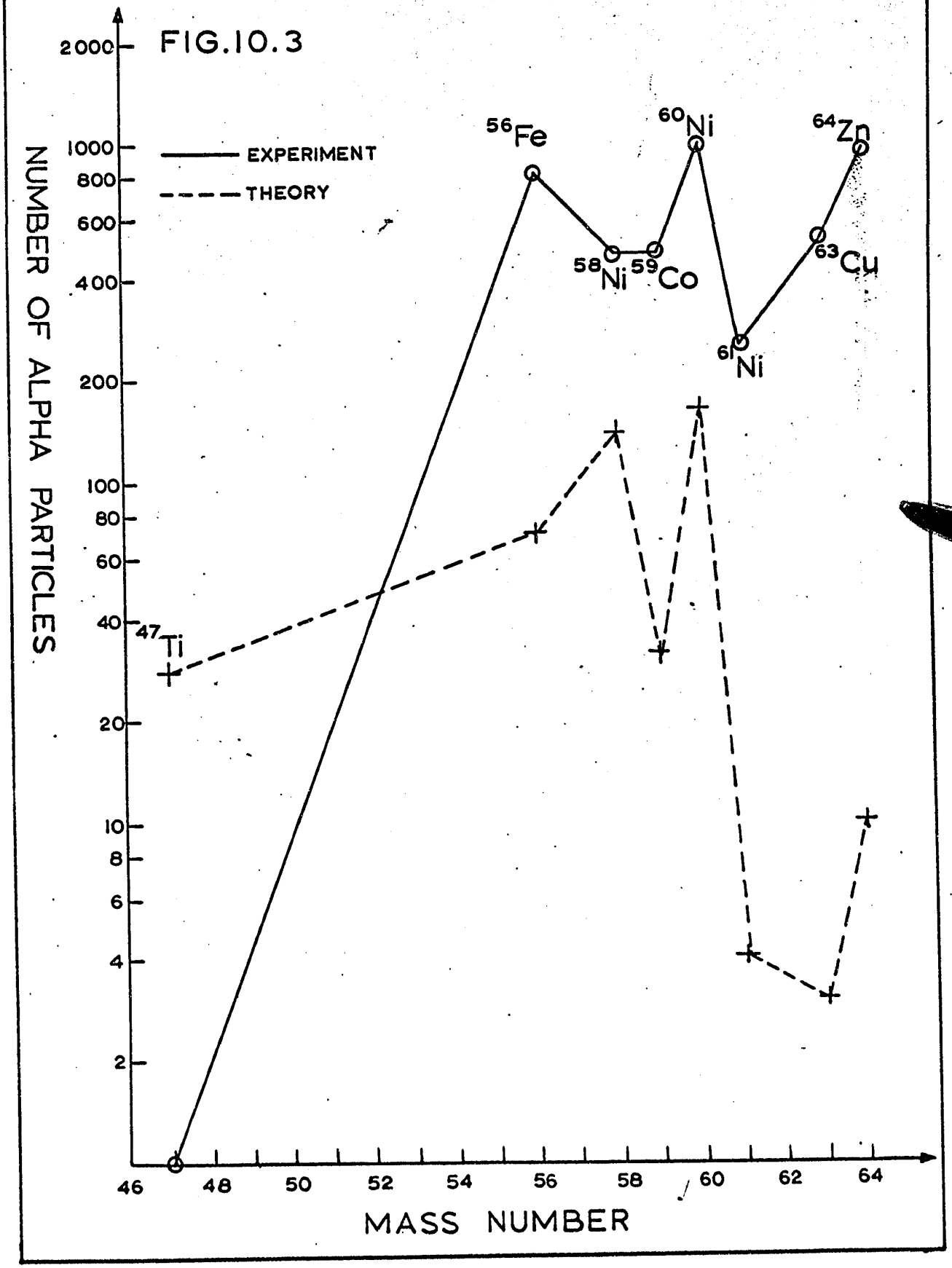

XI - DIRECT INTERACTION MODELS

11.1 Introduction.

Serious discrepancies between the experimental data and the statistical theory were noted in Chapter X. The disagreement was much too large to be accounted for by the experimental uncertainties. This suggests that direct interaction processes play an important role in the transitions to low-lying levels in the residual nucleus. A nuclear reaction is said to be "direct", when the process is completed in a time interval which is comparable to the transit time of the incident particle through the nucleus. The formation of a compound nucleus does not take place and the configuration in the outgoing channel depends strongly on the conditions in the incoming channel. At the present, it is not possible to make accurate predictions of absolute direct reaction cross sections. One or more parameters appear in the final formulae. These cannot be deduced from first principles and are adjusted to make the theoretical curve fit the experimental data.

It will first be shown that the variation of

the ground state transition cross section with target nucleus is in fair agreement with what is anticipated on the ground of a simple pick-up theory.

Next the absolute ground state transition cross section will be calculated for a pick-up process, taking the following approach: the target nucleus is supposed to always present itself in a "^{3}He + core" configuration. The effect of nuclear spins is almost entirely neglected. This calculation gives too large a cross section. It will then be shown that the discrepancy between theory and experiment can roughly be accounted for by the simplifying assumptions.

Finally a plane wave Born approximation calculation, incorporating exchange effects, is introduced. This treatment is similar to the previous one, but here the possibility of "heavy particle stripping" is considered, and the nuclear spins are taken into account. It is shown that reasonable cross sections and angular distributions are obtained for certain values of the adjustable parameters. Distorted wave Born approximation fits were not attempted, because experimental angular

distribution data are not available.

11.2 The successive nucleon pick-up model.

Bayman et al. have attempted to interpret the relative intensities of the ground state transition peaks of (p,α) reactions for even and odd Z targets by means of a simple pick-up mechanism, in which the three constituents of the triton are successively picked-up from the target nucleus (Bayman 1962).

This picture will now be applied to the (n,α) process, in which two protons and one neutron must be picked up. These three nucleons together form a ^{3}He nucleus.

One assumes that the Z' protons outside closed shells are in the state of lowest seniority of the configuration $j_p^{Z'}$. This means that the seniority is zero ($s_p = 0$) for even Z nuclei, and $s_p = 1$ for odd Z nuclei. Similarly $s_n = 0$ and 1 for even and odd N nuclei.

The result of a Born approximation can then be written:

$$\frac{d\sigma(\text{gr.st.})}{d\Omega} = \frac{V_f}{V_i} S \left| \int_R^\infty u_p^2(r) u_n(r) j_\ell(qr) r^2 dr \right|^2 \qquad (11.1)$$

PICK-UP MODEL FOR (n, α) PROCESS.
THE MOMENTUM TRANSFERS.

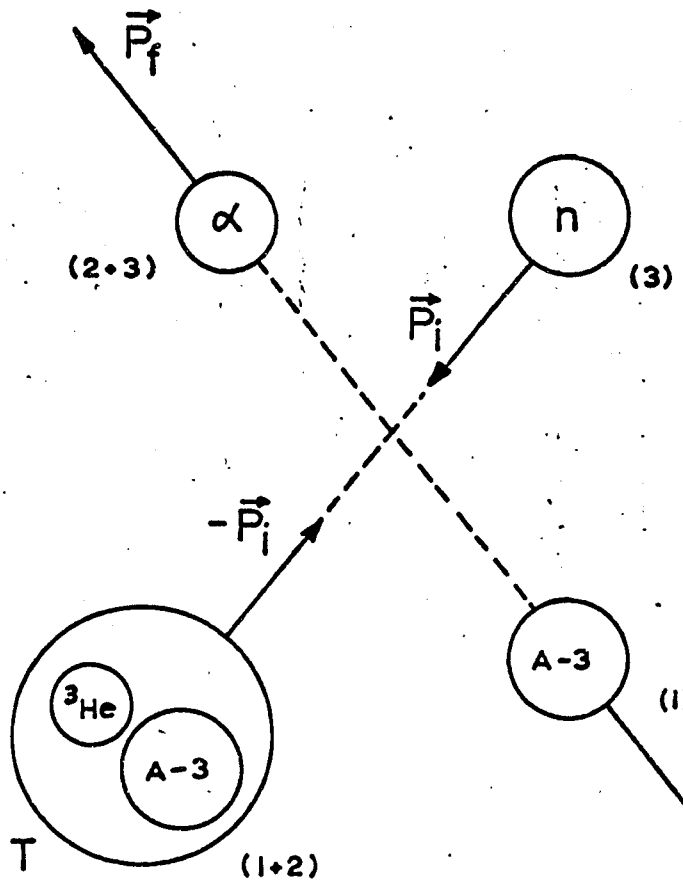

BRACKETED NUMBERS PERTAIN TO SECTION 11.4

FIG. 11.1

V_f and V_i stand for the initial and final relative velocities of the components of the system. R is the interaction radius and $u_n(r)$ and $u_p(r)$ are the radial wave functions of the picked-up protons and neutron. $j_\ell(qr)$ is the spherical Bessel function of order ℓ. $\vec{q}$ is the momentum transfer vector and S is the spectroscopic factor.

$$\frac{V_f}{V_i} = \left(\frac{M_n}{M_\alpha}\frac{E'_\alpha}{E_n}\right)^{\frac{1}{2}}\left(1 + \frac{M_\alpha}{M_R}\right) \qquad (11.2)$$

M_n, M_α and M_R are the masses of the neutron, the alpha particle and the residual nucleus. E_n and E'_α are the neutron laboratory energy and the centre of mass energy of the alpha particle.

The momentum transfer $\vec{q}\hbar$ to the residual nucleus is equal to the sum of the momentum changes of the neutron and the ^{3}He nucleus.

In Table 11.1 the momentum changes are calculated from Fig. 11.1, in which the kinematics of the reaction is illustrated.

Table 11.1

Particle	Initial momentum (*)	Final momentum (*)	Momentum change (*)
n	$\vec{P}_i$	$\frac{M_n}{M_\alpha}\vec{P}_f$	$\frac{M_n}{M_\alpha}\vec{P}_f - \vec{P}_i$

(*) In centre of mass coordinates

^{3}He	$-\frac{M_{^3He}}{M_T}\vec{P}_i$	$\frac{M_{^3He}}{M_\alpha}\vec{P}_f$	$\frac{M_{^3He}}{M_\alpha}\vec{P}_f+\frac{M_{^3He}}{M_T}\vec{P}_i$

From Table 11.1:

$$\vec{q}\hbar = \frac{M_n + M_{^3He}}{M_\alpha}\vec{P}_f + \left(\frac{M_{^3He}}{M_T} - 1\right)\vec{P}_i$$

or $$\vec{q}\hbar \simeq \vec{P}_f - \frac{M_T - M_{^3He}}{M_T}\vec{P}_i$$

Putting $\vec{P}_f = \vec{k}_f\hbar$

$\vec{P}_i = \vec{k}_i\hbar$

it follows that $$\vec{q} \simeq \vec{k}_f - \frac{A-3}{A}\vec{k}_i \qquad (11.3)$$

It should be noted that $\frac{d\sigma}{d\Omega}$ depends on the angle between the reaction products through $\vec{q}$.

The spectroscopic factor S is proportional to the product of the probabilities for pick-up of each of the two protons and neutron, such that the residual nucleus remains in the ground state. It can be deduced from shell theory (Macfarlane 1960), that if the outer shell is occupied by n particles (the expressions are valid for both neutrons and protons), then

$$S(n \to n-1) = n \quad \text{for n even} \qquad (11.4)$$

and

$$S(n \to n-1) = 1 - \frac{n-1}{2j+1} \quad \text{for n odd} \qquad (11.5)$$

where j is the nucleon angular momentum in that shell.

One can see in a qualitative way that (11.4) and (11.5) are valid.

When n is even, all particles in the shell are coupled together in pairs, such that the resultant angular momentum and also the seniority are zero. If one nucleon is picked up, one pair must be broken. The uncoupled nucleon gives rise to a state with $s = 1$, which is by definition the ground state (the state with lowest seniority). Any of the n nucleons gives rise to the same situation when picked up, and therefore the cross section for the ground state transition will be proportional to n: $S = n$.

For odd n the seniority in the shell is $s = 1$. The picked-up particle can either be the uncoupled nucleon, or alternatively one of the pairs can be broken. Since the latter operation increases the seniority in the shell, it is the pick-up of the isolated nucleon, yielding $s = 0$, which gives

rise to the ground state transition. There is only one uncoupled particle available, but $\frac{1}{2}(n - 1)$ coupled pairs. The ground state transition hence becomes less probable with increasing n. Equation (11.5) displays this property, S being a decreasing function factor of n.

The spectroscopic factors for ^{3}He pick-up from even-even, odd-even and even-odd targets (S_{EE}, S_{OE} and S_{EO} respectively) will now be evaluated.

In each case

$$S = S(p_1)\, S(p_2)\, S(n) \qquad (11.6)$$

where p_1, is the first and p_2 the second picked-up proton.

i) S_{EE}

First a proton is picked up from a shell containing Z' protons. (Z' is even).

$S(p_1) = Z'$

The second proton is picked up from shell containing Z' - 1 protons

$$S(p_2) = 1 - \frac{Z' - 2}{2j_p + 1}$$

(j_p is the angular momentum in the last proton shell).

The spectroscopic factor for picking up one neutron from a shell containing N' neutrons (N' is even) is:

$$S(n) = N'$$

Finally

$$S_{EE} = Z'N' \frac{2j_p - Z' + 3}{2j_p + 1} \qquad (11.7)$$

ii) S_{EO}

$$S(p_1) = Z'$$

$$S(p_2) = 1 - \frac{Z' - 2}{2j_p + 1}$$

$$S(n) = 1 - \frac{N' - 1}{2j_n + 1}$$

j_n is the angular momentum in the last neutron shell.

$$S_{EO} = Z' \frac{2j_p - Z' + 3}{2j_p + 1} \frac{2j_n - N' + 2}{2j_n + 1} \qquad (11.8)$$

iii) S_{OE}

$$S(p_1) = 1 - \frac{Z' - 1}{2j_p + 1}$$

$$S(p_2) = Z' - 1$$

$$S(n) = N'$$

$$S_{OE} = (Z' - 1) N' \frac{2j_p - Z' + 2}{2j_p + 1} \qquad (11.9)$$

11.3 Agreement of the successive nucleon pick-up model with experiment.

The variation of the ground state cross section for various nuclei will now be calculated from (11.1), assuming that the value of the radial integral remains constant. This sweeping assumption is obviously unrealistic. The error might be somewhat reduced by comparing the ground state transition cross sections for nuclei which fill up the same neutron shell on one hand and the same proton shell on the other hand.

One also stipulates that both protons are picked up from one shell in all nuclei. This requires that the last unfilled proton shell contains at least 2 protons. In view of these restrictive conditions, equation (11.1) can only be applied to the following nuclides for which experimental cross sections were obtained: ^{56}Fe, ^{58}Ni, ^{59}Co, ^{60}Ni and ^{61}Ni.

The variation of the cross section as given by (11.1) is almost exclusively due to the spectroscopic factor if the integral is taken to remain constant. $(\frac{Vf}{Vi}$ indeed only varies from 0.51 to 0.58

for the 5 above mentioned nuclei). Their shell occupation scheme is given in Table (11.2)

Table 11.2

Nuclide	Z	N	proton shell	neutron shell
^{56}Fe	26	30	$(1f_{7/2})^6$	$(2p_{3/2})^2$
^{58}Ni	28	30	$(1f_{7/2})^8$	$(2p_{3/2})^2$
^{59}Co	27	32	$(1f_{7/2})^7$	$(2p_{3/2})^4$
^{60}Ni	28	32	$(1f_{7/2})^8$	$(2p_{3/2})^4$
^{61}Ni	28	33	$(1f_{7/2})^8$	$(2p_{3/2})^3(1f_{5/2})^2$

Bayman et al. assumed that the neutrons start filling the $1f_{5/2}$ shell after having completed the $1f_{7/2}$ shell. This brings more consistency into their results. It is assumed here that the $2p_{3/2}$ shell fills up after completion of the $1f_{7/2}$ shell, which is a more natural sequence.

Fig. 11.2 shows in dashed line the variation of equation 11.1 for the various nuclides. The results are normalized with respect to the experimental value for ^{58}Ni. The experimental curve is

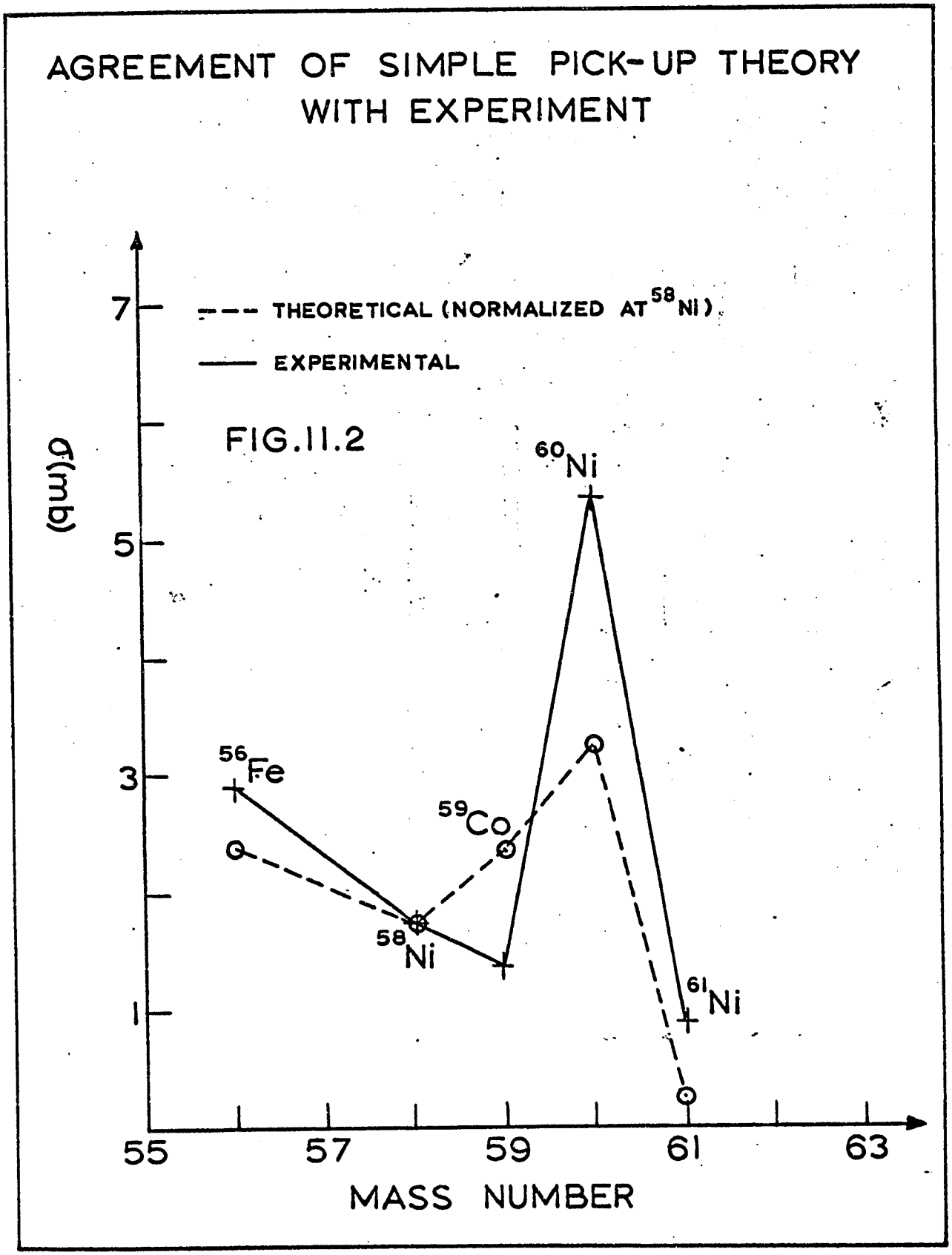
AGREEMENT OF SIMPLE PICK-UP THEORY WITH EXPERIMENT
THEORETICAL (NORMALIZED AT 58Ni)
EXPERIMENTAL
FIG.11.2
σ(mb)
7
5
3
1
56Fe
59Co
58Ni
60Ni
61Ni
55
57
59
61
63
MASS NUMBER

drawn in full line.

It can be seen that the shapes of the experimental and theoretical curves are in good agreement, although the variations of the experimental values are more pronounced.

An explanation must still be found for the low yield from tin, antimony and lead and for the lack of structure in the silver spectrum.

The shell structure of ^{107}Ag and ^{109}Ag is similar to that of ^{103}Rh for which good experimental data were obtained (Table 11.3).

Table 11.3

Nuclide	Z	N	proton shell	neutron shell
^{103}Rh	45	58	$(2p_{1/2})^1(1g_{9/2})^6$	$(1g_{7/2})^2$
^{107}Ag	47	60	$(2p_{1/2})^1(1g_{9/2})^8$	$(1g_{7/2})^4$
^{109}Ag	47	62	$(2p_{1/2})^1(1g_{9/2})^8$	$(1g_{7/2})^6$

All three nuclides in Table 11.3 possess one proton in the $2p_{1/2}$ shell, whereas the $1g_{9/2}$ shell contains in all cases an even number of protons. The incoming neutron can pick up two protons by

either capturing the unpaired proton in the $2p_{1/2}$ shell and then breaking a pair in the $1g_{9/2}$ shell, or by picking up a pair out of the $1g_{9/2}$ shell without interacting with the $2p_{1/2}$ proton. The ground state of the residual nucleus can only be reached through the former process, the latter giving rise to various excitations. Because of the competition between these two processes, the intensity of the ground state transition is considerably reduced. It can be seen from Fig. 9.7 that the "ground state peak" for ^{103}Rh is very broad and that various excitations probably contribute to it.

The ^{107}Ag and ^{109}Ag isotopes, each having about 50% relative abundance, give rise to a spectrum without definite structure. Here too an unpaired proton occupies the $2p_{1/2}$ shell, and sharply resolved ground state peaks might therefore not be expected. The over-all yield from silver is somewhat less than for rhodium.

It is interesting to note in this context that ^{63}Cu (Fig. 9.12) also shows a broad and ill-resolved ground state peak. The proton configuration

of ^{63}Cu which is $(1f_{7/2})^8(2p_{3/2})^1$, suggests that the explanation for this should be sought along the same lines as for ^{103}Rh.

The yields for tin and antimony are so low, one cannot speak of proper spectra. Chatterjee has noted in a survey of experimental data that the total (n,α) cross sections are very low when the Z-number of the residual nucleus is close to 50. (Chatterjee 1964 B). He was able to justify this trend by means of the statistical theory, using a shell-dependent form of the level density (Ericson 1960). One also expects, on the other hand, a low direct interaction yield near Z = 50: the energy gap between neighbouring shells at Z = 50 is considerably larger than for Z = 20 or 28 (Elliott 1957). It is therefore difficult to break the $1g_{9/2}$ shell. The energy gaps at the magic numbers 82 and 126 are even larger. It is not surprising that the direct interaction yield for ^{208}Pb (Z = 82 and N = 126) was found to be extremely low. Also the statistical theory predicts a low cross section for lead in view of the large coulomb barrier.

11.4 Pick-up of a preformed ^{3}He cluster.

In this approach one supposes that the target nucleus consists of a ^{3}He cluster bound to a core. If these constituents are respectively denoted by 2 and 1, and if 3 represents the incident neutron, the (n,α) reaction can be described in terms of the pick-up of particle 2 by 3.

$(1 + 2) + 3 \rightarrow 1 + (2 + 3)$

Neglecting spins and using the Born approximation, Banerjee obtains the following expression for the cross section: (Banerjee 1960).

$$\frac{d\sigma}{d\Omega} = \frac{4\mu_i\mu_f}{\hbar^4}\frac{P_f}{P_i}\left(\varepsilon_{12} + \frac{q_1^2\hbar^2}{2\mu_{12}}\right)^2 (2\ell_{23} + 1)R_1^2(q_1)R_3^2(q_3) \qquad (11.10)$$

$\vec{P}_i$ and $\vec{P}_f$ are the centre of mass momenta in the ingoing and outgoing channels, ε_{12} is the binding energy of the ^{3}He cluster in the target nucleus and ℓ_{23} is the relative orbital angular momentum of the neutron and ^{3}He in the emerging alpha particle.

$$\frac{1}{\mu_i} = \frac{1}{M_1 + M_2} + \frac{1}{M_3} \qquad (11.11)$$

$$\frac{1}{\mu_f} = \frac{1}{M_1} + \frac{1}{M_2 + M_3} \qquad (11.12)$$

$$\frac{1}{\mu_{12}} = \frac{1}{M_1} + \frac{1}{M_2} \qquad (11.13)$$

$\vec{q}_1\hbar$ and $\vec{q}_3\hbar$ are the momentum transfers associated with particles 1 and 3. From Fig. 11.1 one deduces that

$$\vec{q}_1\hbar = -\vec{P}_f + \frac{M_1}{M_1 + M_2}\vec{P}_i \qquad (11.14)$$

$$\vec{q}_3\hbar = \frac{M_3}{M_2 + M_3}\vec{P}_f - \vec{P}_i \qquad (11.15)$$

The integrals $R_1(q_1)$ and $R_3(q_3)$ are given by:

$$R_1(q_1) = \int_0^\infty r_{12}^2 \phi_{12}(r_{12}) j_{\ell_{12}}(q_1 r_{12}) dr_{12} \qquad (11.16)$$

$$R_3(q_3) = \int_0^\infty r_{23}^2 \phi_{23}^*(r_{23}) j_{\ell_{23}}(q_3 r_{23}) dr_{23} \qquad (11.17)$$

r_{12} and r_{23} are the relative coordinates of the particles in the bound systems.

ϕ_{12} and ϕ_{23} are the radial wave functions of the initial and final bound states.

$j_\ell(qr)$ is the spherical Bessel function of order ℓ. ϕ_{12} and ϕ_{23} are taken to be single particle wave functions in a harmonic oscillator potential well. Integrals R_1 and R_3 can then be evaluated.

The radial harmonic oscillator wave functions have the form,

$$\phi_{n\ell} = \frac{1}{r} N_{n\ell} \exp(-1/2\nu r^2) r^{\ell+1} v_{n\ell}(r) \qquad (11.18)$$

$v_{n\ell}(r)$ is an associated Laguerre polynomial and $N_{n\ell}$ a normalization constant. The frequency of the oscillator is found from the relation (Roy 1967):

$$\nu \simeq \frac{41M}{\hbar^2 A^{1/3}} \qquad (11.19)$$

M is the mass of the particle in the well.

The value of ℓ is fixed by the requirements for conservation of spin and parity. n is dictated by the number of particles in the well (The cluster will form in a partially filled shell).

When ϕ_{12} and ϕ_{23} are known, (11.16) and (11.17) can be evaluated and substituted into (11.10). The total (n,α) cross section σ(n,α) can then be calculated:

$$\sigma(n,\alpha) = \int \frac{d\sigma}{d\Omega}\, d\Omega \qquad (11.20)$$

11.5 Agreement of the cluster pick-up mechanism with experiment.

The calculation will be carried out for the target nucleus ^{58}Ni. ϕ_{12} describes the motion of a ^{3}He nucleus around ^{55}Fe in ^{58}Ni. The spins and parities of the three particles are:

$^{3}He : 1/2^{+}$; $^{55}Fe : 3/2^{-}$; $^{58}Ni : 0^{+}$

It is clear that a $1/2^+$ state and a $3/2^-$ state can only combine to 0^+ if $\ell_{12} = 1$. Moreover n = 2 because both the proton and neutron numbers are comprised between 20 and 40 in ^{58}Ni. This yields:

$$\phi_{12} = \left(\frac{2}{\pi}\right)^{\frac{1}{4}} \left(\frac{5}{3}\right)^{\frac{1}{2}} \nu_2^{5/4} \left(r_{12} - 2/5\nu_2 r_{12}^3\right)\exp\left(-\tfrac{1}{2}\nu_2 r_{12}^2\right) \tag{11.21}$$

where ν_2 is the frequency of the oscillator. Similarly $\ell_{23} = 0$ and:

$$\phi_{23} = \left(\frac{2}{\pi}\right)^{\frac{1}{4}} \nu_3^{3/4} \exp\left(-\tfrac{1}{2}\nu_3 r_{23}^2\right) \tag{11.22}$$

One finally obtains:

$$\frac{d\sigma}{d\Omega} = 3.03 \times 10^{-27} \left(17.7 + 0.732 \times 10^{-25} q_1^2\right)^2 I_1^2 I_3^2 \tag{11.23}$$

$$I_1 = \int_0^\infty \left(u^3 - \frac{2u^5}{5}\right)\exp\left(-\frac{u^2}{2}\right) j_1(k_1 u)\,du \tag{11.24}$$

$$I_3 = \int_0^\infty v^2 \exp\left(-\frac{v^2}{2}\right) j_0(k_3 v)\,dv \tag{11.25}$$

$$k_1 = q_1/\nu_2^{\frac{1}{2}}\,, \quad k_3 = q_3/\nu_3^{\frac{1}{2}}$$

q_1 should be expressed in cm^{-1} in (11.23), to find $\frac{d\sigma}{d\Omega}$ in cm^2/stér.

A computer program which uses expressions

(11.14), (11.15), (11.23), (11.24) and (11.25) to evaluate (11.20) has been written. The theoretical angular distribution is shown in Fig. 11.3. The ground state transition cross section (integrated over 4π) was found to be $\sigma(n,\alpha) = 1300mb$. If one adopts the shape of the angular distribution in Fig. 11.3, one finds an experimental ground state transition cross section of 1.1 mb from the experimental data, by carrying out a similar calculation as in section 9.3.

The fact that the pick-up of a preformed ^3He cluster gives rise to a cross section 1200 times too large, can be attributed to four causes:

i) The target nucleus will only consist of a ^3He cluster and a core for a part of the time, whereas the calculation has assumed a permanent cluster structure.

ii) The use of plane waves is unrealistic.

iii) The effects of spin were neglected.

iv) Harmonic oscillator eigenfunctions were chosen for the internal wave functions of the initial and final bound states for mathematical convenience and not for physical reasons.

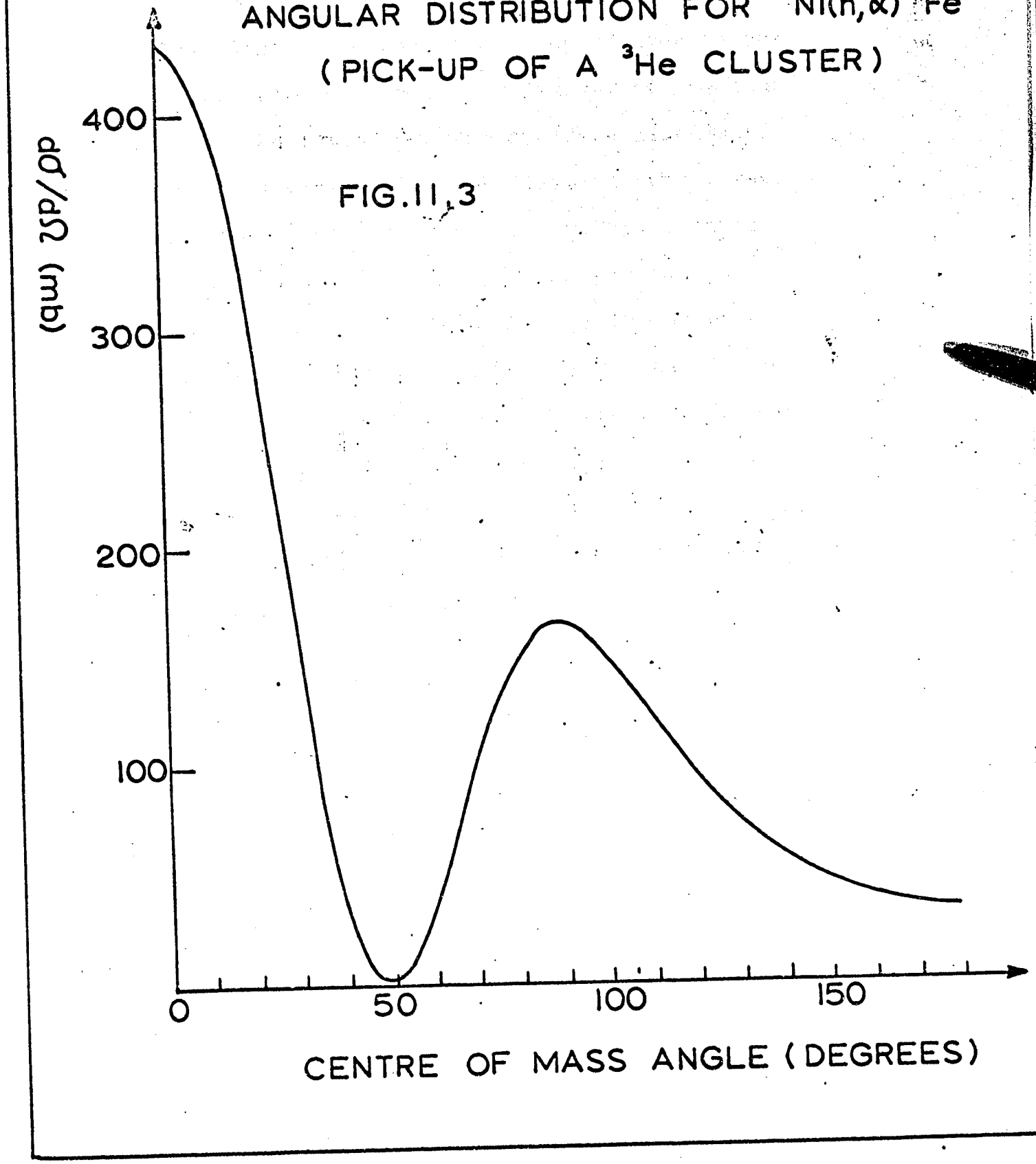
ANGULAR DISTRIBUTION FOR $^{58}Ni(n,\alpha)^{55}Fe$
(PICK-UP OF A ^{3}He CLUSTER)
FIG.11.3
(mb) $\partial\sigma/\partial\Omega$
400
300
200
100
0
50
100
150
CENTRE OF MASS ANGLE (DEGREES)

The first point will be commented upon by outlining the method by which the "amount of ^{3}He clustering" in the target nucleus could be calculated.

In the isotopic spin formalism the total wave function for a nucleus with mass number A can be written $\Psi(\xi;1,\ldots,A)$, where the A nucleons are indistinguishable. ξ groups all quantum numbers which characterize the ground state of the nucleus. Ψ is antisymmetric with respect to the interchange of all coordinates of two nucleons.

The wave function Ψ can be expanded in terms of a set of functions $\phi_n(\xi;A-m,m)$, each ϕ_n representing a different partition of the nucleus in two clusters, containing respectively A-m and m nucleons.

$$\Psi(\xi;1,\ldots,A) = \sum_n a_n \phi_n(\xi;A-m,m) \qquad (11.26)$$

All possible partitions must be included in order that the ϕ_n constitute a complete set. If they are not orthogonal they can be transformed into an orthonormal set by the Schmidt orthogonalization process (Mandl 1957). The sum over n represents a sum over all possible values of m and it is important to note that n takes a range of values for

each m. For instance when m = 1, the one nucleon "cluster" can be a neutron or a proton; m = 1 contributes therefore two terms to (11.26).

Writing ϕ_n in a more explicit form:

$$\phi_n(\xi;A-m,m) = \mathcal{A}\zeta_n^{(1)}(\xi_n^{(1)};A-m)\zeta_n^{(2)}(\xi_n^{(2)};m)\zeta_n^{(3)}(\xi_n^{(3)};\vec{r})\zeta_n^{(4)}(\xi_n^{(4)};\vec{R}) \tag{11.27}$$

$\zeta_n^{(1)}$ and $\zeta_n^{(2)}$ are the internal wave functions of the two clusters; $\zeta_n^{(3)}$ and $\zeta_n^{(4)}$ describe respectively the relative motion of the two clusters and the centre of mass motion of the nucleus. One is reminded by the symbol $\mathcal{A}$ that $\phi_n(\xi;A-m,m)$ must be antisymmetrized.

The expression

$$\xi_n^{(1)} + \xi_n^{(2)} + \xi_n^{(3)} + \xi_n^{(4)} \dashrightarrow \xi \tag{11.28}$$

expresses symbolically that the quantum numbers of the ζ_n combine to yield the set describing the ground state of the target nucleus.

If in the wave function $\phi_n(\xi;A-3,3)$, $\zeta_n^{(2)}(\xi_n^{(2)},3)$ corresponds to a ^{3}He cluster, the probability that the nucleus will assume this configuration is given by:

$$|a_n|^2 = |\langle\Psi(\xi;1,\ldots,A)|\phi_n(\xi;A-3,3)\rangle|^2 \tag{11.29}$$

Expression (11.29) is referred to as the square of an overlap integral. The evaluation of this overlap integral is difficult. The fact that $\Psi(\xi;1,\ldots,A)$ does in fact consist of a sum of various shell model configurations, each having a definite amplitude, complicates matters further. Hird and Li have calculated overlap integrals in the study of the $^{19}F(p,\alpha)^{16}O$ reaction (Hird 1968), but such lengthy calculations are not justified in the present context, where various drastic simplifications were introduced in the calculation of the cross section.

Hird and Li found a value of 0.1 for the square of the overlap integral measuring the probability of triton clustering in ^{19}F. The tendency towards ^{3}He clustering in ^{58}Ni is expected to be considerably less pronounced, in view of the following qualitative arguments:

a) ^{19}F contains one proton and two neutrons outside the closed magic $1p_{1/2}$ shells. Such a configuration is extremely favourable for triton cluster formation.

b) Z = 28 corresponds to the closure of the semi-magic $1f_{7/2}$ proton shell. One does not anticipate strong residual interactions of two components of this closed structure, with one of the two neutrons outside the closed $1f_{7/2}$ neutron shell.

By calculating the ^{3}He pick-up cross section and the overlap integral for each of the 5 nuclei appearing in Fig. 11.2, an absolute fit could be made to the experimental curve in that figure. It would be interesting to see whether the variation of the ground state transition cross section predicted by this calculation would agree better with experiment than the successive nucleon pick-up model. These calculations, however, would be very complicated and are outside the scope of this experimental project.

11.6 PWBA treatment combining pick-up and heavy particle stripping.

Warsh and Edwards have fitted the angular distribution of the ground state transition of the $^{19}F(p,\alpha)^{16}O$ reaction with a plane wave Born approximation treatment which considers the reaction as

a mixture of direct pick-up and pick-up with exchange (Warsh 1965). This treatment will be referred to as the PWBAE theory. Exchange pick-up is also known under the name heavy particle stripping.

Fig. 11.4 illustrates the above process applied to the (n,α) reaction. One assumes that the target nucleus T is found in the ground state in one of two configurations: it consists either of a ^{3}He particle and a component R, which is the residual nucleus of the (n,α) process, or it is made up of a core C bound to an alpha particle. Fig. 11.4(a) shows the direct pick-up mode which has already been discussed in section 11.4. The emerging alpha particle travels mainly in the forward direction. In the heavy particle stripping mode (Fig. 11.4(b)), the incident neutron picks up the core C from the target and the two components combine to form the residual nucleus R, which travels mainly forward. The remaining alpha particle recoils mainly in the backward direction.

The cross section formula obtained by these authors can be written:

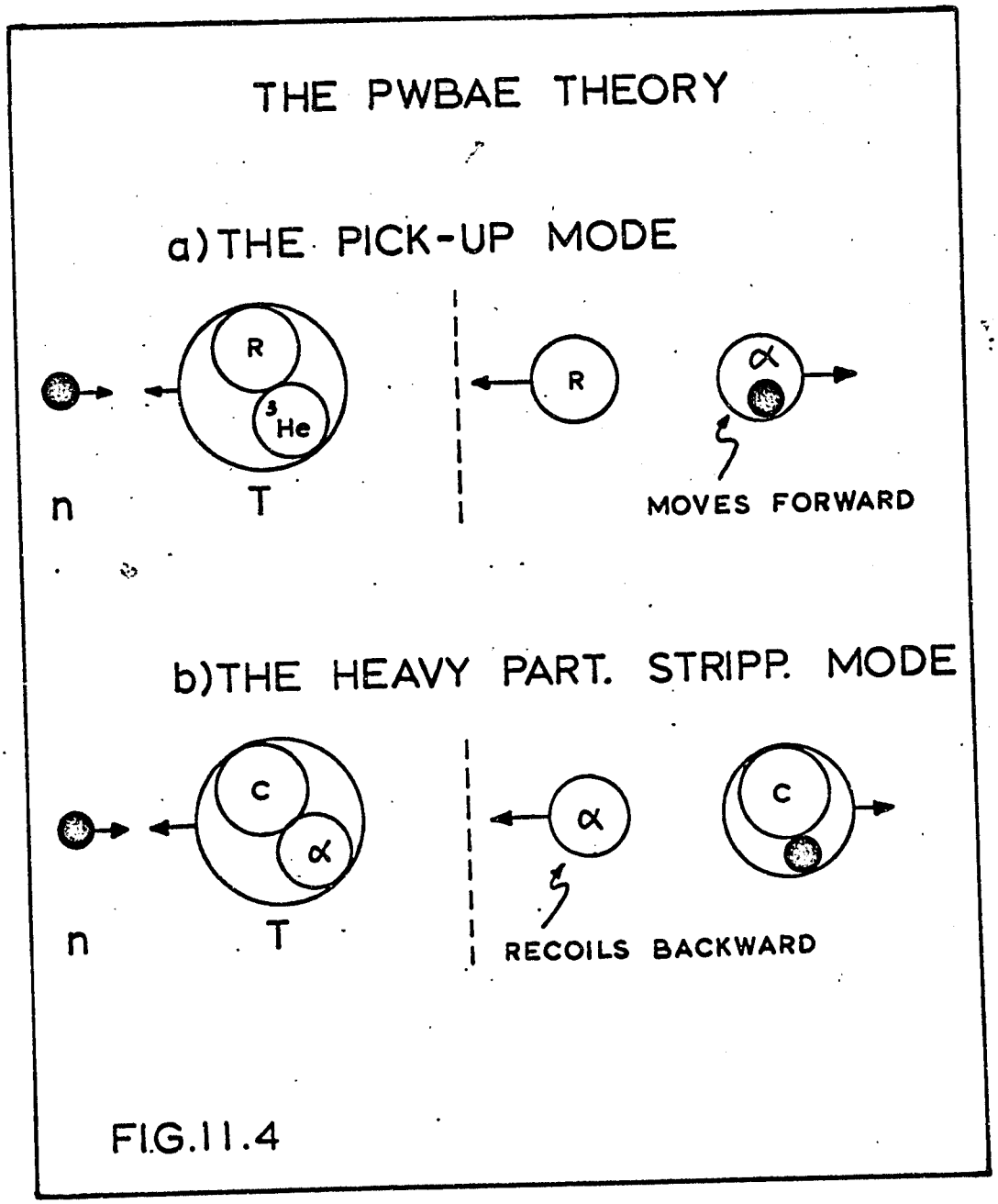
THE PWBAE THEORY
a) THE PICK-UP MODE
R
^{3}He
n
T
R
α
MOVES FORWARD
b) THE HEAVY PART. STRIPP. MODE
c
α
n
T
α
c
RECOILS BACKWARD

FIG.11.4

$$\frac{d\sigma}{d\Omega} = K\left|\Lambda_1^2 A(\theta) + \Lambda_2^2 B(\theta) - 2\Lambda_1\Lambda_2 C(\theta)\right| \qquad (11.30)$$

The three terms A, B and C respectively represent the direct pick-up contribution, the heavy particle stripping and the interference between the two mechanisms. θ is the angle between the incoming neutron and emitted alpha particle. The detailed expression for each term can be found in the original article. K is a constant.

Together with Λ_1 and Λ_2 four other variable parameters appear in (11.30): $A(\theta)$ depends on a_1 and R_1, $B(\theta)$ depends on a_2 and R_2 and $C(\theta)$ is a function of all 4 parameters. a_1, a_2, R_1 and R_2 are cut off radii in integrals containing radial wave functions. The values of the 6 variable parameters determine the relative importance of the direct and exchange pick-up mechanisms and the interference contribution.

A computer program was written to integrate equation (11.30) numerically for the case of ^{58}Ni.

One cannot speak of agreement between theory and experiment in this instance, because any experimental cross section value can be fitted with six

parameters. Fig. 11.5 shows four angular distributions obtained with the PWBAE treatment for four sets of parameters. Each of the four curves yields a total cross section of about 1.7 mb when integrated. When the direct pick-up dominates, the angular distribution is forward peaked; heavy particle stripping causes peaking at backward angles. It is interesting to note that an appropriate mixture of the two processes can give rise to an isotropic distribution.

It is clear that all direct interaction models which have been considered in this chapter will explain the data provided a suitable set of parameters is chosen. This is in contrast with the findings of the statistical theory.

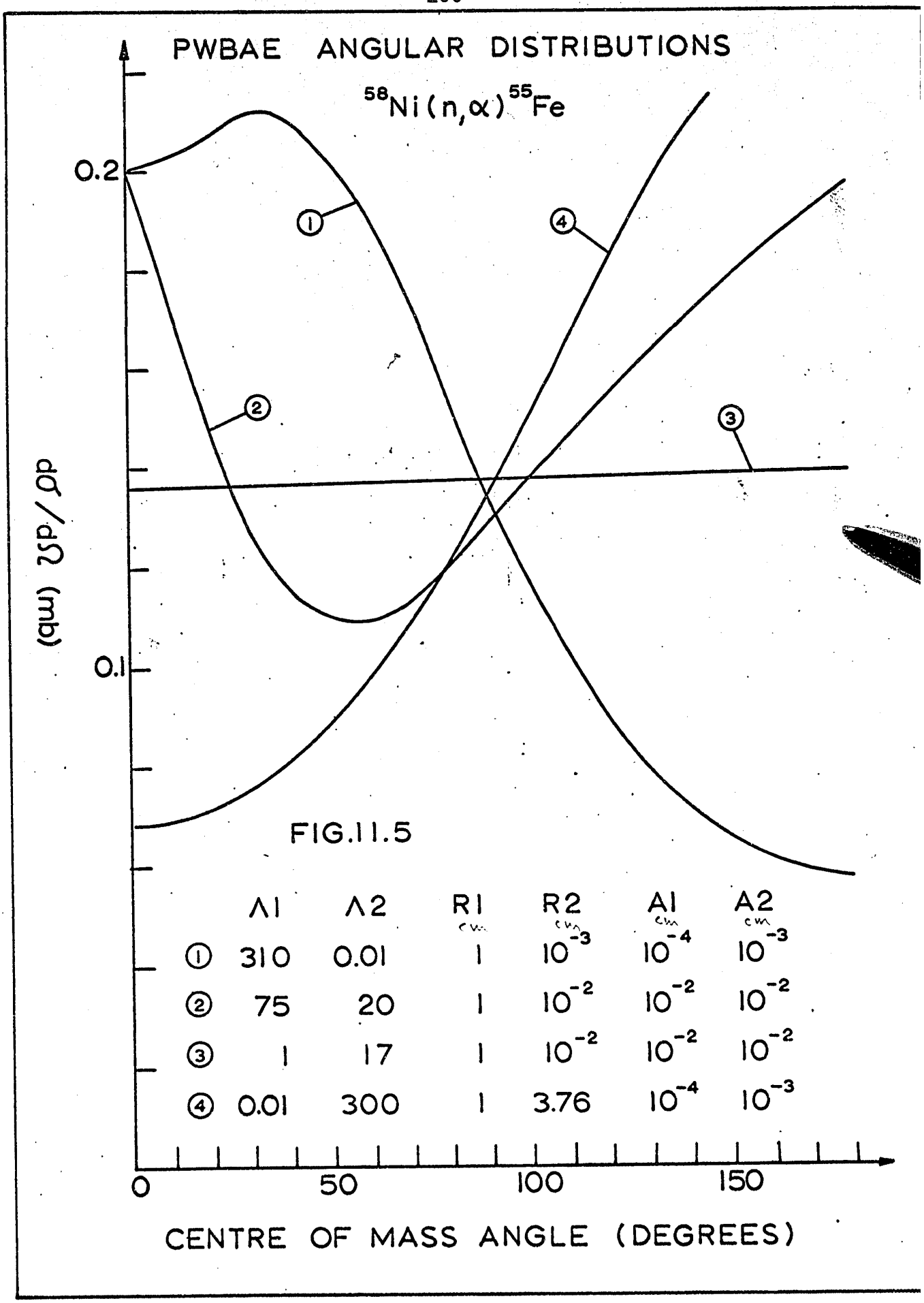

FIG.11.5

	A1	A2	R1 (cm)	R2 (cm)	A1 (cm)	A2 (cm)
①	310	0.01	1	10^{-3}	10^{-4}	10^{-3}
②	75	20	1	10^{-2}	10^{-2}	10^{-2}
③	1	17	1	10^{-2}	10^{-2}	10^{-2}
④	0.01	300	1	3.76	10^{-4}	10^{-3}

XII CONCLUSIONS

In this experimental study of (n,α) reaction spectra, transitions leading to the ground state of the residual nucleus, or to states close to the ground state, have been observed for eight isotopes: ^{58}Ni, ^{60}Ni, ^{61}Ni, ^{64}Zn, ^{56}Fe, ^{59}Co, ^{63}Cu and ^{103}Rh.

The intensities of these transitions are nearly always greater than the predictions of the statistical theory. As this points towards the presence of direct interaction effects, the data were examined in the light of various direct reaction theories.

The relative values of the ground state transition cross sections for five nuclei, which populate respectively the same outer neutron and proton shells (^{56}Fe, ^{58}Ni, ^{59}Co, ^{60}Ni and ^{61}Ni), agree well with a successive nucleon pick-up model.

The attempts to associate definite reaction mechanisms with the various transitions are handicapped by the fact that present direct interaction theories do not predict absolute cross sections well. They do however yield angular distributions, and it is unfortunate that these could not be

measured in this project. Nevertheless, the experimentally observed cross section for the ground state transition of the ^{58}Ni (n,α) ^{55}Fe reaction could be accounted for by means of two cluster pick-up models, by choosing appropriate parameters.

The observed peaks do not always correspond to transitions to a single level in the residual nucleus: sometimes two or more unresolved low-lying levels are involved. The use of targets with a thickness of 200 instead of 400 keV coupled to a reduction of the angular acceptance of the detecting system would improve the resolution and enable angular distributions to be attempted. It would however result in a lower signal to noise ratio and a slower data acquisition rate.

The final conclusion which one can draw from this work is that in (n,α) reactions initiated by 14.6 MeV neutrons, the intensities of transitions to low-lying levels in the residual nucleus are mainly determined by direct interaction processes.

POST-ORAL DISCUSSION

At the oral defence of this thesis, the need for an additional correction factor in the determination of the total neutron production was brought to light.

In section 4.3 the quantity N_n was computed assuming that the neutrons and alpha particles from the $^3H(^2H, n)^4He$ reaction are isotropically distributed in the laboratory system.

It will be shown below that this is a reasonable assumption for the neutrons. The alpha particles, however, are considerably forward peaked.

By monitoring the associated alpha particles at a backward angle of 176°, the neutron production is underestimated.

To evaluate the correction factor one supposes that all neutrons are produced at the centre of the tritium target. Denote by Y_{ni} the number of neutrons striking the sample target in the hypothesis that the emission is isotropic.

$$Y_{ni} = \tfrac{1}{2} (1 - \cos \theta_{max}) N_n$$

θ_{max} is the maximum angle between the deuteron beam and a neutron which still strikes the target.

The quantity Y_{na} for an anisotropic neutron distribution is given by:

$$Y_{na} = N_n \frac{\int_0^{\theta_{max}} \sigma_n(\theta) \sin\theta \, d\theta}{\int_0^{\pi} \sigma_n(\theta) \sin\theta \, d\theta}$$

Values for $\sigma_n(\theta)$, the differential cross section for neutron production in the laboratory system, can be found in Los Alamos Report LAMS-2162 (unpublished). One finds:

$$\frac{Y_{ni}}{Y_{na}} = 0.96$$

One also defines the alpha particle counts $Y_{\alpha i}$ and $Y_{\alpha a}$ in the associated particle detector. These quantities refer respectively to the isotropic and anisotropic distributions. The calculation yields:

$$\frac{Y_{\alpha i}}{Y_{\alpha a}} = 1.18$$

From

$$\frac{Y_{na}}{Y_{\alpha a}} = 1.23 \frac{Y_{ni}}{Y_{\alpha i}}$$

it follows that all cross sections in Table 9.2 must be divided by 1.23

APPENDIX

Mutual inductance of a solenoid and a coaxial circular filament.

Consider a right cylindrical solenoid of radius a and length x, wound with N' turns per cm (Fig.A.1a). Coaxial Concentric with the right hand end plane of the solenoid and at a distance Z of the latter, a circular loop of radius A is placed. The mutual inductance of the solenoid and the circular loop is the sum of two components, each involving a single end plane of the current sheet. If x is very large compared to Z, only the right end plane will contribute significantly. From electro-magnetic theory it follows then that the mutual inductance M(a,A) between solenoid and loop is equal to

$$\frac{M(a,A)}{4\pi N'} = \pi a^2 G(a \to A) \qquad (A.1)$$

where G(a→A) is the average solid angle subtended by A at a divided by 4π.

On the other hand it is shown by Grover (Grover 1946) that the mutual inductance of a right cylindrical solenoid (of radius a and length x) and a coaxial circular loop of radius A in its end plane

is equal to:

$$M(a,A) = 2\pi^2 a\alpha\rho N Q_o(\alpha,\rho^2) \qquad \text{(e.m. units)} \tag{A.2}$$

where $\alpha = \frac{a}{A}$, $\rho^2 = \frac{A^2}{A^2 + x^2}$ and N is the total number of turns ($N = N'x$). The values of Q_o are tabulated as a function of ρ^2 and α. (See also Fig. A.1.b). The last figure is a special case of the previous one with $Z = 0$. Moreover the value $M(a,A)$ for the case with $Z \neq 0$ can be claculated from (A.2) in the following way:

First calculate the mutual inductance M_2 of the right cylinder of length $(x + Z)$ having a winding density N' and the circular loop of radius A in its end plane. Then compute M_3, the mutual inductance of the right cylinder of length Z, having the same loop of radius A in its end plane. It follows that:

$$M(a,A) = M_2 - M_3 \tag{A.3}$$

From (A.2) and (A.3)

$$M(a,A) = \left[2\pi^2 a\alpha\ \rho_2 N_2 Q_o(\alpha,\rho_2^2) - \rho_3 N_3 Q_o(\alpha,\rho_3^2)\right] \tag{A.4}$$

Replacing ρ and α by their value and remembering

that:

$N_2 = N'(x + Z)$ and $N_3 = N'Z$ we obtain

$$M(a,A) = 2\pi^2 a^2 N' \left\{ \frac{Q_o(\alpha,\rho_2^2)}{\left[\left(\frac{A}{x+Z}\right)^2 + 1\right]^{\frac{1}{2}}} - \frac{ZQ_o(\alpha,\rho_3^2)}{[A^2 + Z^2]^{\frac{1}{2}}} \right\} \tag{A.5}$$

In order to substitute (A.5) into (A.1), the limit of (A.5) for large x must be taken, since (A.1) is only valid for a long solenoid.

$$M(a,A) = 2\pi^2 a^2 N' \left\{ Q_o(\alpha,o) - \cos\beta Q_o(\alpha,\rho_3^2) \right\}$$

$x \longrightarrow \infty$ (A.6)

where $\cos\beta = \frac{Z}{(Z^2+A^2)^{\frac{1}{2}}}$, $\rho_3^2 = \frac{A^2}{A^2+Z^2}$, and $Q_o(\alpha,o)=1$ according to Grover's table.

Substitution of (A.6) into (A.1) yields

$$G(a \to A) = \tfrac{1}{2}(1 - Q_o \cos\beta) \tag{A.7}$$

and one can show in a similar manner that

$$G(A \to a) = \tfrac{1}{2}\alpha^2(1 - Q_o \cos\beta) \tag{A.8}$$

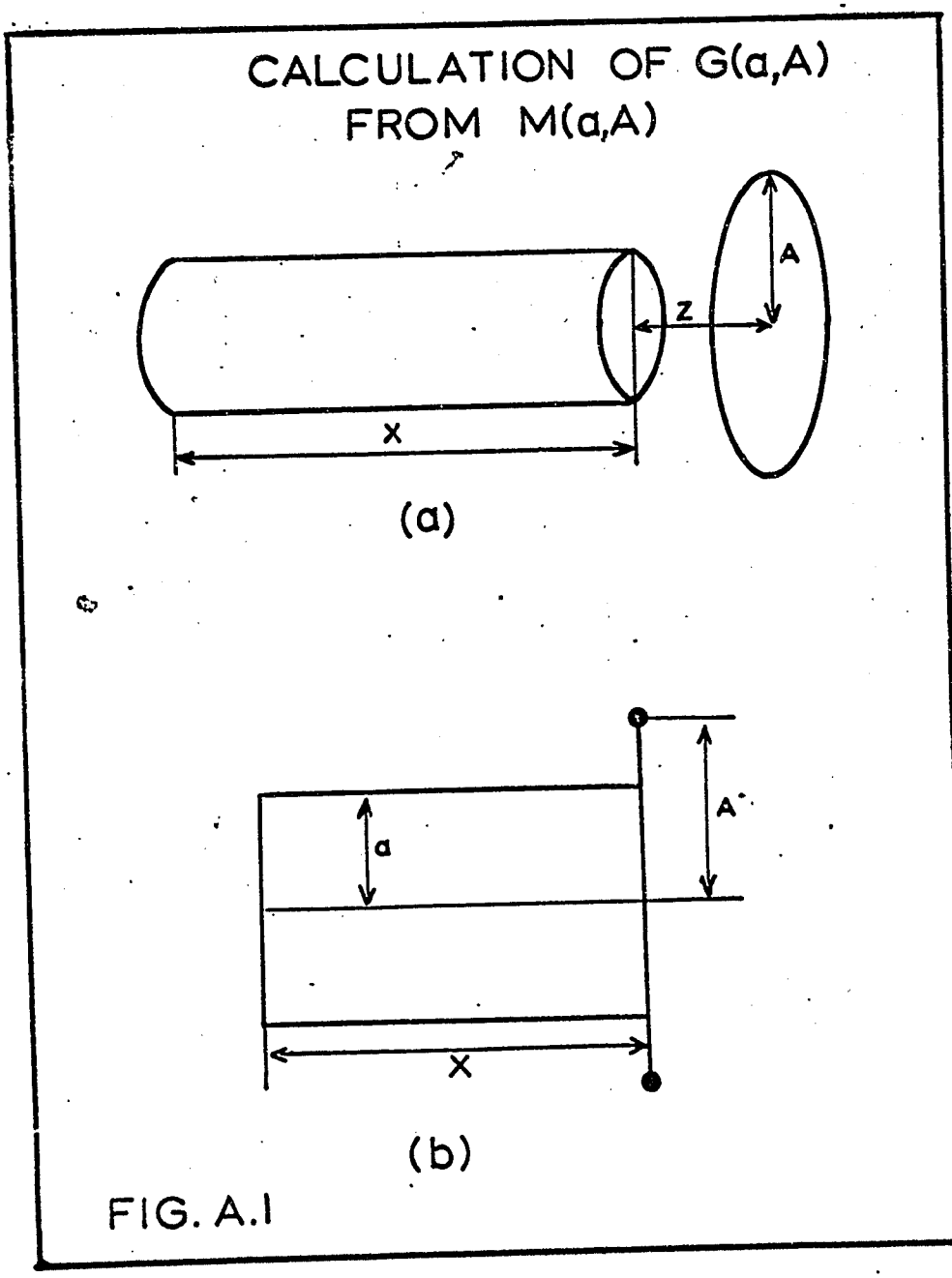

FIG. A.1

REFERENCES

AITKEN 1961 - J.H. Aitken, Nucl. Instrum. and Meth. 14 (1961) 343.

AITKEN 1965 - J.H. Aitken and W.R. Dixon, Nucl. Phys. 67 (1965) 395.

BANERJEE 1960 - M.K. Banerjee, Nuclear Spectroscopy Part B, Academic Press, 1960.

BAYMAN 1961 - B.F. Bayman, F.P. Brady and R. Sherr, Proceedings of the Rutherford Jubilee International Conference on Nuclear Physics, London Heywood, 1961.

BIZZETI 1962 - P.G. Bizzeti, A.M. Bizzeti-Sona and M. Bocciolini, Nucl. Phys. 36 (1962) 38.

BLATT 1952 - J.M. Blatt and V.F. Weisskopf, Theoretical Nuclear Physics. John Wiley & Sons, 1952.

BRISCOE 1958 - W.L. Briscoe, Rev. Sci. Instr. 29 (1958) 401.

CASHWELL 1959 - E.D. Cashwell and C.J. Everett, A Practical Manual on the Monte Carlo Method for Random Walk Problems.

CHASE 1961 A - R.L. Chase, W.A. Higinbotham and G.L. Miller, IRE NS8 (1961) 147.

CHASE 1961 B - R.L. Chase, Nuclear Pulse Spectrometry, McGraw-Hill, (1961) p.39 and foll.

CHATTERJEE 1964 A - A. Chatterjee, Nucleonics 22 (1964) 108.

CHATTERJEE 1964 B - A. Chatterjee, Phys. Rev. 134 (1964) B 374.

CINDRO 1961 - N. Cindro, I. Slaus, P. Tomas and B. Eman, Nucl. Phys 22 (1961) 96.

COLLI 1963 - L. Colli, I. Iori, M.G. Marcazzan and M. Milazzo, Nucl. Phys. 43 (1963) 529.

CUZZOCREA 1964 - P. Cuzzocrea and S. Notarrigo, Nucl. Phys. 55 (1964) 364.

DAVIS 1964 - E.A. Davis, T.W. Bonner, D.M. Worley Jr. and R. Bass, Nucl. Phys. 55 (1964) 643.

DE BENEDETTI 1958 - S. De Benedetti and R.W. Findley, Encyclopedia of Physics, Volume 45, Springer-Verlag (1958).

DOSTROVSKY 1959 - I. Dostrovsky, Z. Fraenkel and G. Friedlander, Phys. Rev. 116 (1959) 683.

ELLIOTT 1957 - J.P. Elliott and A.M. Lane, The Nuclear Shell Model, Encyclopedia of Physics, Volume 39, Springer-Verlag 1957, page 251.

ERICSON 1960 - T. Ericson, Advances in Phys. 9, (1960) 425, Sect. 3.6.

EVANS 1955 - R.D. Evans, The Atomic Nucleus, McGraw-Hill, (1955) p. 637 foll.

FACCHINI 1964 - U. Facchini, E. Saetta-Menichella, F. Tonolini and L. Tonolini-Severgnini Nucl. Phys. 51 (1964) 460.

FORTI 1966 - P. Forti, E. Gadioli and A. Marini, Nuovo Cimento B41 (1966) 52.

GABRIEL 1961 - R. Gabriel and A.M. Segar, Nucl. Instr. and Meth. 12 (1961) 307.

GARRETT 1954 - M.W. Garrett, Rev.Sci.Instr., 25 (1954) 1208.

GIANELLI 1960 - G. Gianelli and L. Stanchi, Nucl. Instr. and Meth., 8(1960) 79.

GILBERT 1965 - A. Gilbert and A.G.W. Cameron, Can. J. Phys., 43 (1965) 1446.

GLENDENNING 1962 - N.K. Glendenning, Nucl. Phys. 29 (1962) 109.

GLENDENNING 1965 - N.K. Glendenning, Phys. Rev. 137 (1965) B102.

GOLDSTEIN 1963 - H. Goldstein, Fast Neutron Physics Part II, Interscience Publishers, (1963), p. 1525.

GROVER 1946 - F.W. Grover, Inductance Calculations, D. Van Nostrand Company 1946, p.115.

HAUSER 1952 - W. Hauser and H. Feshbach, Phys. Rev. 87 (1952) 366.

HIRD 1968 - B. Hird and T.Y. Li, Can. J. Phys. 46 (1968) 1273.

HSU 1967 - Y.C. Hsu, C.Y. Huang and C.C. Chang, Nucl. Phys., A104, (1967) 677.

HUIZENGA 1962 - J.R. Huizenga and G. Igo, Nucl. Phys. 29 (1962) 462.

IRFAN 1963 - M. Irfan and W. Jack, Proc. Phys. Soc. 81 (1963) 800.

JERONYMO 1963 - J.M.F. Jeronymo, G.S. Mani, J. Olkowsky, A. Sadeghi and C.F. Williamson, Nucl. Phys. 47 (1963) 157.

JORDAN 1947 - W.H. Jordan and P.R. Bell, Rev. Sci. Instr. 18 (1947) 703.

KAUL 1962 - O.N. Kaul, Nucl. Phys. 29 (1962) 522.

KNELLWOLF 1966 - T. Knellwolf and J. Rossel, Helv. Phys. Acta 39 (1966) 376.

KÖNIG 1965 - V. König, Nucl. Phys. 71 (1965) 497.

KULISIC 1964 - P. Kulisic, V. Ajdacic, N. Cindro, B. Lalovic and P. Strohal, Nucl. Phys. 54 (1964) 17.

KUMABE 1957 - I. Kumabe, Phys. Rev. 106 (1957) 155.

LAMOT 1967 - G.H. Lamot, C. Fayard, J.W. Massot, E. El-Baz and J. Lafoucrière, Nucl. Phys. **A99 (1967)** 633.

LILLIE 1952 - A.B. Lillie, Phys. Rev. 87 (1952) 716.

MACDONALD 1962 - N. MacDonald, Nucl. Phys. 33 (1962) 110.

MACFARLANE 1960 - H.H. Macfarlane and J.B. French, Rev. Mod. Phys. 32 (1960) 567.

MANDL 1957 - F. Mandl, Quantum Mechanics, Academic Press Inc. (1957) Section 3.

MARCAZZAN 1961 - G.M. Marcazzan, E-Manichella-Saetta and F. Tonolini, Nuovo Cimento 20 (1961) 903.

MARCAZZAN 1963 - G.M. Marcazzan, F. Tonolini and L. Zetta, Nucl. Phys. 46 (1963) 51.

MASSOT 1964 - J.N. Massot, E. El-Baz and J. Lafoucrière, Nucl. Phys. 58 (1964) 273.

MATTAUCH 1965 - J.H.E. Mattauch, W. Thiele and A.H. Wapstra, Nucl. Phys. 67 (1965) 1.

MAXSON 1968 - D.R. Maxson, R.D. Murphy and M.R. Zatzick, Nucl. Phys. A110 (1968) 609.

MCDICKEN 1966 - W.N. McDicken and W. Jack, Nucl. Phys. 88 (1966) 457.

MORGENSTERN 1966 - H. Morgenstern, O. Hilscher and J. Scheer, Nucl. Phys. 83 (1966) 369.

NEWTON 1956 - T.D. Newton, Can. J. Phys. 34 (1956) 804.

PAUL 1953 - E.B. Paul and R.L. Clarke, Can J. Phys. 31 (1953) 267.

PEARLSTEIN 1965 - S. Pearlstein, Nucl. Sci. Eng. 23 (1965) 238.

RIBE 1956 - F.L. Ribe, Phys. Rev. 103 (1956) 741.

ROSEN 1965 - L. Rosen, J.C. Beery and A.S. Goldhaber Ann. of Phys. (New York) 34 (1965) 96.

ROY 1967 - R.R. Roy and B.P. Nigam, Nuclear Physics Theory and Experiment, John Wiley and Sons (1967) Chapter 7.

RUBBINO 1966 - A. Rubbino and D. Zubke, Nucl. Phys. 85 (1966) 606.

SEEBECK 1965 - U. Seebeck and M. Bormann, Nucl. Phys. 68 (1965) 387.

SHAMU 1962 - R.E. Shamu, Nucl. Phys. 31 (1962) 166.

SHAPIRO 1953 - M.M. Shapiro, Phys. Rev. 90 (1953) 171.

SLINN 1963 - W.G. Slinn and J.M. Robson, Can.J.Phys. 41 (1963) 545.

SWENSON 1964 - L.W. Swenson, Nucl. Instr. and Meth. 31 (1964) 269.

VALKOVIC 1965 - V. Valkovic, G. Paic, I. Slaus, P. Tomas and M. Cerineo, Phys. Rev. B139 (1965) 331.

WARSH 1965 - K.L. Warsh and S. Edwards, Nucl. Phys. 65 (1965) 382.

WAUGH 1960 - J.B.S. Waugh and R.W. Nicholson, Nucleonics 18 (1960) 70.

WEISSKOPF 1937 - V.F. Weisskopf, Phys. Rev. 52 (1937) 295.

WILLIAMSON 1966 - C.F. Williamson, J.P.Boujot and J. Picard, Report CEA-R3042 (France) 1966.

YU 1967 - Yu-Wen Yu and D.G. Gardner, Nucl. Phys. A98 (1967) 451.

CURRICULUM VITAE

NAME: Charles Spira

BORN: Antwerp, Belgium 1938.

EDUCATED:-

PRIMARY: Stedelijk Onderwijs Gesticht voor Jongens No. 3. (Antwerp) 1945-1951.

SECONDARY: Koninklijk Atheneum Antwerpen 1951-1957.

UNIVERSITY: Université Libre de Bruxelles. (Licence en Sciences Physiques). 1957-1961.
University of Ottawa 1962-1968.

APPOINTMENTS: Chercheur agréé de l'Institut Interuniversitaire des Sciences Nucléaires. (Belgium) 1961-1962.
Lecturer in the Faculty of Philosophy of the University of Ottawa 1966-1968.